



TECHNISCHE UNIVERSITÄT MÜNCHEN

Fakultät für Medizin

Antiviral properties of species conserved nucleic acid-binding proteins

Lisa Friederike Pennemann

Vollständiger Abdruck der von der Fakultät für Medizin der Technischen Universität München zur Erlangung des akademischen Grades eines

Doktors der Naturwissenschaften (Dr. rer. nat.)

genehmigten Dissertation.

Vorsitzende/-r: Prof. Dr. Dr. Stefan Engelhardt

Prüfende/-r der Dissertation:

1. Prof. Dr. Dr. Andreas Pichlmair

2. Prof. Dr. Dietmar Zehn

Die Dissertation wurde am 04.02.2021 bei der Technischen Universität München eingereicht und durch die Fakultät für Medizin am 10.08.2021 angenommen.



Portrait of a Scientist - Mirre Klatter

“Obviously my method of thought and reasoning is influenced by a scientific training – if that were not so my scientific training will have been a waste and a failure. But you look at science (or at least talk of it) as some sort of demoralizing invention of man, something apart from real life, and which must be cautiously guarded and kept separate from everyday existence. But science and everyday life cannot and should not be separated. Science, for me, gives a partial explanation of life. In so far as it goes, it is based on fact, experience and experiment.”

Rosalind Franklin



Table of Contents

Summary.....	vi
Abbreviations	vii
Introduction	1
Virus-host coevolution influences the immune system	1
Pattern recognition receptors	3
Toll-like receptors	3
C-type lectin receptors	5
NOD-like receptors	6
AIM2-like receptors	6
RIG-I-like receptors.....	6
cGAS	7
EIF2AK2	8
OAS.....	8
PRR induced signaling factors	9
NF- κ B signaling	9
ERK, JNK and p38 dependent transcription factor signaling	10
IRF activation.....	10
Key Cytokines of the Innate Immune System	11
Interleukins	11
Interferons	12
Evolution of NA sensing PRR signaling pathways.....	13
Evolutionary conservation of PRR signaling.....	13
Evolution of PRR induced transcription factors	14
Evolution of cytokines	15
IFN inducing PRRs are older than IFNs	16
Identification of PRRs.....	17

Thesis Aim	20
Materials	22
Devices and instruments	22
Consumables	22
Chemicals and reagents	23
Homemade buffers	26
Commerical kits	28
Enzymes	28
Oligonucleotides	28
Cloning and sequencing oligonucleotides	28
sgRNA oligonucleotides	30
Plasmids	36
Bacteria.....	38
Antibodies	38
Cell lines	39
Viruses.....	41
Lentiviruses	41
Other viruses	48
Software and databases	48
Methods	49
Molecular cloning	49
Polymerase Chain Reaction	49
Agarose gel electrophoresis and gel purification	50
Gateway cloning	50
Sequence and Ligation Independent cloning	51
Lentiviral CRISPR cloning.....	51
Site-directed mutagenesis	51
Bacterial Transformation.....	52



DNA extraction.....	52
Cell culture and handling.....	53
Cell culture.....	53
Freezing and thawing of cells.....	53
Creation of stable KO or overexpression cells	53
Transient overexpression.....	54
Cell viability.....	54
Live cell imaging	54
Virus culture, titration and related experiments	55
Virus stock production.....	55
Plaque assays	55
Lentivirus production.....	55
Virus replication of luciferase tagged viruses	56
Virus replication of fluorescently tagged viruses	56
Protein biochemistry	56
SDS-PAGE	56
Western Blot.....	57
Affinity purification and LC-MS/MS analysis.....	57
Protein production in insect cells.....	59
Fluorescence quenching.....	60
Kinase assay	60
Full proteomic MS analysis	60
Cytokine measurements	62
Bioinformatic analysis	62
Analysis overlap Castello / Metascape IAV and domain enrichment	62
GO-Term enrichment of AP-MS data	62
Orthologue analysis	62
Selection of Candidate Lists	62

Statistical analysis of the KO screening	63
Upstream promoter analysis	63
Results	64
NA interactor identification using proteomic quantification.....	64
Analysis of NA interactome	67
Comparative analysis of NA interactome with viral datasets	71
Intersection of AP-MS from human, mouse and fly	72
Lentivirus based arrayed CRISPR Cas9 screening of the candidate list.....	75
TAO kinases as antiviral proteins	78
Validation of TAOK2 screening phenotypes.....	78
TAOK2 can be transiently, but not stably overexpressed	79
dTao directly interacts with poly(I:C) and the interaction affects kinase activity ..	81
Loss of TAOK2 leads to a decrease in ISG expression.....	82
TAOK2 impacts expression of IFN genes/proteins, but not of TNF- α or ILs	84
Targeting of TAOK2 using kinase inhibitors	85
Discussion.....	88
Candidates from the CRISPR Cas9 KO screening.....	88
The dsRNA interactor PARP12 has pan-antiviral activity	88
The dsDNA interactor RSL1D1 is involved in the DNA damage response	89
The dsRNA interactor SMARCA5 belongs to a family of known antiviral proteins	90
Overlap between human and fly depletion screening	90
ABCF1 and ABCF3 are novel 2'5'OA interactors with antiviral effects	92
NA interactors MSI2 and CDK2AIP have conserved antiviral phenotypes in human and flies	93
Human proviral factor KHDRBS1 is antiviral in flies	93
TAO kinases as antiviral proteins	94
Concluding Remarks.....	96



References.....	97
List of Tables and Figures	118
List of Figures	118
List of Tables	119
Acknowledgements	120

Summary

The cellular antiviral response evolved over millions of years, parallel to viruses attempting to evade it. As viral nucleic acids are one of the few stable components across different viruses, the cellular antiviral response relies heavily on sensing them. Thus in this project affinity proteomics with different viral nucleic acids was used to identify conserved NA interacting proteins in different species (human, mouse and fly). The affinity proteomics were analyzed using mass spectrometry, leading to the identification of 904, 1214 and 1479 NA interactors in human, mouse and fly, respectively. Based on the interaction strength with the viral NA, and factoring in conservation across species and published data, 90 candidates were selected. Cellular knockouts of the 90 candidates were generated using a lentiviral CRISPR Cas9 system, and the knockouts were infected with a panel of four distinct luciferase tagged viruses. Measuring of the luciferase activity as a proxy for viral replication and gene expression identified 43 viral restriction factors and 13 proteins that supported virus growth. One of the viral restriction factors, TAOK2, was selected for follow-up experiments, as it showed conserved NA interaction with dsRNA and a broad antiviral phenotype and had not previously been linked to NA sensing immunity. We furthermore observed that the TAOK2 fly orthologue TAO kinase is a high affinity dsRNA binder and human TAOK2 regulates IRF3-dependent antiviral responses without affecting NF- κ B-dependent cytokine expression. Inhibition of TAOK2 led to an impaired ISG response and increased viral growth. Overall the data, combined with previous studies linking TAOK2 to MAPK based signaling, indicate that TAOK2 has a role in IFN specific immunity, potentially through the MAPK-JNK pathway. Overall, this study shows how considering evolutionary conserved NA binding patterns of proteins, highlights proteins involved in virus-host interactions.



Abbreviations

2'5' OAs	2'-5' oligoadenylates
aa	amino acids
AAA	ATPases associated with a variety of cellular activities
ABC	ATP-binding cassette
AGC	automatic gain control
ALRs	AIM2-like receptors
AMP	Adenosine monophosphate
AP	Affinity purification
AP-1	Activator protein-1
ATF2	activating transcription factor 2
ATM	Ataxia Telangiectasia Mutated kinase
ATP	adenosine 5'triphosphate
ATR	Ataxia Telangiectasia And Rad3-Related Protein kinase
CARD	caspase recruitment domain
CCL	C-C motif chemokine ligand
cGAMP	cyclic GMP-AMP
CLEC4A	C-Type Lectin Domain Family 4 Member A
CLRs	C-type lectin receptors
CRISPR	clustered regularly interspaced short palindromic repeats
CrPV	Cricket paralysis virus
CTD	C-terminal domain
CXCL	C-X-C Motif Chemokine Ligand
DBD	DNA binding domain
DC	dendritic cell
DCV	Drosophila C virus
DD	death domain
DDR	DNA damage response
DEXD/H	DEAD box helicase domain
DIOPT	DRSC Integrative Ortholog Prediction Tool
DMEM	Dublecco's modified Eagle's medium
dTao	<i>D. melanogaster</i> Tao
EDTA	Ethylenediamine tetraacetic acid
EMSA	electrophoretic mobility shift assay
ER	endoplasmic reticulum
ERK	extracellular-signal-regulated kinase
ESCRT-III	endosomal sorting complex required for transport III polymers
EV71	Enterovirus 71
FBS	fetal bovine serum
FHV	Flock house virus
FMDV	Foot-and-mouth-disease virus
GAS	IFN- γ -activated sequence
G-CSF	Granulocyte colony-stimulating factor
GM-CSF	granulocyte/macrophage colony-stimulating factor
GMP	Guanosine monophosphate
GO	Gene Ontology

GOBP	Gene Ontology biological processes
GOCC	Gene Ontology cellular compartments
GOMF	Gene Ontology molecular functions
GPCR	G-coupled protein receptor
GTP	guanosine 5'-triphosphate
HCD	higher-energy collisional dissociation
HDP-RNP	HEXIM1-DNA-PK-paraspeckle components-ribonucleoprotein complex
HIV-1	Human immunodeficiency virus-1
HRP	horseradish peroxidase
HSV-1	Herpes simplex virus 1
IAD	IRF-association domain
IAV	influenza A virus
IFN	interferon
IL	interleukin
IRAKs	IL-1R-associated kinases
IRF	IFN regulatory factors
ISG	interferon-stimulated gene
ISGF3	IFN-stimulated gene factor 3
ISRE	Interferon-Stimulated Response Element
ITAMs	immunoreceptor tyrosine-based activation motifs
ITIMS	immunoreceptor tyrosine-based inhibitory motifs
JAKs	Janus-activated kinases
JNK	JUN N-terminal kinase
KD	knock-down
KEGG	Kyoto Encyclopedia of Genes and Genomes
KO	knockout
LGP2	laboratory of genetics and physiology 2
LRR	leucine rich repeats
M.H.	Matthias Habjan
MAPK	mitogen activated kinase
MDA5	Melanoma differentiation associated gene 5
MHC	Major Histocompatibility complex
MKP1	MAPK phosphatase 1
MS	Mass Spectrometry
MyD88	myeloid differentiation primary-response protein 88
NA	nucleic acids
NCE	normalized collision energy
NEMO	NF- κ B essential modulator
NF- κ B	Nuclear factor κ B
NK	natural killer
NLR	NOD like receptors
NOD	nucleotide-binding oligomerization domain
NTD	N-terminal domain
P/S	penicillin-streptomycin
PAMPs	Pathogen Associated Molecular Patterns
PCR	Polymerase Chain Reaction



pfu	plaque forming units
PI3K	phosphatidylinositol-3-kinase
PRRs	Pattern Recognition Receptors
PTEN	Phosphatase And Tensin Homolog
RIG-I	Retinoic acid-inducible gene 1
RIPK1	Receptor Interacting Serine/Threonine Kinase 1
RLRs	RIG-I like receptors
RNAi	RNA based interference
RNASEH1	Ribonuclease H1
SDS-PAGE	SDS polyacrylamide gel electrophoresis
SFV	Semliki Forest virus
SHP	Sh2-domain-containing protein tyrosine phosphatase
SINV	Sinbid virus
STAT	signal transducers and activators of transcription
STING	Stimulator of Interferon Genes
TAB1	TAK1-binding protein 1
TAB2	TAK1-binding protein 2
TAK1	TGF- β activated kinase 1
TH	T helper
TICAM1	TIR-domain-containing adaptor protein inducing IFN- β
TIR	Toll/interleukin-1 receptor domain
TLRs	Toll-like receptors
TNF	tumor-necrosis factor
TRAF6	TNF receptor associated factor 6
TREX1	Three Prime Repair Exonuclease 1
VSV	Vesicular stomatitis virus
WNV	West Nile Virus



Introduction

Virus-host coevolution influences the immune system

In 1859 naturalist Charles Darwin published 'On the Origin of Species' in which he explains the concept of evolution by natural selection. As it conflicted with the ideals and beliefs of the church, the concepts of the publication were initially quite controversial, but have now become a central dogma of modern evolutionary theory. In short, Darwin's theory of evolution states that any individual that has an advantage, no matter how small, over other individuals of the same species, will have an increased chance of survival and reproduction and its offspring will most likely inherit this advantage. The most famous example of this is of course the Darwin finches, where the most intriguing difference between the finches is the size and shape of their beaks, an adaptation to the different food sources of the birds (Palmer and Kronforst, 2015). In this example, the adaptation is driven by environmental pressure. However, such a driving pressure can also be exerted via another species. For example, for a grazing animal species, which is frequently preyed upon by a predator, it would be beneficial to gain increased athletic capabilities and maneuverability in order to escape more regularly during a hunt. This in turn would exert evolutionary pressure on the predator, as faster predators would now have an advantage (Wilson et al., 2018). The increased speed of the predator negates the increased speed of the prey, and therefore once more exerts evolutionary pressure onto the prey. This dynamic between predator and prey leads to a recurrent and ceaseless evolutionary arms race, known as the Red Queen dynamic (Valen, 1973), and can be observed not only in predator-prey relationships but also in host-pathogen relationships (Daugherty and Malik, 2012).

Virus-host coevolution has been ongoing for millions of years, as evidenced by endogenized viral retroelements in the host genome (Daugherty and Malik, 2012; Theze et al., 2011). This is despite the arms-race between viruses and their hosts being inherently skewed towards the virus, due to higher mutation rates, faster replication rates and a larger population size of the viruses (Daugherty and Malik, 2012). Against this onslaught, hosts rely on a variety of defense mechanisms collectively termed the immune system. Variations of the immune system are found in virtually all living organisms. Bacteria contain clustered regularly interspaced short palindromic repeats (CRISPR), which together with associated proteins serve as an

archive of previously encountered foreign DNA. This allows for quick interference with invading DNA through sequence-specific degradation (Hille et al., 2018). Some eukaryotes, such as plants and insects, rely heavily on RNA based interference (RNAi); a system for sequence specific degradation of foreign RNA (Mussabekova et al., 2017). In mammals, the immune system is divided into two separate strategies: the innate and the adaptive immune system. The innate immune system is considered the broad first line of defense against invading pathogens and includes epithelial barriers, the complement system and germline encoded receptors with a broad specificity for pathogens expressed primarily on phagocytic immune cells, such as dendritic cells (DC), natural killer (NK) cells and macrophages (Medzhitov, 2007) (Fig. 1). Innate immune cells also produce cytokines, small proteins that modulate the local and systemic immune response (Medzhitov, 2007). In contrast, the adaptive immune system allows for a targeted immune response and lasting immunological memory where recognition of pathogens is mediated by B and T lymphocytes, which due to somatic recombination have a diverse range of pathogen specific receptors (Medzhitov, 2007). B cells are primarily known for the production of antibodies, a Y-shaped protein capable of recognizing and neutralizing pathogens (Cyster and Allen, 2019). T cells can be subdivided into two classes CD8+ and CD4+ T cells (Kaech and Cui, 2012). CD8+ T cells are capable of recognizing and killing infected cells (Kaech and Cui, 2012), while CD4+ T cells recruit and influence other immune cells through cytokine signaling (Littman and Rudensky, 2010).

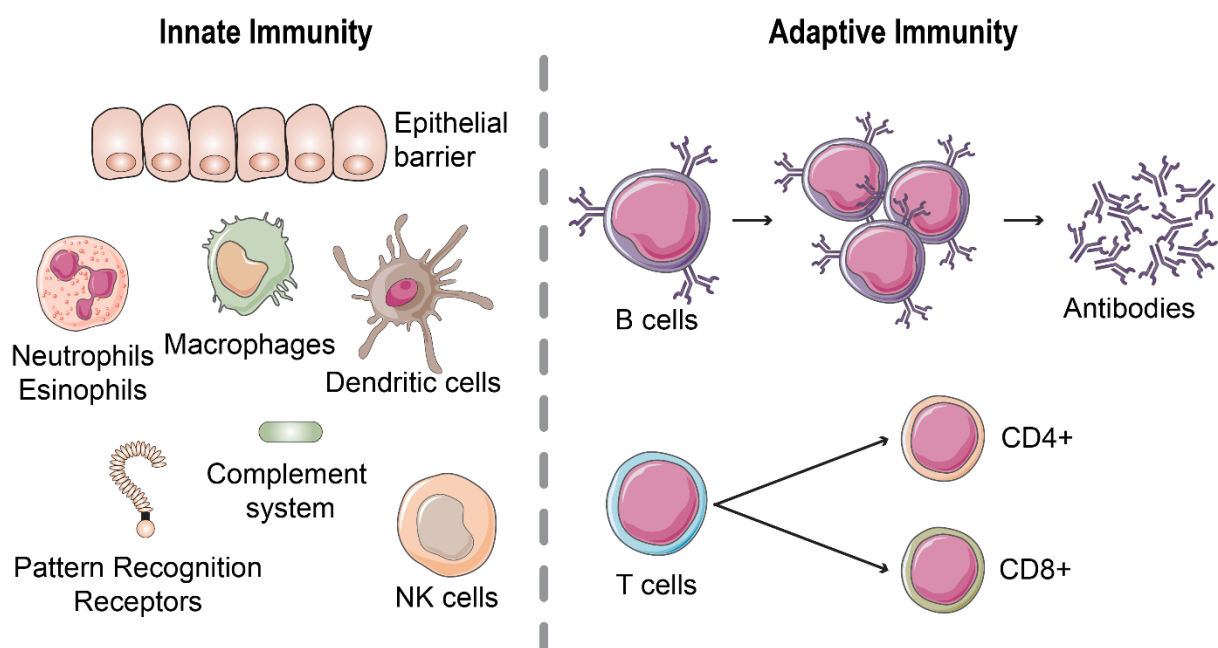


Figure 1: Overview of components of the innate and the adaptive immune system



Pattern recognition receptors

The germline encoded receptors expressed on innate immune cells are known as Pattern Recognition Receptors (PRRs) and detect a wide array of Pathogen Associated Molecular Patterns (PAMPs). Ideal PAMPs are defined as (i) being present across multiple pathogens (ii) being unique to pathogens, to allow discrimination between self and non-self and (iii) having an essential role within the life cycle of the pathogen thereby limiting potential evolutionary changes and ensuring the continued recognition by PRRs (Medzhitov, 2007). The mode of action of several well-established PRRs will be outlined below; however, there are many other proteins with the ability to recognize PAMPs.

Toll-like receptors

The family of Toll-like receptors (TLRs) encompasses 10 different receptors in human and detects a wide array of different PAMPs from bacteria, viruses and fungi (Akira and Takeda, 2004). Four of the 10 TLRs are capable of detecting foreign nucleic acids (NAs), TLR3, 7, 8 and 9 (Table 1). TLRs are transmembrane proteins, found both on the cell surface membrane and, in the case of NA sensing TLRs on membranes of endosomal compartments (Brubaker et al., 2015). They contain three distinct protein domains; leucine rich repeats (LRR), which serves as a binding site for PAMPs, a linker region and a Toll/interleukin-1 receptor domain (TIR), which allows for downstream signaling (Akira and Takeda, 2004). Upon ligand binding, the TLRs dimerize and undergo conformational changes, which leads to the recruitment of adaptor proteins facilitating the downstream signaling.

TLR7, TLR8 and TLR9 rely on interaction with the adaptor Myeloid Differentiation Primary Response Protein MyD88 (MyD88) whereas TLR3 relies on TIR-domain-containing adaptor protein inducing IFN- β (TICAM1, also known as TRIF)(Blasius and Beutler, 2010). MyD88 contains an N-terminal death domain (DD) and a C-terminal TIR domain, which are separated by a short linker region (Akira and Takeda, 2004). MyD88 interacts with the TLR through a TIR-TIR interaction, and upon interaction MyD88 recruits serine/threonine kinase IRAK4 through a DD-DD interaction (Akira and Takeda, 2004). IRAK4 phosphorylates family members IRAK1 and IRAK2, which in turn activates TNF receptor associated factor 6 (TRAF6) (Blasius and Beutler, 2010). TRAF6 is an E3 ubiquitin ligase and, after autoubiquitination, binds to NF- κ B essential modulator (NEMO) via TAK1-binding protein 2 (TAB2). In chaining itself to TAB2 and

NEMO, TRAF6 activates NEMO and a protein complex consisting of TAB2, TGF- β activated kinase 1 (TAK1) and TAK1-binding protein 1 (TAB1) (Blasius and Beutler, 2010). TAK1 phosphorylates IKK- β , which in turn phosphorylates I κ B. Phosphorylation of I κ B leads to its degradation, initiating the nuclear translocation of the NF- κ B complex (Blasius and Beutler, 2010) (Fig. 2).

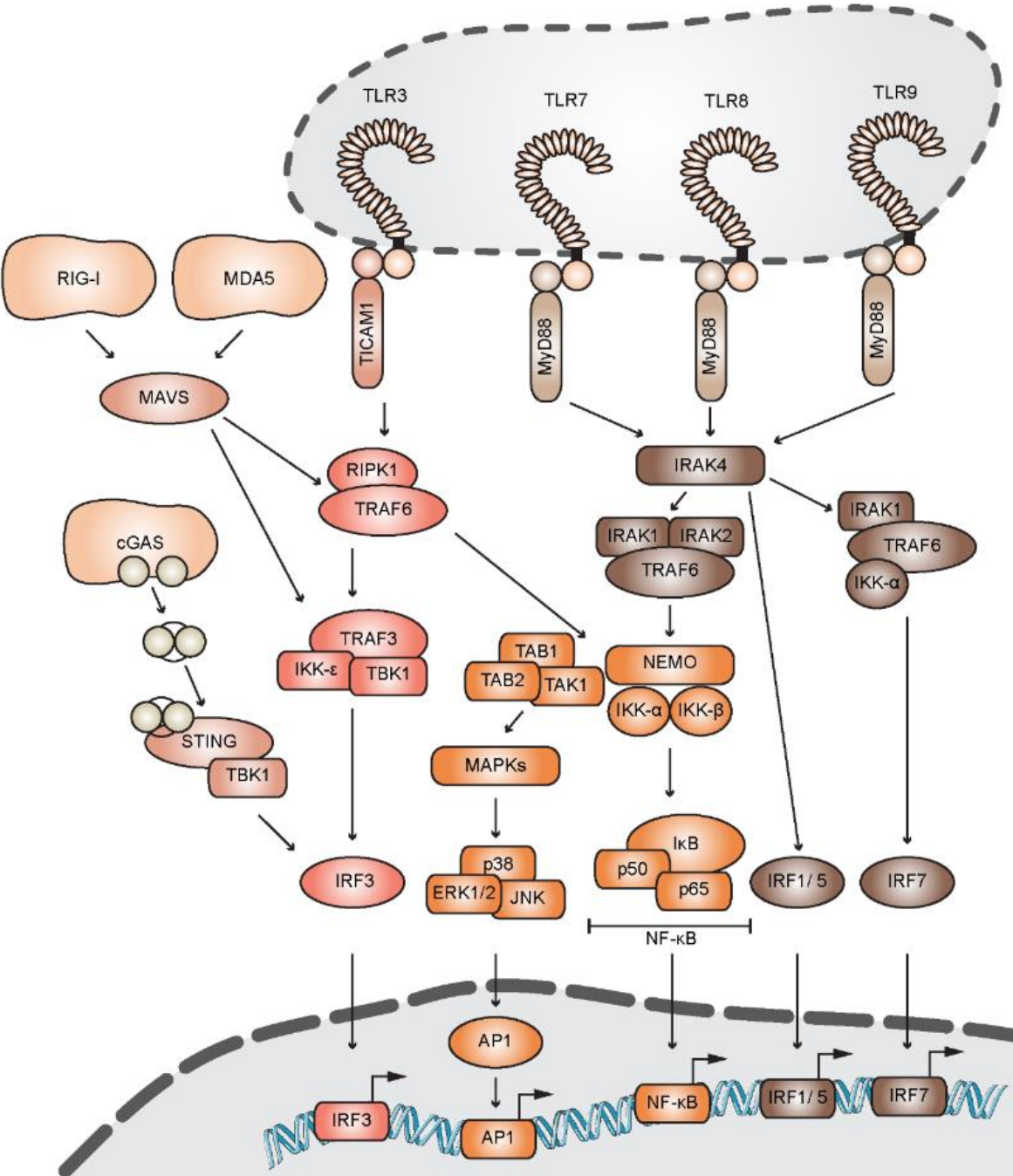


Figure 2: Schematic of NA sensing PRR signaling. Adapted from: (Ablasser and Hur, 2020; Akira and Takeda, 2004; Belgnaoui et al., 2011; Blasius and Beutler, 2010; Cervantes et al., 2012; Kosugia et al., 2009; Schlee and Hartmann, 2016)



In addition to the phosphorylation of IKK- β , TAK1 also activates the mitogen activated kinase (MAPK) cascade (Liu et al., 2007). Activation of the MAPK cascade results in the activation of p38, extracellular-signal-regulated kinase (ERK) and JUN N-terminal kinase (JNK). Once activated, these kinases translocate across the nuclear membrane and phosphorylate selected transcription factors, including activating transcription factor 2 (ATF2) and activator protein 1 (AP-1) (Liu et al., 2007) (Fig. 2).

Interferon (IFN) regulatory factors (IRF) 1 and 5 directly associate with MyD88-IRAK4 and are thus activated, while IRF7 is activated by a complex of IRAK1, TRAF6 and IKK- α (Blasius and Beutler, 2010). Upon activation, all three IRFs translocate to the nucleus and induce the production of IFN (Blasius and Beutler, 2010).

As opposed to the other endosomal TLRs, TLR3 signaling relies on the adaptor TICAM1. Similar to MyD88, TICAM1 interacts with TLR3 through a TIR domain (Matsumoto et al., 2011). Once activated, TICAM1 also activates the aforementioned NEMO and MAPK pathways, but through TRAF6 in a complex with Receptor Interacting Serine/Threonine Kinase 1 (RIPK1) instead of the IRAK proteins. In addition, TLR3 signaling through RIPK1 and TRAF6 also links to TRAF3, which in combination with TBK1 and IKK ϵ activates IRF3 (Blasius and Beutler, 2010) (Fig. 2).

C-type lectin receptors

The C-type lectin receptor (CLR) family consists of over a 1000 different proteins, all containing a carbohydrate binding C-type lectin-like domain. CLRs are found both as secreted and as transmembrane proteins. Their function ranges from cell homeostasis to growth factors and of course PRRs (Brown et al., 2018). CLRs can recognize viruses, such as Hepatitis C virus, human immunodeficiency virus (HIV) and Dengue virus, through viral carbohydrate structures, e.g. mannose glycans found on the viral envelope (Bermejo-Jambrina et al., 2018). CLRs can also contain immunoreceptor tyrosine-based activation motifs (ITAMs), hemi-ITAMs, or immunoreceptor tyrosine-based inhibitory motifs (ITIMs), all of which are signaling motifs involved in the regulation of the immune response. While the precise signaling pathways are unclear, CLR members have been shown to impact the immune response. For example, C - Type Lectin Domain Family 4 Member A (CLEC4A, also known as DCIR) and BDCA-2 impact the IFN response and DC-SIGN, MR and MDL-1 the interleukin response (Bermejo-Jambrina et al., 2018). One hypothesis suggests that CLEC4A using its ITIM domain, recruits two phosphatases: Sh2-domain-containing protein tyrosine

phosphatase (SHP) 1 and SHP2. When active SHP2 can deactivate signal transducers and activators of transcription (STAT) 1, thereby disrupting interferon signaling. Through the binding of SHP2, CLEC4A prevents the deactivation of STAT1, maintaining IFN signaling (Troegeler et al., 2017). Additionally, CLRs are involved in antigen presentation via major histocompatibility complex (MHC) class II on CD4+ T cells and cross-presentation via MHC class I on CD8+ T cells (Bermejo-Jambrina et al., 2018).

NOD-like receptors

Nucleotide-binding oligomerization domain (NOD)-like leucine-rich repeat containing receptors (NLRs) are a family of 22 intracellular cytoplasmic PRRs. They contain an N-terminal domain, a central NACHT domain and a ligand binding C-terminal LRR domain. The receptors are categorized into four subfamilies based on the N-terminal effector domain: NLRA, NLRB, NLRC, NLRP and NLRX (Saxena and Yeretssian, 2014; Ting et al., 2008). The two most well studied NLRs are NOD1 and NOD2, which detect bacterial components, e.g. bacterial peptidoglycans such as muramyl-dipeptid. Upon activation, NOD1 and NOD2 self-oligomerize and recruit RIPK2 (Saxena and Yeretssian, 2014). This induces a signaling cascade leading to the activation of NF- κ B, via NEMO, and MAPK, via the TAK1 TAB1 TAB2 complex (Dolasia et al., 2018; Saxena and Yeretssian, 2014).

AIM2-like receptors

The AIM2-like receptor (ALR) family consists of four proteins, AIM2, IFI16, PYHIN1 and MNDA. Each of the receptors contains a DNA binding HIN-200 domain and a PYHIN domain, which enables protein-protein interactions (Fernandes-Alnemri et al., 2009). Upon the detection of intracellular DNA, AIM2 interacts with the adaptor protein ASC and promotes inflammasome formation (Fernandes-Alnemri et al., 2009). The inflammasome is a protein complex capable of activating pro-inflammatory caspases (Medzhitov, 2007). Although IFI16 also directly interacts with foreign DNA, recent studies have shown that IFI16 is a cofactor for another PRR, cGAS, rather than an independent PRR (Jonsson et al., 2017). No receptor function has been identified for PYHIN1 or MNDA (Muñoz-Wolf and Lavelle, 2016).

RIG-I-like receptors

The human family of retinoic acid-inducible gene I-like receptors (RLRs) consists of three cytoplasmic NA sensing PRRs; retinoic acid-inducible gene 1 (RIG-I; also called



DDX58), melanoma differentiation associated gene 5 (MDA5; also called IFIH1) and laboratory of genetics and physiology 2 (LGP2; also called DHX58). The RLRs share a DExD/H-box helicase domain and a C-terminal domain. Additionally both RIG-I and MDA5 have an N-terminal caspase recruitment domain (CARD), which allows for interaction with the downstream adaptor (Yoneyama et al., 2015). While LGP2 can interact with dsRNA, it lacks the CARD domain responsible for downstream signaling (Yoneyama et al., 2015). However, LGP2 appears to act as a cofactor to both RIG-I and MDA5 (Habjan and Pichlmair, 2015).

Both RIG-I and MDA5 interact with dsRNA through the helicase domain, which for RIG-I induces a conformational change exposing the CARD domain (Loo and Gale, 2011). Through CARD-CARD domain interactions, both RIG-I and MDA5 interact with the adaptor protein mitochondrial antiviral signaling protein (MAVS) at the mitochondrial membrane (Ablasser and Hur, 2020; Loo and Gale, 2011). Once active, MAVS oligomerizes and recruits TRAF proteins, including TRAF3 and TRAF6. TRAF3 activates IKK- ϵ and TBK1 (Belgnaoui et al., 2011), which in turn phosphorylate MAVS. The phosphorylation creates a docking site for IRF3, which once in proximity is phosphorylated and thus activated by TBK1 (Liu et al., 2015). Similarly, IKK- ϵ and TBK1 can also activate IRF7 (Belgnaoui et al., 2011). Akin to TLR3 signaling, TRAF6, in combination with RIPK1, activates NF- κ B through NEMO (Belgnaoui et al., 2011) (Fig. 2).

cGAS

cGAS, a dsDNA sensor contains an unstructured N-terminal domain and a C-terminal nucleotidyl transferase domain consisting of two lobes, the C-lobe and the N-lobe, which are connected by a zinc ribbon (Ablasser and Chen, 2019; Sun et al., 2012). Together, the C-lobe and the N-lobe create a positively charged catalytic pocket (Ablasser and Chen, 2019). Upon binding of dsDNA to the zinc ribbon, the catalytic pocket of cGAS undergoes a conformational change, allowing for the binding of ATP and GTP (Ablasser and Hur, 2020). ATP and GTP are then converted to cyclic guanosine monophosphate (GMP) - adenosine monophosphate (AMP) (cGAMP), which contains two phosphodiester bonds; 2'-hydroxyl GMP to 5'-phosphate AMP and 3'-hydroxyl AMP to 5'-phosphate GMP (Ablasser and Chen, 2019). cGAMP is a second messenger, of which the only known downstream target is the endoplasmic reticulum (ER) membrane protein stimulator of interferon genes (STING) (Ablasser and Hur,

2020). Upon binding of cGAMP, STING translocates from the ER to the Golgi complex, where STING then recruits TBK1 (Ablasser and Hur, 2020). TBK1 phosphorylates STING, allowing for IRF3 interaction and phosphorylation through TBK1 (Ablasser and Hur, 2020) (Fig. 2). Interestingly, cGAMP can also cross gap junctions from one cell to another, inducing inflammatory signaling in neighboring cells (Ablasser and Hur, 2020).

EIF2AK2

EIF2AK2 (also known as dsRNA-dependent Protein kinase R (PKR)) is a dsRNA-dependent protein kinase that is transcriptionally upregulated by interferon and activated through dsRNA binding (Hur, 2019). EIF2AK2s best known target for phosphorylation is eIF2 α , which has a pivotal role during cap-dependent translation. By constitutively phosphorylating eIF2 α , EIF2AK2 essentially leads to a global stop of protein synthesis, and therefore inhibition of cell cycle progression and viral replication (Hur, 2019).

OAS

The 2'-5'-Oligoadenylate synthetase (OAS) family consists of three catalytically active (OAS1, OAS2, OAS3) and one inactive (OASL) members, which recognize dsRNA (Schwartz and Conn, 2019). OAS1 has one repeat of the OAS domain, OAS2 contains two and OAS3 contains three. OASL contains one OAS domain and a C-terminal domain (Hartmann et al., 2003). Upon binding dsRNA, the three catalytically active OAS proteins synthesize 2'-5' oligoadenylates (2'5' OAs). 2'5'OAs is a second messenger, activating RNase L, which then cleaves unpaired RNA. This cleavage is minimally sequence specific and therefore targets a broad range of RNAs, e.g. tRNAs, mRNAs and rRNAs, leading to similar effects as those observed for EIF2AK2 (Hur, 2019). While catalytically inactive, OASL also plays a role in the innate immune response, acting as a cofactor to RIG-I (Ibsen et al., 2015).

Table 1: Overview of selected NA binding PRRs

PRR	Family	Ligand	Location	References
TLR3	TLR	dsRNA	Endosomal compartment membrane	(Akira and Takeda, 2004; Brubaker et al., 2015)
TLR7	TLR	ssRNA dsRNA	Endosomal compartment membrane	(Akira and Takeda, 2004; Brubaker et al., 2015; Schlee and Hartmann, 2016)
TLR8	TLR	ssRNA	Endosomal compartment membrane	(Akira and Takeda, 2004; Brubaker et al., 2015)

TLR9	TLR	CpG-containing DNA	Endosomal compartment membrane	(Akira and Takeda, 2004; Brubaker et al., 2015)
AIM2	ALRs	dsDNA	Cytoplasmic	(Fernandes-Alnemri et al., 2009)
RIG-I	RLR	PPP-dsRNA	Cytoplasmic	(Habjan and Pichlmair, 2015; Yoneyama et al., 2015)
MDA5	RLR	Long dsRNA, AU-rich RNA	Cytoplasmic	(Habjan and Pichlmair, 2015; Yoneyama et al., 2015)
cGAS	-	dsDNA	Cytoplasmic	(Ablasser and Chen, 2019)
EIF2AK2	-	PPP-dsRNA	Cytoplasmic	(Habjan and Pichlmair, 2015; Schlee and Hartmann, 2016)
OAS1	OAS	>17 bp dsRNA	Cytoplasmic	(Schlee and Hartmann, 2016; Schwartz and Conn, 2019)
OAS2	OAS	>35-40 bp dsRNA	Cytoplasmic	(Schwartz and Conn, 2019)
OAS3	OAS	>50 bp dsRNA	Cytoplasmic	(Schwartz and Conn, 2019)

PRR induced signaling factors

NF- κ B signaling

In humans, the NF- κ B signaling complex has up to five different members which act as dimers; p65, p50, RelB, Relc and p52 (Mitchell et al., 2016), which are normally kept in the cytoplasm by inhibitory proteins, such as I κ B (Liu et al., 2017). Upon activation of NEMO through PRR signaling, or through ribotoxic, genotoxic or shear stress (Mitchell et al., 2016), I κ B is phosphorylated, which triggers ubiquitin dependent proteasomal degradation (Liu et al., 2017). Degradation of the inhibitory protein causes NF- κ B translocates to the nucleus, where it acts as a transcription factor for pro-inflammatory cytokines, chemokines and other inflammatory proteins (Liu et al., 2017). Key cytokines induced by NF- κ B are IL-1, IL-2, IL-6, IL-8, IL-12, TNF- α , C-C motif chemokine ligand (CCL) CCL2, C-X-C Motif Chemokine Ligand (CXCL) 1, CXCL2 and CXCL10 (Liu et al., 2017). Additionally, NF- κ B impacts the expression of cell cycle regulators, e.g. PAI2 and cyclin, and anti-apoptotic factors, e.g. caspase, as well as T-cell and macrophage differentiation and activation, dendritic cell maturation and neutrophil recruitment (Liu et al., 2017).

ERK, JNK and p38 dependent transcription factor signaling

Translocation of the MAPK activated kinases ERK, JNK and p38 to the nucleus leads to the activation of the transcription factors including AP-1 and ATF2. These transcription factors are known to regulate the proinflammatory tumor-necrosis factor (TNF) cytokines, interleukins (IL)-1 β and -6, though effects have also been observed on CCL2, CCL4 and granulocyte/macrophage colony-stimulating factor (GM-CSF) (Liu et al., 2007). There is also evidence that MAPK signaling can affect IFN production (Yoshizawa et al., 2008), potentially through IRF3 (Zhang et al., 2009), though the exact pathway is unknown. Concurrently to enhancing the transcription of cytokine mRNA, the transcription factors also induce the transcription of MAPK phosphatase 1 (MKP1). Accumulation of MKP1 in the nucleus causes the dephosphorylation of JNK and p38, thereby terminating the signal driving the pro-inflammatory response (Liu et al., 2007). It is worth noting that in addition to being activated through PRR signaling pathways, the MAPK cascade can also be activated by various other pathways including growth factors, hormones and cytokines and activation impacts proliferation, differentiation, senescence and apoptosis (Plotnikov et al., 2011; Yang et al., 2013). In line with this, the MAPK cascade has been implicated in multiple diseases, including cancer, diabetes and arthritis (Liu et al., 2007; Plotnikov et al., 2011).

IRF activation

Most vertebrates have 10 IRFs, though humans only have nine, IRF1-9 (Nehyba et al., 2009). Each has a DNA binding domain (DBD) as well as one IRF-association domains (IAD), either IAD1 or IAD2, in the C-terminal region, which allows for the dimerization with other IRF family members (Antonczyk et al., 2019; Mogensen, 2019). The DBD recognizes a DNA sequence termed Interferon-Stimulated Response Element (ISRE), an element found in the promoters of type I and III IFNs as well as interferon-stimulated genes (ISGs) (Negishi et al., 2018). The four main IRFs acting as transcription factors upon PRR stimulation are IRF1, IRF3, IRF5 and IRF7 (Negishi et al., 2018). Of these IRF3 and IRF7 are the two key mediators of IFN induction downstream of PRRs (Jefferies, 2019). IRF3 is constitutively expressed and is therefore generally activated early during infection, while IRF7 is an ISG and is thus activated in the later stages (Honda et al., 2006). IRF3 preferentially activates IFN- β over IFN- α , whereas IRF7 activates both equally (Honda et al., 2006).

Table 2: Overview of IRFs induced by NA sensing PRRs



	Activation Pathway	Impact	References
IRF1	TLR7, TLR8, TLR9 signaling, Type II IFN signaling	Type I IFN expression in DCs Induction of apoptosis	(Blasius and Beutler, 2010; Negishi et al., 2018)
IRF3	TLR3 signaling, cGAS-STING signaling, RLR signaling	Early stage type I and type III IFNs expression, e.g. IFN- β , IFN- α 1 and IFN- α 4	(Ablasser and Hur, 2020; Loo and Gale, 2011; Matsumoto et al., 2011; Mogensen, 2019)
IRF5	TLR7, TLR8, TLR9 signaling	Induction of type I IFN gene expression Induction of pro-inflammatory cytokines, e.g. IL-12 β , IL-6 and TNF- α	(Blasius and Beutler, 2010; Negishi et al., 2018)
IRF7	TLR7, TLR8, TLR9 signaling, RLR signaling, type I IFN signaling	Delayed type I IFNs expression, e.g. IFN- α 2, IFN- α 5, IFN- α 6, IFN- α 8, IFN- β 2 and IFN- β 3	(Blasius and Beutler, 2010; Loo and Gale, 2011; Mogensen, 2019)

Key Cytokines of the Innate Immune System

Interleukins

There are well over 40 different ILs in humans, which are generally divided into four groupings, based on their structural features: IL-1 like cytokines, class I helical cytokines, class II helical cytokines and IL-17-like cytokines (Brocker et al., 2010). There are also ILs that, due to unique or lacking structure, are not sorted into the aforementioned groups (Brocker et al., 2010). In line with the large number of different ILs, functions also vary vastly, as ILs modulate not only the immune response but also cellular growth and differentiation (Brocker et al., 2010). Functions of ILs within the immune response include (i) induction of pro-inflammatory proteins, as observed for IL-1 and IL-17, (ii) functioning as a chemoattractant for immune cells, e.g. IL-16 and (iii) operating as a crossover point between the innate immune system and the adaptive immune system. ILs convey signaling between the innate and the adaptive immune system by inducing activation and differentiation of B- and T-cells (Akdis et al., 2011). For instance, IL-1, IL-4 and IL-12 induce T_H cell differentiation (Akdis et al., 2011; Dinarello, 2011; Gee et al., 2009), IL-6 and IL-15 induce T-cell activation, proliferation and differentiation (Akdis et al., 2011) and IL-2, IL-6 and IL-14 induce proliferation and activation of B cells (Akdis et al., 2011).

Interferons

Interferons are typically divided into three groups: type I, type II and type III IFNs. Type I IFNs are predominantly expressed by innate immune cells (Mogensen, 2019) and consist of 19 cytokines: 12 types of IFN- α , IFN- β , IFN- δ , IFN- ζ , IFN- ϵ , IFN- κ , IFN- ω and IFN- τ (Li et al., 2018b). IFN- α and IFN- β are well characterized, while less is known about the others, in part due to tissue specificity and overlapping functions with other interferons (Negishi et al., 2018).

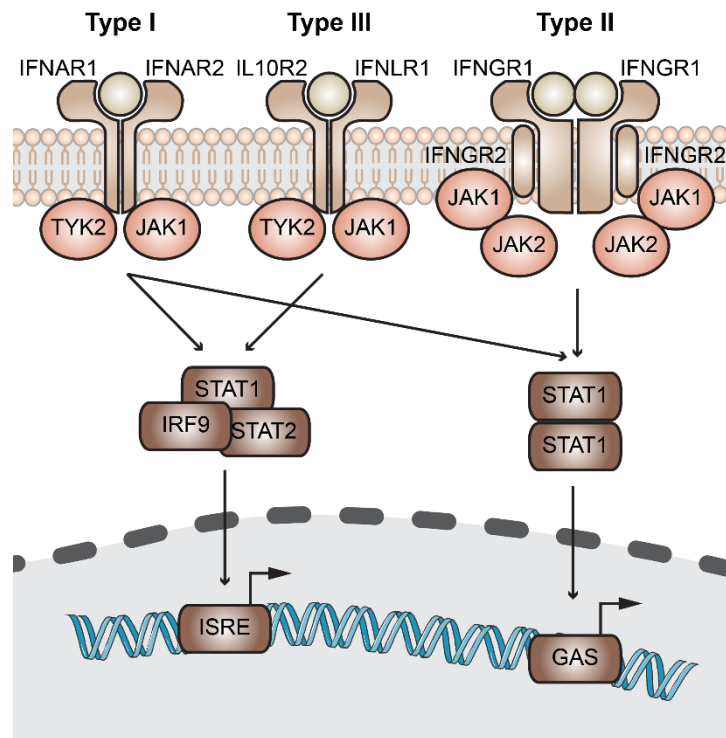


Figure 3: Schematic of IFN signaling pathways. Adapted from (Guo et al., 2013; Negishi et al., 2018)

Type I IFNs bind to a heterodimeric receptor, consisting of the IFNAR1 and IFNAR2 receptor chains. Upon binding Janus-activated kinases (JAKs) TYK2 and JAK1 are recruited to the receptor. TYK2 and JAK1 phosphorylate STAT1 and STAT2. Activated STAT1 and STAT2 then form a complex with IRF9, known as IFN-stimulated gene factor 3 (ISGF3). ISGF3 translocates to the nucleus and binds to the ISRE, thereby initiating transcription of IFNs and ISGs, such as OAS1, IFIT1 and MX1 (Negishi et al., 2018). JAK1 and TYK2 activation also causes the phosphorylation and formation of STAT1 homodimers, which bind to IFN- γ -activated sequence (GAS) and initiate transcription of ISGs such as IRF8, GBP1, IDO1 and CXCR3 (Decker et al., 1997; Negishi et al., 2018) (Fig. 3). Furthermore, type I IFN signaling can induce MAPK activated JNK signaling (Negishi et al., 2018).

Type II IFNs consist of a single IFN, IFN- γ , and is expressed by both innate and adaptive immune cells, most notably, NK cells and T cells (Negishi et al., 2018). IFN- γ differs structurally from the other IFNs and also activates a different cell surface receptor, namely a tetramer of two IFNGR1 and two IFNGR2 receptor chains (Negishi et al., 2018). Upon binding, STAT1 is recruited to the receptor and phosphorylated by JAK1 and JAK2, leading to the formation of STAT1 homodimers. The homodimer then



translocates to the nucleus, where it induces transcription of ISGs via GAS (Decker et al., 1997; Negishi et al., 2018) (Fig. 3).

Type III IFNs consists of four different IFNs, IFN- λ 1, IFN- λ 2, IFN- λ 3 and IFN- λ 4 and are structurally related to type I IFNs and IL-10 (Negishi et al., 2018; Zhou et al., 2020). Similar to type I IFN, type III IFNs bind to a heterodimeric receptor consisting of the IL10R2 and IFNLR1 receptor chains, which in a similar manner to activation of the type I IFN receptor, leads to the activation of ISGF3, followed by the transcription of ISGs and IFNs (Negishi et al., 2018) (Fig. 3).

Evolution of NA sensing PRR signaling pathways

There is a large variety of viruses, with high mutation rates than observed in their hosts (Daugherty and Malik, 2012; Peck and Lauring, 2018). Viral mutations impact drug resistance, vaccination strategies and immune detection (Sanjuán et al., 2010). While the mutations effect the DNA or RNA sequence of a given virus, it does not affect the structure of the nucleic acids. Therefore, one of the main virus-associated PAMPs are viral nucleic acids (NA) (Schlee and Hartmann, 2016). NA sensing PRRs are an integral part of the innate immune system and as such are frequently conserved across species.

Evolutionary conservation of PRR signaling

The first PRR orthologue, termed Toll, was identified in *Drosophila melanogaster*, and is an orthologue of the mammalian TLRs (Akira and Takeda, 2004). The most distant functional orthologues of TLRs were identified in sea anemone and coral (Brennan et al., 2018). For example, a TLR identified in the sea anemone *Nematostella vectensis* is capable of inducing NF- κ B in human cells, upon exposure to bacterial PAMPs (Brennan et al., 2018). The two key domains of TLRs, LRR and TIR, have also been identified in a sponge belonging to the porifera phylum, *Amphimedon queenslandica* (Brennan et al., 2018). Similarly, the most distant cGAS orthologue was identified in sea anemone demonstrates that this PRR was already present over 500 million years ago (Kranzusch et al., 2015).

Interestingly, the TLR7, TLR8 and TLR9 key adaptor MyD88 was identified in the porifera genus *Amphimedon* and downstream signaling effector protein families IRAK and TRAF have been identified in the holozoa genus *Capsaspora*, by which they predate TLR evolution (Gilmore and Wolenski, 2012). NF- κ B activators, IKK- α and IKK-

β appear to have evolved in the same period as TLRs, though their protein complex member NEMO evolved far later and has up until now not been identified in arthropods (Gilmore and Wolenski, 2012).

Another notable example of a family of highly conserved NA sensing PRRs are the RLRs. Orthologues of RIG-I have been found across vertebrates as well as in invertebrates like *C. elegans* and *D. melangoaster* (Paro et al., 2015; Zou et al., 2009). The RLR related *D. melanogaster* DEAD-box RNA helicase Dicer is also a well-known dsRNA binder and antiviral protein, as well as a major player in the RNAi pathway (Deddouche et al., 2008; Paro et al., 2015). The *C. elegans* orthologue DRH1 is also involved in dsRNA binding and RNAi mediated antiviral activity (Paro et al., 2015). Additionally, DRH1 can induce cytokines Upd and VAGO, which in turn induce the JAK/STAT pathway in a manner similar to IFNs (Paro et al., 2015). A closer look at the protein domains identified in RIG-I and its *C. elegans* orthologue DRH1, exemplifies the high degree of conservation of this PRR. Both proteins contain the DEAD box superfamily domain (DExD/H), as well as a helicase domain and a C-terminal domain (CTD) (Fig. 4).

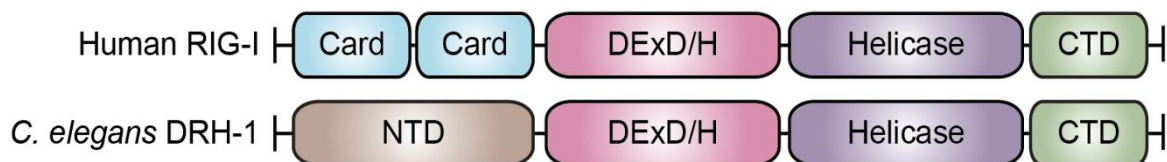


Figure 4: Comparative view of the domains identified in human RIG-I and *C. elegans* orthologue DRH1. Adapted from (Paro et al., 2015).

Another example of a conserved NA sensor is ADAR1. ADAR1 binds dsRNA and catalyzes the C6 deamination of adenosine in RNA, causing a conversion from adenosine to inosine. During translation, inosine is read as guanosine, and in that way the A -> I editing of ADAR1 leads to the translation of altered, and potentially not functional viral proteins (Samuel, 2019; Schlee and Hartmann, 2016). This function of ADAR1 has been documented in worms, flies and mammals (Deng et al., 2020; Reich et al., 2018; Samuel, 2001).

Evolution of PRR induced transcription factors

Similar to the high degree of conservation observed in PRRs and their signaling pathways, transcription factors are also highly conserved. For example, IRFs appear



to have initially evolved in parallel to multicellular animals, as they are found in porifera, but not in holozoa (Nehyba et al., 2009). The number of IRF genes vary from species to species, though no IRF orthologues have been identified in Nematodes (Nehyba et al., 2009). The key transcription factor activating kinases induced via MAPK signaling, ERK, JNK and p38 have also been identified in *Drosophila* and *Caenorhabditis elegans* (Yang et al., 2013).

Orthologues of NF- κ B have been identified in two separate unicellular organisms *Capsaspora owczarzaki* and *Sphaeroforma arctica*, as well as in sea sponges, sea anemone, hydra, coral, insects, fish, amphibians, reptiles and birds (Gilmore and Wolenski, 2012). This indicates that NF- κ B evolved in the clade holozoa, following the divergence between animals and related single-cell organisms and fungi approximately 1000 million years ago (Gilmore and Wolenski, 2012). Similarly, NF- κ B regulator, I κ B has been identified in the holozoa genus *Capsaspora*, indicating it evolved alongside NF- κ B (Gilmore and Wolenski, 2012). Therefore, both NF- κ B and I κ B seem to have evolved at around the same time as signaling proteins IRAK and TRAF, and well before TLRs, IKK α/β and MyD88 (Gilmore and Wolenski, 2012).

Evolution of cytokines

In line with the previously noted age of the NF- κ B signaling complex, a potential orthologue of IL-2 was identified in the marine protozoan, *Euplotes raikovi* (Brockner et al., 2010). The *Euplotes raikovi* pheromone and IL-2 shared structural similarities and the pheromone is capable of binding mammalian IL-2 receptors, while IL-2 can also bind the protozoan pheromone receptor (Brockner et al., 2010). This would make interleukins the oldest part of the immune signaling pathway (Brockner et al., 2010; Gilmore and Wolenski, 2012).

While IFNs are prominent antiviral factors in mammals, they appear to be a relatively young group of cytokines. Due to their identification in most vertebrates, but not in invertebrates, current theory places the origin of IFNs in early vertebrates (Langevin et al., 2013; Secombes and Zou, 2017; Wang and He, 2019). The number of IFN genes varies, even within the same species; fugu and medaka have a single IFN gene, zebrafish has four and Atlantic salmon has 11 (Langevin et al., 2013). Fish IFNs are divided into two families, type I and type II interferons, both with comparable signaling pathways to human type I and type II IFNs (Langevin et al., 2013). Type III IFN, the

third IFN family identified in humans, is believed to have diverged from type I IFNs in early tetrapods (Qi et al., 2010).

IFN inducing PRRs are older than IFNs

The more recent evolution of IFNs allows for an interesting perspective on the PRR pathway evolution. As opposed to TLR based NF- κ B dependent IL induction, where the first identifiable orthologue belongs to the IL, then NF- κ B and finally TLR (Brocker et al., 2010; Gilmore and Wolenski, 2012), IFNs seem to have evolved following the evolution of the cGAS and RLR (Kranzusch et al., 2013; Paro et al., 2015; Qi et al., 2010).

The change in signaling caused by the evolution of IFNs is observable in the protein structure of both RLRs and the cGAS downstream signaling protein STING. For example, the key difference in RIG-I and DRH1 is in the domain responsible for downstream signaling. DRH-1 contains a N-terminal domain (NTD), which is crucial for antiviral RNAi carried out by DRH-1 (Guo et al., 2013). RIG-I contains two CARD domains, which are responsible for the interaction with the adaptor MAVS (Ablasser and Hur, 2020; Guo et al., 2013) (Fig. 4). Similarly, cGAS activation in both human and *N. vectensis* causes STING activation through a cyclic dinucleotide, and while human STING induces the IFN response, sea anemone STING orthologue induces autophagy (Cheng et al., 2020; Kranzusch et al., 2013). In arthropods, STING induces both autophagy and NF- κ B signaling (Cheng et al., 2020), while in fish, STING activation induces both NF- κ B activation and IFN- β production (de Oliveira Mann et al., 2019). In mammals, STING primarily induces IFN- β , though it can still activate NF- κ B (de Oliveira Mann et al., 2019). This gradual shift from signaling via NF- κ B to signaling via IRFs is due to the emergence of the unstructured C-terminal tail of STING (de Oliveira Mann et al., 2019). It is particularly noteworthy, that despite the change of downstream signaling, cGAS itself remains conserved, with *N. vectensis* cGAS able to activate human STING (Kranzusch et al., 2013).

Considering that due to the previously mentioned evolutionary pressure from virus-host coevolution, immune genes evolved disproportionality faster than non-immune related genes (Hurst and Smith, 1999), the high degree of conservation observed for PRR is remarkable and speaks to their relevance (Fig. 5).

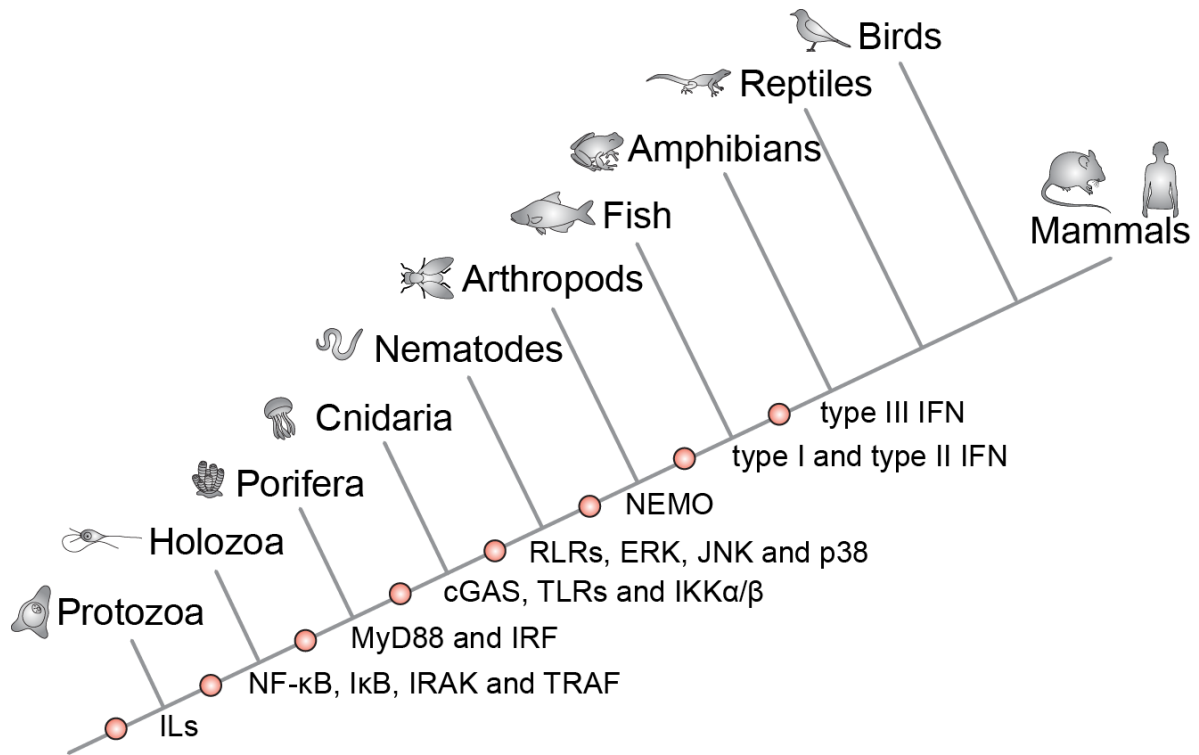


Figure 5: Cladogram indicating the evolution of various elements of the innate immune system.

Identification of PRRs

Identification of NA interacting proteins is of particular interest as it not only allows for a deeper understanding of cellular biology, but in the case of viral NA interactors, also allows for the development of more targeted drugs. Due to the effectiveness of NA PRR sensing pathways in initiating an immune response and the cross-reactivity to the anti-tumor response, NA sensing PRRs are currently under consideration as targets for cancer immunotherapies (Iurescia et al., 2018). For example, stimulation of cancer cells with RLR ligands causes cancer cells to mimic a viral infection. The resulting type I IFN response activates dendritic cells, which migrate to the tumor which may result in the presentation of tumor antigens during the priming of CD8 T cells (Iurescia et al., 2018). Furthermore, identifying novel PRRs could also benefit development of PRR blockers for the treatment of autoimmune disease such as Type I interferonopathies (Rodero and Crow, 2016) and identification of new adjuvant candidates for vaccines (Yong and Luo, 2018).

Different approaches can be utilized to identify NA interactors, depending on the NA of interest and whether a targeted or unbiased approach is desired. While in an unbiased approach (e.g. proteome or genome wide studies), all interactors can be identified, in a targeted approach NA interactions of individual known proteins can be validated. A

classic example of a targeted NA interaction verification experiment is the electrophoretic mobility shift assay (EMSA). There, the protein of interest is recombinantly produced and diluted with the NA. The protein-NA mixture is analyzed via gel electrophoresis, where interaction between protein and NA leads to decreased migration and a visible shift of the NA band compared to NA without protein.

The advantage of an unbiased approach is that the targets do not need to be selected in advance. Rather, they allow for the 'blind' detection of a large amount of interactors. One such method is affinity purification (AP)- mass spectrometry (MS). In the classical AP-MS protocol, the NA in question is coupled to beads, usually through a chemical interaction such as biotin-tagged NA coupled to streptavidin beads. The NA-coupled beads are then incubated with proteins from cellular lysate, followed by a wash to remove non-specifically bound proteins. The thus purified proteins are digested by proteases such as Lys-C and trypsin into peptides, which are then analyzed via MS (Fig. 6). MS peptide spectra are processed and searched against an organism-specific database to identify and quantify proteins that were present in the sample. Further statistical analyses are used to compare bait and control NA and identify relevant NA interactors.



Figure 6: Schematic detailing AP-MS procedure.

Each of the steps involved in preparation of the MS samples has its own potential pitfalls. The crosslinking between the NA and bead could be unsuccessful. The tag introduced to NA could interfere with the binding domain of potential interactors. One of the inherent disadvantages of cell lysis is that proteins that are normally in separate compartments and do not interact can suddenly bind to one another. The stringency of the washing can affect which proteins are identified, while a highly stringent wash reduces background noise, it can also result in the loss of low affinity interactors. In addition, it is not possible to know if the protein identified interacts with the NA directly or is part of a complex. The choice of protease, ionization procedure and MS system



can also influence the results. Finally, in order to exclude non-specific binders each AP-MS experiment needs to be carefully controlled.

Despite these potential pitfalls, AP-MS has several advantages. In addition to being an unbiased detection method, it allows for high throughput preparations and equal handling of samples and controls. Variations of the above noted basic AP-MS procedure have been used to successfully study NA–protein interactions in the past. For example, a recently published study deployed UV crosslinking coupled to oligo(dT) based mRNA isolation followed by MS in Sindbis virus (SINV) infected cells and identified 274 proteins of interest which interacted with the viral NA (Garcia-Moreno et al., 2019). Another recent study used Chikungunya virus particles with 4-thiouridine -labelled genomes to infect cells. Subsequent irradiation of the 4-thiouridine -labelled viral RNA caused crosslinking between viral RNA and interactors, but not between host mRNA and interactors. The viral RNA was then purified and the bound proteins were analyzed via MS, leading to the detection of ~400 viral NA interactors (Kim et al., 2020).

While both of these studies focused on identification of NA interactors involved in the antiviral response, neither study took the high degree of evolutionary conservation into account.

Thesis Aim

Given the high degree of conservation observed for NA sensing PRRs, it stands to reason that cross-species conservation could be used to identify novel NA sensors.

To test this, 11 baits and 6 control NAs, with various chemical and structural components were coupled to beads and incubated with cell lysates from three different species (human, mouse and fly). NA binding proteins were precipitated and analyzed by LC-MS/MS by my predecessor Matthias Habjan (M.H.). After initial statistical analysis of the data, M.H. calculated a score for each bait-control comparison to determine the strength of the NA-protein interaction, intersected the data from human and mouse, and selected 90 candidates for further study (Fig. 7).

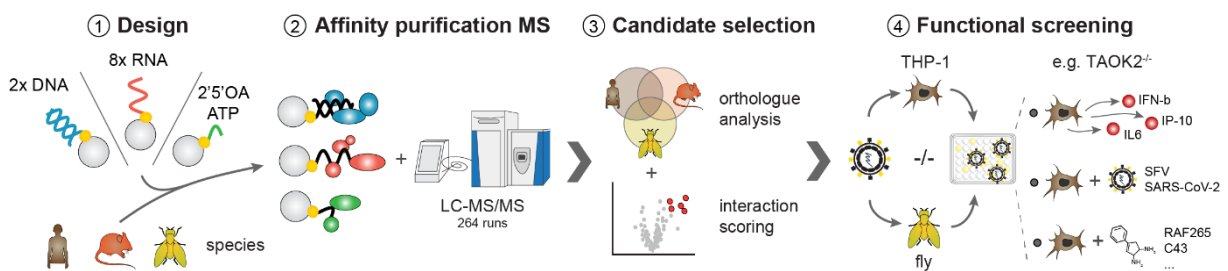


Figure 7: Schematic representation of experimental design and outline. NA baits were coupled to beads and used to precipitate NA interactors from human, mouse and fly cell lysates. The interactors were identified using LC-MS/MS analysis. Candidates were then selected factoring in enrichment and cross species conservation. We conducted a functional screen in human cells, while our collaborators conducted a functional screen in flies to identify relevant immune related proteins. Follow-up studies were conducted on one particular candidate of interest, TAOK2.

The aim of my thesis is to further analyze the NA affinity purification data set in all three species and perform a gene knockout screening on the selected 90 candidates to assess their relevance for viral replication as well as perform follow up experiments for individual interesting candidates (Fig. 7). One of the candidates I will be primarily focusing on is TAOK2. TAOK2 is one of three human TAO kinases, all Ste20p related serine/threonine kinases (Hutchison et al., 1998). TAO kinases are particularly interesting as they are well conserved across vertebrates, which express at least three kinases (Xenopus expresses four and zebrafish six). Invertebrates, like *D. melanogaster* and *C. elegans*, each only express one TAO kinase. Potential orthologues have also been predicted in *N. vectensis* and *A. queenslandica* (Huerta-Cepas et al., 2019). The main characteristic of TAO kinases is the N-terminal serine/threonine kinase domain. The C-terminus is largely unstructured, containing coiled-coil domains and in the case of human and mouse TAOK2, a transmembrane region (Fig. 8A).

One of the key reasons why TAO kinases were selected for follow-up experiments is that they had previously not been linked to a direct antiviral phenotype. In humans, TAOs act as MAP kinase kinase kinases within the MAPK pathway. Signaling via TAO is induced by ATM/ATR upon DNA damage and by a G protein-coupled receptor (GPCR) (Raman et al., 2007). Once activated, the TAOs phosphorylate and activate MEK3/6, which in turn activate p38 (Chen et al., 2003). TAO2 specifically has also been shown to phosphorylate and activate MEK4/7 and thereby inducing JNK signaling (Zihni et al., 2007) (Fig. 8B).

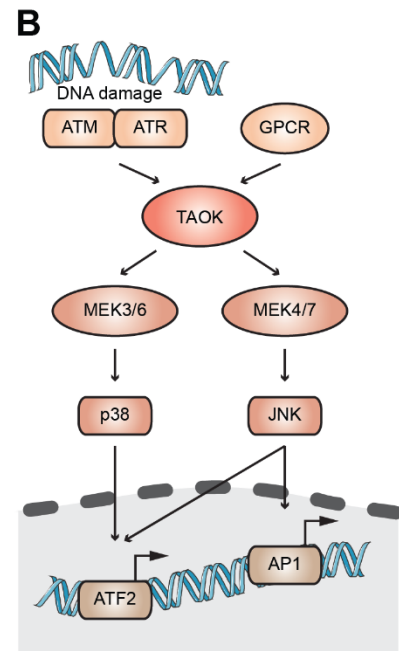
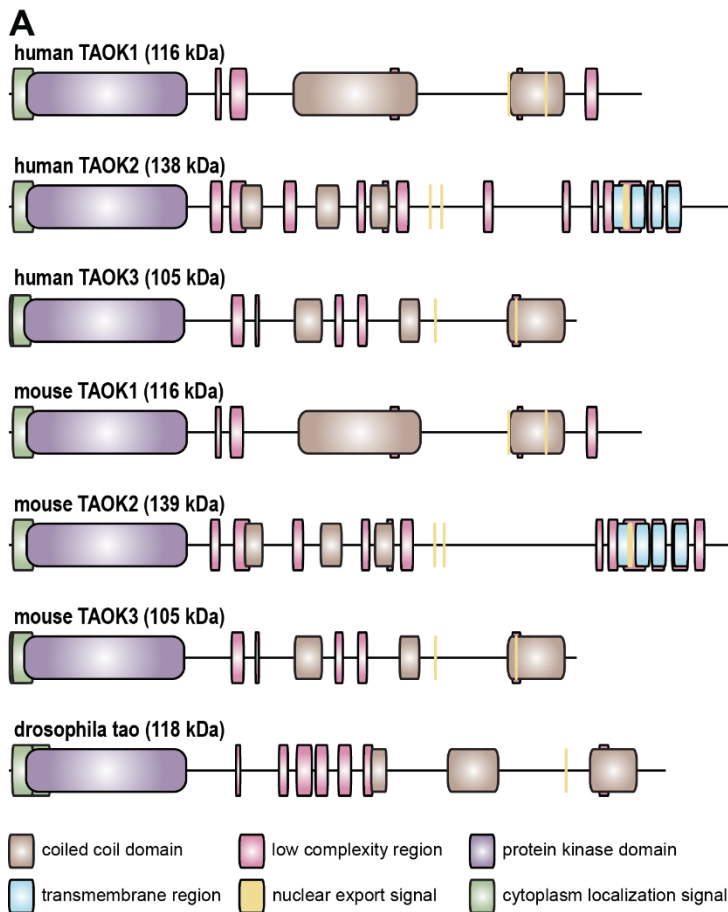


Figure 8: TAO kinase structures and functions. (A) Overview of predicted TAO kinase domains (la Cour et al., 2004; Letunic and Bork, 2018). (B) Schematic of theoretical TAO kinase signaling pathway.

Materials

Devices and instruments

Device or instrument	Manufacturer
Bio-Plex 200 Luminex Technology	BioRad
Bioruptor Plus	Diagenode
ChemiDoc™ XRS+	BioRad
Countess	invitogen
EASY-nanoLC system	Proxeon Biosystems
FastPrep-24	MPBio
Incucyte S3 light microscopy screening platform	Sartorius
Infinite 200 PRO series micro plate reader	Tecan
InGenius3	Syngene
LTQ-Orbitrap XL mass spectrometer	Thermo Fisher Scientific
Mini Trans-Blot® Cell	BioRad
Monolith NT.115	Nanotemper Technologies
PowerPac™ Basic Power Supply	BioRad
Protein electrophoresis chamber	BioRad
Q-Exactive HF mass spectrometer	Thermo Fisher Scientific
QuantStudio3	Thermo Fisher Scientific
T100™ Thermal Cycler	BioRad
Vi-CELL XR Cell Viability Analyzer System	Beckman Coulter

Consumables

Consumable	Manufacturer
10 mL Stripette™ Serological Pipets	Corning
25 mL Stripette™ Serological Pipets	Corning
5 mL Stripette™ Serological Pipets	Corning
50 mL Stripette™ Serological Pipets	Corning
96-well multiscreen filter plates	Millipore
Amersham™ Protran® Western blotting membranes, nitrocellulose 0.22 µm	GE Healthcare
Amersham™ Protran® Western blotting membranes, nitrocellulose, 0.45 µm	GE Healthcare
C18 Empore filter discs	Empore
Cell culture 12-well-plate	Sigma-Aldrich
Cell culture 24-well-plate	Sigma-Aldrich
Cell culture 48-well-plates	Sigma-Aldrich
Cell culture 6-well-plate	Sigma-Aldrich
Cell culture dishes 10cm	Sigma-Aldrich
Cell culture dishes 15cm	Sigma-Aldrich
Countess™ Cell Counting Chamber Slides, 500 slides	Thermo Fisher
Eppendorf Safe-Lock 1,5ml	Fisher Scientific
Eppendorf Safe-Lock 2ml	Fisher Scientific
Falcon 14ml Corning (500)	VWR
Filter tips 10µl	Kisker Biotech



Filter tips 100µl	Kisker Biotech
Filter tips 1000µl	Kisker Biotech
Filter tips 200µl	Kisker Biotech
GE Healthcare Whatman™ 3MM Chr Chromatography Paper X100	Fisher Scientific
3MMCHR 460X570MM	
Glaskugeln, 5 ± 0,3 mm	Carl Roth
Lysing Matrix D	MPBio
Microplate 384 Well Flat bottom White	Greiner
Nunc™ 96-MicroWell™ plate, flat bottomed wells	Fisher Scientific
Nunc™ Cryogenic Tubes (pack 1800)	Fisher Scientific
Petri dishes Greiner (480)	VWR
Polyester films for ELISA	VWR
Reagent Reservoirs (200ST)	VWR
Reprosil-Pur 120 C18-AQ, 1.8 µM, 200 x 0.075 mm	Dr. Maisch
Reprosil-Pur 120 C18-AQ, 3 µM, 150 x 0.075 mm	Dr. Maisch
ReproSil-Pur C18-AQ 1.9 µm silica beads	Dr. Maisch
Stripette-Pipettes 5ml	Omnilab
Tips BRAND 10 grey (10.000)	neoLab
Tips BRAND 1000 blue (5.000)	neoLab
Tips BRAND 200 yellow (10.000)	neoLab

Chemicals and reagents

Chemical or reagent	Manufacturer
2'5'OAs	Rune Hartmann
2-chloroacetamide, CAA	Sigma-Aldrich
2-Propanol AnalaR normapur acs/reag.pe/reag.usp kst.-flasche 2,5l	VWR
30% Acrylamide/Bis Solution, 29:1	Bio-Rad
5x GC Buffer	Thermo Fisher Scientific
5x Rapid Ligation	NEB
6X DNA Loading Dye	Thermo Fisher Scientific
Acetic Acid 100%	Merck
Acetic Acid 96%	AppliChem
Acetonitril	VWR
Agarose, BioReagent, for molecular biology, low EEO, 500g	Sigma-Aldrich
Ammonium Persulfate	BioRad
Ammonium Persulfate	Sigma-Aldrich
Ammonium Persulfate	GE Healthcare
Ampicillin sodium crystalline	Sigma-Aldrich
ATP disodium salt	Sigma-Aldrich
Biotin-16-UTP, 30 µl (10 mM)	Jena Bioscience
biotin-N-hydroxysuccinimide ester	Epicentre
Blasticidin S-Hydrochloride	Sigma-Aldrich
Bovine Serum Albumin, heat shock fraction, pH 7, ≥98%, 500g	Sigma-Aldrich
Bromophenol Blue	Sigma-Aldrich
Calciumchlorid Dihydrat, ACS reagent ≥99%	Sigma-Aldrich

Carboxymethylcellulose (CMC) Sodium Salt 1 * 250 g	Sigma-Aldrich
Chloramphenicol	Roth
Coelenterazine	Sigma-Aldrich
Coenzyme A trilithium salt	Sigma-Aldrich
cOmplete™, EDTA-free Protease Inhibitor Cocktail, Roche (3 x 20 tabLets)	Sigma-Aldrich
Coomassie brilliant blue	Thermo Fisher Scientific
Copper(II) sulphate pentahydrate ≥98%, 1kg	VWR
Crystal violet 25g	Carl Roth GmbH
Dabrafenib	Cayman Chemical
Digestion Buffer 3.1	NEB
D-Luciferin sodium salt	Sigma-Aldrich
DMEM	Sigma-Aldrich
dNTPs	Thermo Fisher Scientific
DPBS	Sigma-Aldrich
DTT	Sigma-Aldrich
Ethanol 99.8 % denatured with IPA, MEK and Bitrex pure, 10 L	OmniLab
Ethylene glycol-bis(2-aminoethylether)-N,N,N',N'-tetraacetic acid (EGTA)	Sigma-Aldrich
Ethylenediamine tetraacetic acid (EDTA)	Sigma-Aldrich
FastAP	Fermentas
fetal bovine serum	Sigma-Aldrich
Formaldehyd 35 %	VWR
Formic Acid	Sigma-Aldrich
GelRed™ Nucleic Acid Stain, 10.000x in water - 500 ul	Biotium
GeneRuler 1 kb DNA Ladder	Thermo Fisher Scientific
GeneRuler 100 bp Plus DNA Ladder (5x50µg)	Thermo Fisher Scientific
Glycerin 86 %	Roth
Glycerol 87%	Sigma-Aldrich
Glycine (6X1KG)	Sigma-Aldrich
Guanidine Hydrochloride	Sigma-Aldrich
Hydrochloric acid 1N	VWR
Hydrochloric acid 5N	VWR
Hydrogen Peroxyde H2O2, 100ml	Sigma-Aldrich
IFN-α B/D	Peter Stäheli
IGEPAL CA-630 (NP-40)	Sigma-Aldrich
iodoacetamide	Sigma-Aldrich
Kaliumacetat (Potassium acetate)	Fluka
Kanamycin	Sigma-Aldrich
LB Agar (Lennox L Agar)	invitrogen
LB Broth Base	invitrogen
LysC	WAKO Chemicals USA
Magnesium chloride, anhydrous, ≥98%	Sigma-Aldrich
Magnesium Sulfate Heptahydrate	Fluka
Manganese Chloride	Sigma-Aldrich
Metafectene Pro	Biontex



Methanol ≥99.9%, EMSURE® ACS, ISO, Reag. Ph. Eur. for analysis, Supelco®	VWR
Methanol, 99.9%, for spectroscopy, ACROS Organics™	Thermo Fisher Scientific
MOPS (3-(N-morpholino)propanesulfonic acid)	Fluka
Opti-MEM I Reduced-Serum Medium (100ml), Gibco™ 31985062	Thermo Fisher Scientific
PageRuler™ Prestained Protein Ladder, 10 to 180 kDa (10 x 250µL)	Thermo Fisher Scientific
Passive Lysis 5X Buffer	Promega
Penicillin-Streptomycin (100ml)	Sigma-Aldrich
PMA	Sigma-Aldrich
poly(A)	Sigma-Aldrich
Poly(I:C) (HMW), fluorescent	InvivoGen
Polycytidylic acid–Agarose	Sigma-Aldrich
Polyethylenimine (PEI)	Polysciences
Polyinosinic acid potassium salt (Poly I)	Sigma-Aldrich
Polyinosinic–polycytidylic acid potassium salt	Sigma-Aldrich
Polyuridylic acid–Agarose	Sigma-Aldrich
Potassium Bromide	VWR
Potassium chloride (KCl), 1kg	Carl Roth GmbH
Potassium Phosphate Monobasic	Sigma-Aldrich
Puromycin dihydrochloride, cell culture	Sigma-Aldrich
RAF265	Cayman Chemical
resazurin	Sigma-Aldrich
RNase inhibitor	Fermentas
RNaseZAP	Sigma-Aldrich
RPMI 1640	Sigma-Aldrich
Rubidium chloride, 99% (metals basis), 25 g (Alfa Aesar)	VWR
SDS Pellets 1kg	Carl Roth GmbH
Skim Milk Powder	Sigma-Aldrich
Sodium acetate trihydrate	Sigma-Aldrich
Sodium Chloride (NaCl), ACS	Sigma-Aldrich
Sodium-phosphat dibasisch Dihydrat	Sigma-Aldrich
Sorafenib 10mg	BIOZOL
Strep-Tactin® Sepharose® resin	IBA Life Sciences
Swine MBP Protein 1mg	BIOZOL
T4 DNA Ligase Buffer (10X)	Thermo Fisher Scientific
TCEP HCl (Tris(2-carboxyethyl)phosphin Hydrochlorid) (C ₉ H ₁₆ ClO ₆ P)	Sigma-Aldrich
TE buffer	Qiagen
TEMED 50ml	Sigma-Aldrich
Thiourea	Amersham
Tricine	Sigma-Aldrich
Tris	Roth
Trizma® base	Sigma-Aldrich
Trypsin	Promega
Trypsin 0.25%, 100mL	Sigma-Aldrich
Tween 20	Sigma-Aldrich

UltraPure™ DNase/RNase-Free Distilled Water (10 x 500 mL)

Urea

Urea

Urea

Thermo Fisher
Scientific

Fluka

ICN Biomed

Qiagen

Homemade buffers

Buffer	Recipe
10x Electrophoresis Running Buffer	250 mM Trizma base 1.92 M Glycine 1% SDS
10x PBS	1.4 M NaCl 27 mM KCl 17 mM KH ₂ PO ₄ 100 mM Na ₂ HPO ₄ 2H ₂ O
10x Wet-Blotting Transfer Buffer	250 mM Trizma base 1.5 M Glycine pH adjusted to 8.3
1x Resolving/separating Gel Buffer	1.5 M Trizma base 0.4% SDS pH adjusted to 8.8
1x SDS buffer	62.5 mM Tris HCl pH 6.8 2% SDS 10% glycerol 50 mM DTT 0.01% Bromophenol Blue
1x Stacking Gel Buffer	1 M Trizma base 0.8% SDS pH adjusted to 6.8
1x Transfer Buffer	10% 10x Wet-Blotting Transfer Buffer 10% Methanol
5x Lämmli buffer	10% SDS 250mM Tris HCl, pH 6.8 100mM DTT 50% glycerol 0.1% Bromophenol Blue
ammonium bicarbonate buffer	50mM ammonium bi-carbonate (NH ₄ HCO ₃) pH 8
buffer A	0.1% formic acid
buffer B	80% acetonitrile 0.1% formic acid
Coomassie staining solution	0.1% Coomassie Brilliant Blue 30% Methanol 10% HAc
Destaining solution	40% Methanol 10% HAc



firefly substrate	20 mM Tricine 3.74 mM MgSO ₄ 33.3 mM DTT 0.1 mM EDTA 270 μM Coenzyme A trilithium salt 470 μM D-Luciferin sodium salt 530 μM ATP disodium salt pH adjusted to 7.8-8
FP lysis buffer	6 M GdmCl 10 mM TCEP 40 mM CAA 100 mM Tris HCl pH 8
Gaussia Luciferase buffer	20 mM MOPS 75 mM KBr 1 mM EDTA 5 mM MgCl ₂ pH adjusted to 7.8
LB	25% w/v LB broth base
LB-agarose	15% w/v LB agar
PBST	10% 10x PBS 0.25% Tween20
Storage Buffer	20 mM Tris 200 mM NaCl 10 % Glycerin 0.2 mM EGTA 1 mM TCEP pH 8
TAE	600 mM Sodium acetate trihydrate 120 mM Tris 38 mM EDTA
TAP buffer	50 mM Tris pH 7.5 100 mM NaCl 5% (v/v) glycerol 0.2 % (v/v) Nonidet-P40 1.5 mM MgCl ₂ protease inhibitor cocktail (cOmplete)
TB1	100mM RbCl 50mM MnCl ₂ 30mM Ka-Acetate 10mM CaCl ₂ 0,15% Glycerol Adjust pH to 5,8 with acetic acid
TB2	75 mM CaCl ₂ 10mM RbCl 10mM MOPS 15% Glycerol

Commerical kits

Kit	Manufacturer
ADP-Glo(TM) Kinase Assay, 1000 Assays	Promega
Bio-Plex Pro Human Cytokine 17-plex	Bio-Rad
Dual-Luciferase® Reporter Assay System, 10-Pack	Promega
human IFN- β DuoSet ELISA	R&D Systems
human IP-10 OptEIA ELISA Set	BD Biosciences
m7G Capping System	CellScript
NucleoBond™ AX 100 Columns	Macherey-Nagel
Nucleobond™ PC 500 (100)	Macherey-Nagel
NucleoSpin® Gel and PCR Clean-up	Macherey-Nagel
NucleoSpin® Plasmid (NoLid) (250)	Macherey-Nagel
NucleoSpin® RNA Plus (250)	Macherey-Nagel
QIAEX II Gel Extraction Kit (150)	Qiagen
SP6 RiboMAX™ Large Scale RNA Production Systems	Promega
SuperSignal™ West Femto, 200ml	Thermo Fisher Scientific
T7 RiboMAX™ Large Scale RNA Production Systems	Promega
Western Lightning Plus-ECL, Enhanced Chemiluminescence Substrate (340 mL)	Perkin-Elmer

Enzymes

Enzyme	Manufacturer
BP clonase® II	Invitrogen
BsmBI	NEB
DpNI	NEB
HincII	NEB
LR clonase® II	Invitrogen
pfu polymerase	Promega
Phusion Hot Start II DNA Polymerase (2 U/ μ L)	Thermo Fisher
Proteinase K	NEB
RecA recombinase	NEB
T4 DNA Ligase	Thermo Fisher

Oligonucleotides

Cloning and sequencing oligonucleotides

Oligonucleotides were purchased at Eurofins Genomics, Ebersberg, Germany.

Primer Name	Target	Sequence(5'->3')
TAOK2 midseq rat	rat TAOK2 sequencing	GAATGAATCCCCTGCTCTC



TAOK2 rat midseq2	rat TAOK2 sequencing	GCACAGTGGGCGGTTGCA
attB TAOK1 fw	gateway cloning human TAOK1	GGGG ACA AGT TTG TAC AAA AAA GCA GGC TCCCCTCCTCC
attB TAOK1 rev	gateway cloning human TAOK1	GGGG AC CAC TTT GTA CAA GAA AGC TGG GTN CTA TTTTTTTTTTTTTTTTGTG
attB TAOK2 fw	gateway cloning human TAOK2	GGGG ACA AGT TTG TAC AAA AAA GCA GGC TCTCCATCTTGAATTGGG
attB TAOK2 rev	gateway cloning human TAOK2	GGGG AC CAC TTT GTA CAA GAA AGC TGG GTN CTA TTTTTTTTTTTCCAAAGGCACA
attB TAOK3 fw	gateway cloning human TAOK3	GGGG ACA AGT TTG TAC AAA AAA GCA GGC GTGCTCGGCG
attB TAOK3 rev	gateway cloning human TAOK3	GGGG AC CAC TTT GTA CAA GAA AGC TGG GTN CTA TTTTTTTTTTTTTTTTTGTGAT
pC1_NHis6_TAOK2_fw	SLIC cloning TAOK2	AAGTTCTGTTCCAGGGGCCCATGCCAGC TGGGGGC
pC1_NHis6_TAOK2_rev	SLIC cloning TAOK2	CCCCAGAACATCAGGTTAATGGCGCTAC CTCCAGGGGGGC
pC36_CHis_TAOK2_fw	SLIC cloning TAOK2	GAGCGGATAACAATCCCCTCTAGAGAA GGAGATATACCATGCCAGCTGGGGGC
pC36_CHis_TAOK2_rev	SLIC cloning TAOK2	GTGGTGATGATGATGATGCTCCCTCCAG GGGGGCAG
pC1_NHis6_RN_TAOK2_fw	SLIC cloning rat TAOK2	AAGTTCTGTTCCAGGGGCCCATGGAGCA GAAGCTGATCAGCG
pC1_NHis6_RN_TAOK2_rev	SLIC cloning rat TAOK2 1-993 truncated	CCCCAGAACATCAGGTTAATGGCGTTAG GCCAGCAGTGCTGC
p36_CHis_RN_TAOK2_fw	SLIC cloning rat TAOK2	GAGCGGATAACAATCCCCTCTAGAGAA GGAGATATACCATGGAGCAGAAGCTGAT CAGCG
p36_CHis_RN_TAOK2_rev	SLIC cloning rat TAOK2 1-993 truncated	GTGGTGATGATGATGATGCTCGGCCAGC AGTGCTGC
attB_RN_TAOK2_fw	gateway cloning rat TAOK2	GGGG ACA AGT TTG TAC AAA AAA GCA GGC TTC ATGGAGCAGAAGCTGATCA
attB_RN_TAOK2_rev	gateway cloning rat TAOK2 1-993 truncated, no stop	GGGG AC CAC TTT GTA CAA GAA AGC TGG GTC GGCCAGCAGTGCTGC
attB_RN_TAOK2_stop_rev	gateway cloning rat TAOK2 1-993 truncated, with stop	GGGG AC CAC TTT GTA CAA GAA AGC TGG GTC TTAGGCCAGCAGTGCTG
pC1_NHis6_RN451_TAOK2_rev	SLIC cloning rat TAOK2 1-451 truncated	CCCCAGAACATCAGGTTAATGGCGTCAG GTGGAGGTGGGAGG
p36_CHis_RN451_TAOK2_rev	SLIC cloning rat TAOK2 1-451 truncated	GTGGTGATGATGATGATGCTCGGTGGAG GTGGGAGGG
attB_RN451TAOK2_rev	gateway cloning rat TAOK2 1-451 truncated, no stop	GGGG AC CAC TTT GTA CAA GAA AGC TGG GTC GGTGGAGGTGGGAGGG
attB_RN451TAOK2_stop_rev	gateway cloning rat TAOK2 1-451 truncated, with stop	GGGG AC CAC TTT GTA CAA GAA AGC TGG GTC TCAGGTGGAGGTGGGAG
taok2_151A_fw	rat TAOK2 mutate D151A	CAACATGATCCATAGAGCTGTGAAGGCT GGGAACA

taok2_151A_rev	rat TAOK2 mutate D151A	TGTTCCCAGCCTTCACAGCTCTATGGATC ATGTTG
RatTAOK2_21_46C>T_fw	point mutation in rat TAOK2	CAGGCTGTCCAGTGCACACGTGCTG
RatTAOK2_21_46C>T_rev	point mutation in rat TAOK2	CAGCACGTGTGCACTGGACAGCCTG
attB eGFP FW	GW cloning eGFP, N-tag able	GGG GAC AAG TTT GTA CAA AAA AGC AGG CTC CAT GGT GAG CAA GGG CGA GGG GAC CAC TTT GTA CAA GAA AGC TGG GTC CTT GTA CAG CTC GTC CAT GC
attB eGFP no_stop REV	GW cloning eGFP, C-tag able	GGG GAC CAC TTT GTA CAA GAA AGC TGG GTC TTA CTT GTA CAG CTC GAG CAT CAT CAT CAT CAC CAC GGT ATA TCT CCT TCT CTA GAG GGG AAT TGT TAT CCG CTC
attB eGFP stop REV	GW cloning eGFP, stop codon	AA GTT CTG TTC CAG GGG CCC
SLICLP2His10	SLIC linerization	GGGCCCCTGGAACAGAACTTCCAG
SLICLP1tagless	SLIC linerization	CGCCATTAACCTGATGTTCTGGGG
SLICGOIHis6 LP1	SLIC linerization	AGCGCTTGGAGCCACCCGCAG
PreScission LP2 ccdB	SLIC linerization	
LP2 StrepOne	SLIC linerization	

sgRNA oligonucleotides

sgRNA sequences were selected using the GPP sgRNA designer (Doench et al., 2016) in the lab of our collaborator Giulio Superti-Furga.

Construct Name	Insert
ABCF1_gRNA1	CACCGGCAACACATCAATGTTGGGA
ABCF1_gRNA2	CACCGTAAGCCAGATGACAGCGTTG
ABCF1_gRNA3	CACCGTGTAATTGCCCTATAGTAG
ABCF3_gRNA1	CACCGCAGCGGCTAGATGGTTACCG
ABCF3_gRNA2	CACCGTGCGAGAGGATTTGCTACGG
ABCF3_gRNA3	CACCGGCAGAGTGTTGTACATGCGC
ADAR_gRNA1	CACCGTTCTTGTAGGGTGAACACCG
ADAR_gRNA2	CACCGAGGCAATCAACACCTCTCTG
ADAR_gRNA3	CACCGTTGAGTGATGCACAAATTG
ADARB1_gRNA1	CACCGGGTGAATACATGAGTGATCG
ADARB1_gRNA2	CACCGTCAGGTCACCAAACCTTACCC
ADARB1_gRNA3	CACCGTTGGAGCCCACGTAAAAGGG
ANGEL2_gRNA1	CACCGGCAGAGACTGGACTACACCG
ANGEL2_gRNA2	CACCGCTGTTGTATAATCCAAGGCG
ANGEL2_gRNA3	CACCGGCCGGCGGCCAGTATTACAC
APEX1_gRNA1	CACCGTTTCATTTCTATAGGCGATG
APEX1_gRNA2	CACCGCCAAGAGCAGATCTTGAGTG
APEX1_gRNA3	CACCGACAGCATATGTACCTAATGC
APTX_gRNA1	CACCGAATTACGACTGAGTCAATGC
APTX_gRNA2	CACCGTCCACGGTAAGACCAGCCAA
APTX_gRNA3	CACCGAAGAAATGTTCTCGACAGCA



AQR_gRNA1 CACCGAGGTCCAAAAAACTTGACCA
AQR_gRNA2 CACCGACATCATGCTTACGAAGACC
AQR_gRNA3 CACCGACGATTGCAAAAGAGTCTAG
ASCC1_gRNA1 CACCGTCCACCTCGTAGGCATCACA
ASCC1_gRNA2 CACCGGTGTAATTTTCAGCCCGAACA
ASCC1_gRNA3 CACCGAGTACTGGCGAAGTGCTCCA
BANF1_gRNA1 CACCGAGTCCTGGGCAAGAAGCTGG
BANF1_gRNA2 CACCGGGACTTCACCAATCCCAGCC
BANF1_gRNA3 CACCGGCCCATGGGGGAGAAGCCAG
C8orf88_gRNA1 CACCGGTTTAACAGTGTAAGACGAA
C8orf88_gRNA2 CACCGTACAATCTATTACTCACCTG
C8orf88_gRNA3 CACCGTGTATGCACTGAGTGTTGCA
CAPRIN1_gRNA1 CACCGGGGTGATCGACAAGAACTT
CAPRIN1_gRNA2 CACCGTTTGGTATCATCCACAAGTG
CAPRIN1_gRNA3 CACCGAGTGCCAATATTGTCCGAAG
CDKN2AIP_gRNA1 CACCGCAGTTCAACGTGTATAGGGT
CDKN2AIP_gRNA2 CACCGAGAGGGATATCGAGTAGCAA
CDKN2AIP_gRNA3 CACCGGGCAGCTTCATCCGTGCTAG
CHAF1A_gRNA1 CACCGGAAAGCGGTCCGACGCCGAG
CHAF1A_gRNA2 CACCGCCAAGAGGGCCTCTAAATCG
CHAF1A_gRNA3 CACCGAGGGCGACGGTGTTCGCGAG
CHAF1B_gRNA1 CACCGTTATGTCCAAGGAGTAACCT
CHAF1B_gRNA2 CACCGATTGGACAAAAATTCCACGA
CHAF1B_gRNA3 CACCGAGATGTGTATGATATTTGCT
CMTR1_gRNA1 CACCGATATTAACCTCAATCAGCTG
CMTR1_gRNA2 CACCGAAATCCGCGGGACTCTTATG
CMTR1_gRNA3 CACCGTCGACAGGCAGAGATACGGA
CMTR2_gRNA1 CACCGCCAATGACAAGGAAACCGAT
CMTR2_gRNA2 CACCGAGGAAACTCCGAAGTCTATG
CMTR2_gRNA3 CACCGCTGAACTTTGTAICTCAAGCA
CSDE1_gRNA1 CACCGTTGAAGTATCATCGGACCGA
CSDE1_gRNA2 CACCGGATGTCAGACTATTGCCTCA
CSDE1_gRNA3 CACCGTGTATGCTACGAACGTAATG
DDX1_gRNA1 CACCGTGAGAGCTTTCGGAGCATTG
DDX1_gRNA2 CACCGACACTTACCTAGGTCCAAAG
DDX1_gRNA3 CACCGCAGATGAACCCATATGACAG
DDX20_gRNA1 CACCGAAGCAGCAGTGACTCGAAGT
DDX20_gRNA2 CACCGTTCAAGCTAAATCTGGCACC
DDX20_gRNA3 CACCGTTCAATTCAAGACTTCTCGT
DDX41_gRNA1 CACCGATGCTCAGAACATAACGGGG
DDX41_gRNA2 CACCGAGCCTGTGACCATCAATGTG
DDX41_gRNA3 CACCGGCTGACCGCATGATCGACAT
DDX42_gRNA1 CACCGCCTGATCGACCCTATTTCGAG
DDX42_gRNA2 CACCGAGTGATTGTGTGTCCTACCA
DDX42_gRNA3 CACCGGCGGCCAATCCTATGCGTGT
DEK_gRNA1 CACCGTCTAGAAAAGAGTCTCATCG
DEK_gRNA2 CACCGCATGTAAAGAGCATCTGTG

DEK_gRNA3	CACCGAAGAATGTGGGTCAGTTCAG
DHX36_gRNA1	CACCGTGTCCAATGATACATATACC
DHX36_gRNA2	CACCGTGTGGTACGCGAAAAACAG
DHX36_gRNA3	CACCGAATGAACTGAGTAACTTGAG
DHX58_gRNA1	CACCGCGGGTGAAGATGATACCCCG
DHX58_gRNA2	CACCGTCTGTGCCAACTTGGACACG
DHX58_gRNA3	CACCGGACCGTGACAACCCTGAGTG
DHX9_gRNA1	CACCGCAAACATTATACTGGCATG
DHX9_gRNA2	CACCGTCAATCACAGCATCCAAAGG
DHX9_gRNA3	CACCGGGAGATTTACCAACAACCAT
DTYMK_gRNA1	CACCGATGCGTATCTGTCCACGACG
DTYMK_gRNA2	CACCGGGAACCGGAGCAGTTCGGCG
DTYMK_gRNA3	CACCGAAGTGACGTGGAGGATCACT
EEA1_gRNA1	CACCGACTAACCAAGTCTAATATAG
EEA1_gRNA2	CACCGTGTAACACTGCTCAGACAAG
EEA1_gRNA3	CACCGACGGCAACATCTTCTATACC
EIF2S1_gRNA1	CACCGGATGACAAGTACAAGAGACC
EIF2S1_gRNA2	CACCGTAATAGGCGCTTGACCCAC
EIF2S1_gRNA3	CACCGGTGTGTGGTTGTCATTAGGG
EIF2S3_gRNA1	CACCGTATCACTTACCAATAAGCCG
EIF2S3_gRNA2	CACCGTTGGTCCCTGGAATGTCCGT
EIF2S3_gRNA3	CACCGTCTTACCTTGGACAAATGCA
ELAVL1_gRNA1	CACCGTATCCGGTTTGACAAACGGT
ELAVL1_gRNA2	CACCGTTGGGCGGATCATCAACTCG
ELAVL1_gRNA3	CACCGTGTGAACTACGTGACCGCGA
ERI3_gRNA1	CACCGAATCTGTGGCTTGTGCGCAG
ERI3_gRNA2	CACCGGCTTACCCATTCTGTACAG
ERI3_gRNA3	CACCGCGGCTTTGGCGCATCCATGG
EXOSC2_gRNA1	CACCGCGTAGTGGGACGAATCACAG
EXOSC2_gRNA2	CACCGCGACACTAAGAAACATCTAG
EXOSC2_gRNA3	CACCGAAGCGCAGGATACACTGATA
EXOSC4_gRNA1	CACCGACTATATTGACAGTTCACTA
EXOSC4_gRNA2	CACCGGCGCAAGCGACGGCCACATG
EXOSC4_gRNA3	CACCGGGCTCGGCCTACATTGAGCA
FAM98B_gRNA1	CACCGGTTTTATTAACATTCGTCGG
FAM98B_gRNA2	CACCGAGAGCAAGCCCTTACAAAGG
FAM98B_gRNA3	CACCGACCCAAGACAACGATTACAA
IFI27_gRNA1	CACCGACAACACTGTAGCAATCCTGGC
IFI27_gRNA2	CACCGTGTGGCCAAAGTGGTCAGGG
IFI27_gRNA3	CACCGATTGCTACAGTTGTGATTGG
ILF2_gRNA1	CACCGAATTGAAGAAGTTCGACAGG
ILF2_gRNA2	CACCGACTAGTAGGTCAAGGATCCA
ILF2_gRNA3	CACCGAAACAGGCACACTCACACGT
ILF3_gRNA1	CACCGCGTCCCTCCGACACGCCAAG
ILF3_gRNA2	CACCGAAAGGGCCTCCTACTCAAGG
ILF3_gRNA3	CACCGTACGCCCATGAAACGCCCAA
ISY1_gRNA1	CACCGGAGGTCCGGATAAAGGAGCT



ISY1_gRNA2	CACCGTCAAACAGCTCTCTAACACC
ISY1_gRNA3	CACCGGACACGTGCTGAGCTCATGA
KHDRBS1_gRNA1	CACCGACGGCGTCTGACGCACCGAG
KHDRBS1_gRNA2	CACCGAGAGCATAAGCCTCACATGG
KHDRBS1_gRNA3	CACCGTTCAGGTACTCCATTCAAGT
KIF2A_gRNA1	CACCGGTTTACTGCTAGACCACTAG
KIF2A_gRNA2	CACCGGTGTTGTGAACAGATTGACC
KIF2A_gRNA3	CACCGGTACTGAAACTCATTGACAT
LARP1_gRNA1	CACCGTAGTGAATACTACTTCAGCG
LARP1_gRNA2	CACCGAACCTAAAGACACTACCCAA
LARP1_gRNA3	CACCGTGTGAATAATCCACTATTGG
LRRC59_gRNA1	CACCGCGGCGGCTGGAAGTAGAACG
LRRC59_gRNA2	CACCGGGATCCTAGTCGGATTTCTG
LRRC59_gRNA3	CACCGGAGCCTCAGCGACCTGAATG
MAVS_gRNA1	CACCGAGTACTTCATTGCGGCACTG
MAVS_gRNA2	CACCGACTGGAGCAGATGATAGGCT
MAVS_gRNA3	CACCGGTGTCTTCCAGGATCGACTG
MKRN2_gRNA1	CACCGTGTTTAGATATGACCACACG
MKRN2_gRNA2	CACCGAAAATAACTCACATGAACC
MKRN2_gRNA3	CACCGTTGACGTTCGAACACGAGA
MNDA_gRNA1	CACCGTGATGTGGAAGACTTTCACA
MNDA_gRNA2	CACCGAAACTGACATCGGAAGCAAG
MNDA_gRNA3	CACCGCCAAAACGACCCAGTGACAG
MOV10_gRNA1	CACCGAGCCGCCCTCAGTGCTACG
MOV10_gRNA2	CACCGAGCTGGTCTTACAATGGACA
MOV10_gRNA3	CACCGCCTGGATTTGAACCGCAAAG
MSI2_gRNA1	CACCGACCTTGGGTTGCGCTCGACG
MSI2_gRNA2	CACCGACGCGTTCATGCTTGGCATG
MSI2_gRNA3	CACCGTTACCTGGAGCGTTTCGTAG
N4BP2_gRNA1	CACCGAGAAAGAAGACATCTTACGT
N4BP2_gRNA2	CACCGTTGAAGTTGAACCCTTCGGA
N4BP2_gRNA3	CACCGTTGATAAGACTATTGGTCAG
neg_control1	CACCGAACCGGATCGCCACGCGTCC
neg_control10	CACCGAACATCGTTTACGTCTAGA
neg_control11	CACCGAGCTTGACAATGCACACTAC
neg_control12	CACCGCTTCCTAGCCATAGCCGCGT
neg_control2	CACCGTCCGGAGCTTCTCCAGTCAA
neg_control3	CACCGTGCAAAGTTCAGGGTAATGG
neg_control4	CACCGACCGGAAACGATGAGTGGGG
neg_control5	CACCGTCCACTAGAATTCCGTGGCC
neg_control6	CACCGCGTTGTACGGGGGCCTTGTG
neg_control7	CACCGAATAACGCGTAACTCCCACC
neg_control8	CACCGAAGCGGTGGGTGTCGATAAT
neg_control9	CACCGCTGGCCCGACGAGAATGAGC
NTPCR_gRNA1	CACCGATGCCGAGTTGGGCAGTATG
NTPCR_gRNA2	CACCGTATACCGAAGAAGTCAGACA
NTPCR_gRNA3	CACCGGTACTCACATTCCCTCAAGAC

NUDT16_gRNA1	CACCGGCGTGTCCACGAATCCGCCG
NUDT16_gRNA2	CACCGGGTAGTCAGTGCCTCCACG
NUDT16_gRNA3	CACCGTGCCAAGCGTCTGACGCTCG
NUMB_gRNA1	CACCGGGCCACCTTACCCGAACATG
NUMB_gRNA2	CACCGGATGACCAAACCAGTGACAG
NUMB_gRNA3	CACCGATCCTCATGCCATCCCACGC
PARP1_gRNA1	CACCGCGATGCCTATTACTGCACTG
PARP1_gRNA2	CACCGTACCGATCACCGTACCCACA
PARP1_gRNA3	CACCGAGCTAGGCATGATTGACCGC
PARP12_gRNA1	CACCGACCTGGCCTACTGTACACCG
PARP12_gRNA2	CACCGCTTGGATAGAGGCAAATGGG
PARP12_gRNA3	CACCGATAGCTCATTATAGCTCAGG
PARP2_gRNA1	CACCGCATGCAATGAATTCTACACC
PARP2_gRNA2	CACCGAATACCAAGAAAGCCCCACT
PARP2_gRNA3	CACCGGGGGGCGCAAGGCACAATGT
PATL1_gRNA1	CACCGTTTCTGAACGAGCATTACCA
PATL1_gRNA2	CACCGTGTGTCCGGTCTAAACATTG
PATL1_gRNA3	CACCGCCATAGGGAGCAGGATAACG
PDAP1_gRNA1	CACCGAAAAGCGCAAAGGCGTTGAA
PDAP1_gRNA2	CACCGGAGGCAGTATACAAGCCCTG
PDAP1_gRNA3	CACCGACTGGATCTGGACGGGCCAA
PDIA5_gRNA1	CACCGGAAAGTTGACCTGAGCCCGA
PDIA5_gRNA2	CACCGGTACTCAAATAGCAGATGG
PDIA5_gRNA3	CACCGGTGGAACATGACGAGGACAG
PHF6_gRNA1	CACCGCTTTATCATGCAATGCACAG
PHF6_gRNA2	CACCGAAAACACTGCACATAACTCCGA
PHF6_gRNA3	CACCGGGCAGCGCACCATAAAGTGCA
PRMT1_gRNA1	CACCGAAAGCCAACAAGTTAGACCA
PRMT1_gRNA2	CACCGGATGGCCGTCACATACAGCG
PRMT1_gRNA3	CACCGACATGGAGTTGCGGTAAGTG
PYHIN1_gRNA1	CACCGAGAAGACCCAATAATCGCGA
PYHIN1_gRNA2	CACCGCAAACGTAATAGTCTCCTAG
PYHIN1_gRNA3	CACCGTCAGCAAGGTCTCCCAGTGT
QKI_gRNA1	CACCGGGATGTAAAATCATGGTCCG
QKI_gRNA2	CACCGAAATAGAGGCAAGCCCAATT
QKI_gRNA3	CACCGGGGAGAATCCTTGGACCTAG
R3HCC1_gRNA1	CACCGCAGGGTGGACCCAAACCGTG
R3HCC1_gRNA2	CACCGGGAGACCCCAACTCTGATCA
R3HCC1_gRNA3	CACCGTTCTATGGATCAGGTACCGG
RACK1_gRNA1	CACCGCTTGCCTTGTGAGATCCCAG
RACK1_gRNA2	CACCGTTAGTCCGTACCTCGAGAGG
RACK1_gRNA3	CACCGAGTGTATTTGCACACACCCA
RBM14_gRNA1	CACCGGGAGCCACATAAGAGGCTCG
RBM14_gRNA2	CACCGGCCGTTGAGCTGCGCGATTG
RBM14_gRNA3	CACCGCTGGGCTCCATAAGCTAGTG
RBMS1_gRNA1	CACCGGATTCCAGTGGTACAAGTCG
RBMS1_gRNA2	CACCGTGGGAAAATAGTCTCCACAA



RBMS1_gRNA3	CACCGAACATACCAGAAACTCCTGG
RBMS2_gRNA1	CACCGCTACAATAGAAACAACAAGA
RBMS2_gRNA2	CACCGTTGGCCAAGGAATGCAGACA
RBMS2_gRNA3	CACCGGCCTCACCTGGTACTCCAGG
RSL1D1_gRNA1	CACCGGCTATACGTATTGGTCACGT
RSL1D1_gRNA2	CACCGAAATGTCTCCAATGAGTGA
RSL1D1_gRNA3	CACCGTGATCGAATACTATGAGGCA
SMARCA5_gRNA1	CACCGCATCAGCCTTAATTCGACGA
SMARCA5_gRNA2	CACCGATGCATCTAGTAACCAACAG
SMARCA5_gRNA3	CACCGCCGTAGAACAGAGCAAGAGG
STAT1_gRNA1	CACCGTCCCATTACAGGCTCAGTCG
STAT1_gRNA2	CACCGGACGTTGGAGATCACCACAA
STAT1_gRNA3	CACCGAGAACACGAGACCAATGGTG
STAU1_gRNA1	CACCGCCTGCATCACAAACTCCCTG
STAU1_gRNA2	CACCGACCTATAACTACAACATGAG
STAU1_gRNA3	CACCGGAAAACAAAACCCATAGTCA
STRBP_gRNA1	CACCGATCACCTTCAAAGTTAGCGT
STRBP_gRNA2	CACCGGTGCAACAGAGTCCCCACAT
STRBP_gRNA3	CACCGGGACATTGTGTGGTGTAATG
SYNCRIP_gRNA1	CACCGTATTCTAAGAGTAAAACCA
SYNCRIP_gRNA2	CACCGGATGACAAGAAAAAACAG
SYNCRIP_gRNA3	CACCGTGAGCGAGATGGTGCTGTCA
TAOK1_gRNA1	CACCGGATTTGTGACGAGATACTTG
TAOK1_gRNA2	CACCGGAAATAGCAGCAATTACACA
TAOK1_gRNA3	CACCGTGGGCGTCATAACTTAGAGC
TAOK2_gRNA1	CACCGTCAAGACAGACCAACCTCAG
TAOK2_gRNA2	CACCGCCCAACACCATTAGTACCG
TAOK2_gRNA3	CACCGGCCAGGGTTAGTGAAGCTAG
TAOK3_gRNA1	CACCGCCTAATACTATTGAGTACAA
TAOK3_gRNA2	CACCGGTATTCATAAGGGATGAGGC
TAOK3_gRNA3	CACCGTTCATTAGACTGTAACGTTG
TOE1_gRNA1	CACCGCAGAACTCCAGGGTAAGGTG
TOE1_gRNA2	CACCGAGGTCAATATCGTGAGACTG
TOE1_gRNA3	CACCGCCAGATAGGAATGTTACCC
TOP1_gRNA1	CACCGCGACCATGAATATACTACCA
TOP1_gRNA2	CACCGACTCACTCATCCTCATCTCG
TOP1_gRNA3	CACCGTGGAAGAGGCTCATATGGTG
TSEN2_gRNA1	CACCGGAGACCTTCTGTGGTAAACG
TSEN2_gRNA2	CACCGGGTATCAGCATAGTGTTGAG
TSEN2_gRNA3	CACCGGGAGTGTGCCATGAGCGAGA
UHRF1_gRNA1	CACCGGCGGGAACCTCTACGCCAACG
UHRF1_gRNA2	CACCGTGCTCGGGACACGAACATGG
UHRF1_gRNA3	CACCGCCATACCCTCTTCGACTACG
VRK1_gRNA1	CACCGTTTTGTAGCCCCATCAAGACG
VRK1_gRNA2	CACCGCCCAATACTTAGGAACACCC
VRK1_gRNA3	CACCGGTAGGATTACCCATTGGCCA
XAB2_gRNA1	CACCGCCGACACGAGAACTACGATG

XAB2_gRNA2	CACCGGAAACGCTCGTCGTTACCA
XAB2_gRNA3	CACCGTCTGGGGTGTGCGATACGC
XRN1_gRNA1	CACCGGATTCCAAGTGTATCACACC
XRN1_gRNA2	CACCGAGATAAAGAACAATCTAACT
XRN1_gRNA3	CACCGTATTCTATAAAGTACAACCC
YTHDC2_gRNA1	CACCGGGTTTGCTGACAGTACACAT
YTHDC2_gRNA2	CACCGACAAGTGGGCGACTCAACAA
YTHDC2_gRNA3	CACCGGTTTCAAGCCTGAATCTCAG
ZC3H11A_gRNA1	CACCGGTAAGACTCAATCTAACCAA
ZC3H11A_gRNA2	CACCGTAAAACAAAGTCTATGCAGG
ZC3H11A_gRNA3	CACCGTCCTGGCTGAAAAAAAAACAT
ZC3H15_gRNA1	CACCGGTATGTGCATTCTTCAAGCA
ZC3H15_gRNA2	CACCGTTTGGTAACATTTGGACCTA
ZC3H15_gRNA3	CACCGTGGTCAACAAAATCCACGTC
ZC3HAV1_gRNA1	CACCGGCAACTATTCGCAGTCCGAG
ZC3HAV1_gRNA2	CACCGACTTCCATCTGCCTTACCGG
ZC3HAV1_gRNA3	CACCGTCTGGTAGAAGTTATATCTG
ZFP91_gRNA1	CACCGTCACTGACCTGCAAATAGCG
ZFP91_gRNA2	CACCGGCTGCATCTAGACCTAGCCG
ZFP91_gRNA3	CACCGAGGCCGAGTATCCCCGCCGG
ZNF207_gRNA1	CACCGGGAACACCTGGCATTAAATGG
ZNF207_gRNA2	CACCGATGCAATGAATAGCTAAGCC
ZNF207_gRNA3	CACCGTGGAAGAACAGACATAGAGT
ZNF346_gRNA1	CACCGGCAAACCTTACACTGGGTGT
ZNF346_gRNA2	CACCGCAGCAGTCCACTAAGGTGGA
ZNF346_gRNA3	CACCGATACCTAGCAATCCATGGAA
ZNF385A_gRNA1	CACCGCAGCTTGAGGCACATAACAA
ZNF385A_gRNA2	CACCGACTGGTCAGGGTGTAACCAA
ZNF385A_gRNA3	CACCGAGGCAGCACCCCAACAAATG
ZNFX1_gRNA1	CACCGTCTGCAGGTAAGTTCCCGT
ZNFX1_gRNA2	CACCGTGGAAGTTGTCATTGGACCA
ZNFX1_gRNA3	CACCGGGTGGTCCCCAATCAAATG

Plasmids

Plasmid	Origin
pBS SK drosophila tao	Drosophila Gold Collection
pCMVmyc#1-ratTAOK2(1-451aa)	Melanie Cobb
pCMVmyc#1-ratTAOK2(1-451aa)-D151A	this study
pCMVmyc#1-ratTAOK2(1-993aa)	Melanie Cobb
pCMVmyc#1-ratTAOK2(1-993aa)-D151A	this study
pCoofy1	CoreFacility, Max Planck Institute for Biochemistry
pCoofy1-ratTAOK2(1-993aa)	this study
pCoofy27	CoreFacility, Max Planck Institute for Biochemistry
pCoofy27_dTao	this study



pCoofy27-ratTAOK2(1-451aa)	this study
pCoofy27-ratTAOK2(1-993aa)	this study
pCoofy36	CoreFacility, Max Planck Institute for Biochemistry
pCoofy36-drosophila tao	this study
pCoofy36-ratTAOK2(1-451aa)	this study
pCoofy36-ratTAOK2(1-451aa)-D151A	this study
pCoofy36-ratTAOK2(1-993aa)	this study
pCoofy36-ratTAOK2(1-993aa)-D151A	this study
pDONR221	Invitrogen
pDONR221_eGFP	this study
pDONR221-drosophila tao no_stop_codon	this study
pDONR221-drosophila tao STOP_codon	this study
pDONR221-ratTAOK2(1-451aa)D151A no_stop_codon	this study
pDONR221-ratTAOK2(1-451aa)D151A STOP_codon	this study
pDONR221-ratTAOK2(1-451aa)D151N no_stop_codon	this study
pDONR221-ratTAOK2(1-451aa)D151N STOP_codon	this study
pDONR221-ratTAOK2(1-451aa)no_stop_codon	this study
pDONR221-ratTAOK2(1-451aa)STOP_codon	this study
pDONR221-ratTAOK2(1-993aa)D151A no_stop_codon	this study
pDONR221-ratTAOK2(1-993aa)D151A STOP_codon	this study
pDONR221-ratTAOK2(1-993aa)D151N no_stop_codon	this study
pDONR221-ratTAOK2(1-993aa)no_stop_codon	this study
pDONR221-ratTAOK2(1-993aa)STOP_codon	this study
pETG-N-His/Venus-GW	Andreas Osterman
pETG-N-His/Venus-GW-ratTAOK2(1-451aa)	this study
pETG-N-His/Venus-GW-ratTAOK2(1-993aa)	this study
pLentiCMV/To-Hygro_GW_ratTAOK2(1-993aa)	this study
pLentiCMV/To-Hygro_GW_ratTAOK2(1-993aa)D151A	this study
pLentiCRISP_v2	Addgene
pLENTICRISPR_v2_MAVS_gRNA1	Guilio Superti-Furga
pLENTICRISPR_v2_MAVS_gRNA2	Guilio Superti-Furga
pLENTICRISPR_v2_MAVS_gRNA3	Guilio Superti-Furga
pLENTICRISPR_v2_neg_control1	Guilio Superti-Furga
pLENTICRISPR_v2_neg_control10	Guilio Superti-Furga
pLENTICRISPR_v2_neg_control11	Guilio Superti-Furga
pLENTICRISPR_v2_neg_control12	Guilio Superti-Furga
pLENTICRISPR_v2_neg_control2	Guilio Superti-Furga
pLENTICRISPR_v2_neg_control3	Guilio Superti-Furga
pLENTICRISPR_v2_neg_control4	Guilio Superti-Furga

pLENTICRISPR_v2_neg_control5	Guilio Superti-Furga
pLENTICRISPR_v2_neg_control6	Guilio Superti-Furga
pLENTICRISPR_v2_neg_control7	Guilio Superti-Furga
pLENTICRISPR_v2_neg_control8	Guilio Superti-Furga
pLENTICRISPR_v2_neg_control9	Guilio Superti-Furga
pLENTICRISPR_v2_NTC	Beatrice Laudenbach
pLENTICRISPR_v2_STAT1_gRNA1	Guilio Superti-Furga
pLENTICRISPR_v2_STAT1_gRNA2	Guilio Superti-Furga
pLENTICRISPR_v2_STAT1_gRNA3	Guilio Superti-Furga
pLENTICRISPR_v2_TAOK1_gRNA1	Guilio Superti-Furga
pLENTICRISPR_v2_TAOK1_gRNA2	Guilio Superti-Furga
pLENTICRISPR_v2_TAOK1_gRNA3	Guilio Superti-Furga
pLENTICRISPR_v2_TAOK2_gRNA1	Guilio Superti-Furga
pLENTICRISPR_v2_TAOK2_gRNA2	Guilio Superti-Furga
pLENTICRISPR_v2_TAOK2_gRNA3	Guilio Superti-Furga
pLENTICRISPR_v2_TAOK3_gRNA1	Guilio Superti-Furga
pLENTICRISPR_v2_TAOK3_gRNA2	Guilio Superti-Furga
pLENTICRISPR_v2_TAOK3_gRNA3	Guilio Superti-Furga
pLIX403_cV5_GW	Addgene
pLIX403_cV5_GW_eGFP	this study
pLIX403_cV5_GW_ratTAOK2(1-451aa)	this study
pLIX403_cV5_GW_ratTAOK2(1-451aa)D151A	this study
pLIX403_cV5_GW_ratTAOK2(1-993aa)	this study
pLIX403_cV5_GW_ratTAOK2(1-993aa)D151A	this study
pLIX403_cV5_ratTAOK2(1-993aa)_2146C>T	this study
pMD2G	Annika Frauenstein
psPAX2	Annika Frauenstein
pTM1-eGFP	Friedemann Weber

Bacteria

Bacterial strain	Origin
BL21ai	Max Planck Institute for Biochemistry, Core Facility
STbl3	Invitrogen
TOP10	Max Planck Institute for Biochemistry, Core Facility

Antibodies

Antibody	Species	Manufacturer
α-ABCF1	rabbit	Aviva Sytems Biology (ARP43631_P050)
α-ABCF3	rabbit	Sigma (HPA036332)
α-mouse-IgG-HRP	goat	Sigma-Aldrich (A0168)
α-MX1	mouse	Georg Koch
α-PARP12	rabbit	Sigma (HPA063872)
α-rabbit-IgG-HRP	goat	Cell Signaling Technology (7074)

THP-1_DHX58-KO	this study
THP-1_DHX9-KO	this study
THP-1_DTYMK-KO	this study
THP-1_EEA1-KO	this study
THP-1_EIF2S1-KO	this study
THP-1_EIF2S3-KO	this study
THP-1_ELAVL1-KO	this study
THP-1_ERI3-KO	this study
THP-1_EXOSC2-KO	this study
THP-1_EXOSC4-KO	this study
THP-1_FAM98B-KO	this study
THP-1_IFI27-KO	this study
THP-1_IFIT1-Gluc	Veit Hornung
THP-1_ILF2-KO	this study
THP-1_ILF3-KO	this study
THP-1_ISY1-KO	this study
THP-1_KHDRBS1-KO	this study
THP-1_KIF2A-KO	this study
THP-1_LARP1-KO	this study
THP-1_LRRC59-KO	this study
THP-1_MAVS-KO	this study
THP-1_MKRN2-KO	this study
THP-1_MNDA-KO	this study
THP-1_MOV10-KO	this study
THP-1_MSI2-KO	this study
THP-1_N4BP2-KO	this study
THP-1_neg..control3-KO	this study
THP-1_neg.control1-KO	this study
THP-1_neg.control2-KO	this study
THP-1_neg.control4-KO	this study
THP-1_NTC-KO	this study
THP-1_NTPCR-KO	this study
THP-1_NUDT16-KO	this study
THP-1_NUMB-KO	this study
THP-1_PARP12-KO	this study
THP-1_PARP1-KO	this study
THP-1_PARP2-KO	this study
THP-1_PATL1-KO	this study
THP-1_PDAP1-KO	this study
THP-1_PDIA5-KO	this study
THP-1_PHF6-KO	this study
THP-1_pLIX403_cV5_GW_eGFP	this study
THP-1_pLIX403_cV5_GW_ratTAOK2(1-451aa)	this study
THP-1_pLIX403_cV5_GW_ratTAOK2(1-451aa)D151A	this study
THP-1_pLIX403_cV5_GW_ratTAOK2(1-993aa)	this study
THP-1_pLIX403_cV5_GW_ratTAOK2(1-993aa)D151A	this study
THP-1_PRMT1-KO	this study
THP-1_PYHIN1-KO	this study
THP-1_QKI-KO	this study



THP-1_R3HCC1-KO	this study
THP-1_RACK1-KO	this study
THP-1_RBM14-KO	this study
THP-1_RBMS1-KO	this study
THP-1_RBMS2-KO	this study
THP-1_RSL1D1-KO	this study
THP-1_SMARCA5-KO	this study
THP-1_STAT1-KO	this study
THP-1_STAU1-KO	this study
THP-1_STRBP-KO	this study
THP-1_SYNCRIP-KO	this study
THP-1_TAOK1-KO	this study
THP-1_TAOK2_gRNA1-KO	this study
THP-1_TAOK2_gRNA2-KO	this study
THP-1_TAOK2_gRNA3-KO	this study
THP-1_TAOK2-KO	this study
THP-1_TAOK3-KO	this study
THP-1_TOE1-KO	this study
THP-1_TOP1-KO	this study
THP-1_TSEN2-KO	this study
THP-1_UHRF1-KO	this study
THP-1_VRK1-KO	this study
THP-1_XAB2-KO	this study
THP-1_XRN1-KO	this study
THP-1_YTHDC2-KO	this study
THP-1_ZC3H11A-KO	this study
THP-1_ZC3H15-KO	this study
THP-1_ZC3HAV1-KO	this study
THP-1_ZFP91-KO	this study
THP-1_ZNF207-KO	this study
THP-1_ZNF346-KO	this study
THP-1_ZNF385A-KO	this study
THP-1_ZNFX1-KO	this study
Vero E6	Michael Bergmann

Viruses

Lentiviruses

Virus

pLENTICRISPR_v2_ABCF1_gRNA1
pLENTICRISPR_v2_ABCF1_gRNA2
pLENTICRISPR_v2_ABCF1_gRNA3
pLENTICRISPR_v2_ABCF3_gRNA1
pLENTICRISPR_v2_ABCF3_gRNA2
pLENTICRISPR_v2_ABCF3_gRNA3
pLENTICRISPR_v2_ADAR_gRNA1
pLENTICRISPR_v2_ADAR_gRNA2

Origin

Giulio Superti-Furga
Giulio Superti-Furga

pLENTICRISPR_v2_ADAR_gRNA3	Giulio Superti-Furga
pLENTICRISPR_v2_ADARB1_gRNA1	Giulio Superti-Furga
pLENTICRISPR_v2_ADARB1_gRNA2	Giulio Superti-Furga
pLENTICRISPR_v2_ADARB1_gRNA3	Giulio Superti-Furga
pLENTICRISPR_v2_ANGEL2_gRNA1	Giulio Superti-Furga
pLENTICRISPR_v2_ANGEL2_gRNA2	Giulio Superti-Furga
pLENTICRISPR_v2_ANGEL2_gRNA3	Giulio Superti-Furga
pLENTICRISPR_v2_APEX1_gRNA1	Giulio Superti-Furga
pLENTICRISPR_v2_APEX1_gRNA2	Giulio Superti-Furga
pLENTICRISPR_v2_APEX1_gRNA3	Giulio Superti-Furga
pLENTICRISPR_v2_APTX_gRNA1	Giulio Superti-Furga
pLENTICRISPR_v2_APTX_gRNA2	Giulio Superti-Furga
pLENTICRISPR_v2_APTX_gRNA3	Giulio Superti-Furga
pLENTICRISPR_v2_AQR_gRNA1	Giulio Superti-Furga
pLENTICRISPR_v2_AQR_gRNA2	Giulio Superti-Furga
pLENTICRISPR_v2_AQR_gRNA3	Giulio Superti-Furga
pLENTICRISPR_v2_ASCC1_gRNA1	Giulio Superti-Furga
pLENTICRISPR_v2_ASCC1_gRNA2	Giulio Superti-Furga
pLENTICRISPR_v2_ASCC1_gRNA3	Giulio Superti-Furga
pLENTICRISPR_v2_BANF1_gRNA1	Giulio Superti-Furga
pLENTICRISPR_v2_BANF1_gRNA2	Giulio Superti-Furga
pLENTICRISPR_v2_BANF1_gRNA3	Giulio Superti-Furga
pLENTICRISPR_v2_C8orf88_gRNA1	Giulio Superti-Furga
pLENTICRISPR_v2_C8orf88_gRNA2	Giulio Superti-Furga
pLENTICRISPR_v2_C8orf88_gRNA3	Giulio Superti-Furga
pLENTICRISPR_v2_CAPRIN1_gRNA1	Giulio Superti-Furga
pLENTICRISPR_v2_CAPRIN1_gRNA2	Giulio Superti-Furga
pLENTICRISPR_v2_CAPRIN1_gRNA3	Giulio Superti-Furga
pLENTICRISPR_v2_CDKN2AIP_gRNA1	Giulio Superti-Furga
pLENTICRISPR_v2_CDKN2AIP_gRNA2	Giulio Superti-Furga
pLENTICRISPR_v2_CDKN2AIP_gRNA3	Giulio Superti-Furga
pLENTICRISPR_v2_CHAF1A_gRNA1	Giulio Superti-Furga
pLENTICRISPR_v2_CHAF1A_gRNA2	Giulio Superti-Furga
pLENTICRISPR_v2_CHAF1A_gRNA3	Giulio Superti-Furga
pLENTICRISPR_v2_CHAF1B_gRNA1	Giulio Superti-Furga
pLENTICRISPR_v2_CHAF1B_gRNA2	Giulio Superti-Furga
pLENTICRISPR_v2_CHAF1B_gRNA3	Giulio Superti-Furga
pLENTICRISPR_v2_CMTR1_gRNA1	Giulio Superti-Furga
pLENTICRISPR_v2_CMTR1_gRNA2	Giulio Superti-Furga
pLENTICRISPR_v2_CMTR1_gRNA3	Giulio Superti-Furga
pLENTICRISPR_v2_CMTR2_gRNA1	Giulio Superti-Furga
pLENTICRISPR_v2_CMTR2_gRNA2	Giulio Superti-Furga
pLENTICRISPR_v2_CMTR2_gRNA3	Giulio Superti-Furga
pLENTICRISPR_v2_CSDE1_gRNA1	Giulio Superti-Furga
pLENTICRISPR_v2_CSDE1_gRNA2	Giulio Superti-Furga
pLENTICRISPR_v2_CSDE1_gRNA3	Giulio Superti-Furga
pLENTICRISPR_v2_DDX1_gRNA1	Giulio Superti-Furga



pLENTICRISPR_v2_DDX1_gRNA2	Giulio Superti-Furga
pLENTICRISPR_v2_DDX1_gRNA3	Giulio Superti-Furga
pLENTICRISPR_v2_DDX20_gRNA1	Giulio Superti-Furga
pLENTICRISPR_v2_DDX20_gRNA2	Giulio Superti-Furga
pLENTICRISPR_v2_DDX20_gRNA3	Giulio Superti-Furga
pLENTICRISPR_v2_DDX41_gRNA1	Giulio Superti-Furga
pLENTICRISPR_v2_DDX41_gRNA2	Giulio Superti-Furga
pLENTICRISPR_v2_DDX41_gRNA3	Giulio Superti-Furga
pLENTICRISPR_v2_DDX42_gRNA1	Giulio Superti-Furga
pLENTICRISPR_v2_DDX42_gRNA2	Giulio Superti-Furga
pLENTICRISPR_v2_DDX42_gRNA3	Giulio Superti-Furga
pLENTICRISPR_v2_DEK_gRNA1	Giulio Superti-Furga
pLENTICRISPR_v2_DEK_gRNA2	Giulio Superti-Furga
pLENTICRISPR_v2_DEK_gRNA3	Giulio Superti-Furga
pLENTICRISPR_v2_DHX36_gRNA1	Giulio Superti-Furga
pLENTICRISPR_v2_DHX36_gRNA2	Giulio Superti-Furga
pLENTICRISPR_v2_DHX36_gRNA3	Giulio Superti-Furga
pLENTICRISPR_v2_DHX58_gRNA1	Giulio Superti-Furga
pLENTICRISPR_v2_DHX58_gRNA2	Giulio Superti-Furga
pLENTICRISPR_v2_DHX58_gRNA3	Giulio Superti-Furga
pLENTICRISPR_v2_DHX9_gRNA1	Giulio Superti-Furga
pLENTICRISPR_v2_DHX9_gRNA2	Giulio Superti-Furga
pLENTICRISPR_v2_DHX9_gRNA3	Giulio Superti-Furga
pLENTICRISPR_v2_DTYMK_gRNA1	Giulio Superti-Furga
pLENTICRISPR_v2_DTYMK_gRNA2	Giulio Superti-Furga
pLENTICRISPR_v2_DTYMK_gRNA3	Giulio Superti-Furga
pLENTICRISPR_v2_EEA1_gRNA1	Giulio Superti-Furga
pLENTICRISPR_v2_EEA1_gRNA2	Giulio Superti-Furga
pLENTICRISPR_v2_EEA1_gRNA3	Giulio Superti-Furga
pLENTICRISPR_v2_EIF2S1_gRNA1	Giulio Superti-Furga
pLENTICRISPR_v2_EIF2S1_gRNA2	Giulio Superti-Furga
pLENTICRISPR_v2_EIF2S1_gRNA3	Giulio Superti-Furga
pLENTICRISPR_v2_EIF2S3_gRNA1	Giulio Superti-Furga
pLENTICRISPR_v2_EIF2S3_gRNA2	Giulio Superti-Furga
pLENTICRISPR_v2_EIF2S3_gRNA3	Giulio Superti-Furga
pLENTICRISPR_v2_ELAVL1_gRNA1	Giulio Superti-Furga
pLENTICRISPR_v2_ELAVL1_gRNA2	Giulio Superti-Furga
pLENTICRISPR_v2_ELAVL1_gRNA3	Giulio Superti-Furga
pLENTICRISPR_v2_ERI3_gRNA1	Giulio Superti-Furga
pLENTICRISPR_v2_ERI3_gRNA2	Giulio Superti-Furga
pLENTICRISPR_v2_ERI3_gRNA3	Giulio Superti-Furga
pLENTICRISPR_v2_EXOSC2_gRNA1	Giulio Superti-Furga
pLENTICRISPR_v2_EXOSC2_gRNA2	Giulio Superti-Furga
pLENTICRISPR_v2_EXOSC2_gRNA3	Giulio Superti-Furga
pLENTICRISPR_v2_EXOSC4_gRNA1	Giulio Superti-Furga
pLENTICRISPR_v2_EXOSC4_gRNA2	Giulio Superti-Furga
pLENTICRISPR_v2_EXOSC4_gRNA3	Giulio Superti-Furga

pLENTICRISPR_v2_FAM98B_gRNA1	Giulio Superti-Furga
pLENTICRISPR_v2_FAM98B_gRNA2	Giulio Superti-Furga
pLENTICRISPR_v2_FAM98B_gRNA3	Giulio Superti-Furga
pLENTICRISPR_v2_IFI27_gRNA1	Giulio Superti-Furga
pLENTICRISPR_v2_IFI27_gRNA2	Giulio Superti-Furga
pLENTICRISPR_v2_IFI27_gRNA3	Giulio Superti-Furga
pLENTICRISPR_v2_ILF2_gRNA1	Giulio Superti-Furga
pLENTICRISPR_v2_ILF2_gRNA2	Giulio Superti-Furga
pLENTICRISPR_v2_ILF2_gRNA3	Giulio Superti-Furga
pLENTICRISPR_v2_ILF3_gRNA1	Giulio Superti-Furga
pLENTICRISPR_v2_ILF3_gRNA2	Giulio Superti-Furga
pLENTICRISPR_v2_ILF3_gRNA3	Giulio Superti-Furga
pLENTICRISPR_v2_ISY1_gRNA1	Giulio Superti-Furga
pLENTICRISPR_v2_ISY1_gRNA2	Giulio Superti-Furga
pLENTICRISPR_v2_ISY1_gRNA3	Giulio Superti-Furga
pLENTICRISPR_v2_KHDRBS1_gRNA1	Giulio Superti-Furga
pLENTICRISPR_v2_KHDRBS1_gRNA2	Giulio Superti-Furga
pLENTICRISPR_v2_KHDRBS1_gRNA3	Giulio Superti-Furga
pLENTICRISPR_v2_KIF2A_gRNA1	Giulio Superti-Furga
pLENTICRISPR_v2_KIF2A_gRNA2	Giulio Superti-Furga
pLENTICRISPR_v2_KIF2A_gRNA3	Giulio Superti-Furga
pLENTICRISPR_v2_LARP1_gRNA1	Giulio Superti-Furga
pLENTICRISPR_v2_LARP1_gRNA2	Giulio Superti-Furga
pLENTICRISPR_v2_LARP1_gRNA3	Giulio Superti-Furga
pLENTICRISPR_v2_LRRC59_gRNA1	Giulio Superti-Furga
pLENTICRISPR_v2_LRRC59_gRNA2	Giulio Superti-Furga
pLENTICRISPR_v2_LRRC59_gRNA3	Giulio Superti-Furga
pLENTICRISPR_v2_MAVS_gRNA1	Giulio Superti-Furga
pLENTICRISPR_v2_MAVS_gRNA2	Giulio Superti-Furga
pLENTICRISPR_v2_MAVS_gRNA3	Giulio Superti-Furga
pLENTICRISPR_v2_MKRN2_gRNA1	Giulio Superti-Furga
pLENTICRISPR_v2_MKRN2_gRNA2	Giulio Superti-Furga
pLENTICRISPR_v2_MKRN2_gRNA3	Giulio Superti-Furga
pLENTICRISPR_v2_MNDA_gRNA1	Giulio Superti-Furga
pLENTICRISPR_v2_MNDA_gRNA2	Giulio Superti-Furga
pLENTICRISPR_v2_MNDA_gRNA3	Giulio Superti-Furga
pLENTICRISPR_v2_MOV10_gRNA1	Giulio Superti-Furga
pLENTICRISPR_v2_MOV10_gRNA2	Giulio Superti-Furga
pLENTICRISPR_v2_MOV10_gRNA3	Giulio Superti-Furga
pLENTICRISPR_v2_MSI2_gRNA1	Giulio Superti-Furga
pLENTICRISPR_v2_MSI2_gRNA2	Giulio Superti-Furga
pLENTICRISPR_v2_MSI2_gRNA3	Giulio Superti-Furga
pLENTICRISPR_v2_N4BP2_gRNA1	Giulio Superti-Furga
pLENTICRISPR_v2_N4BP2_gRNA2	Giulio Superti-Furga
pLENTICRISPR_v2_N4BP2_gRNA3	Giulio Superti-Furga
pLENTICRISPR_v2_neg_control1	Giulio Superti-Furga
pLENTICRISPR_v2_neg_control10	Giulio Superti-Furga



pLENTICRISPR_v2_neg_control11	Giulio Superti-Furga
pLENTICRISPR_v2_neg_control12	Giulio Superti-Furga
pLENTICRISPR_v2_neg_control2	Giulio Superti-Furga
pLENTICRISPR_v2_neg_control3	Giulio Superti-Furga
pLENTICRISPR_v2_neg_control4	Giulio Superti-Furga
pLENTICRISPR_v2_neg_control5	Giulio Superti-Furga
pLENTICRISPR_v2_neg_control6	Giulio Superti-Furga
pLENTICRISPR_v2_neg_control7	Giulio Superti-Furga
pLENTICRISPR_v2_neg_control8	Giulio Superti-Furga
pLENTICRISPR_v2_neg_control9	Giulio Superti-Furga
pLENTICRISPR_v2_NTPCR_gRNA1	Giulio Superti-Furga
pLENTICRISPR_v2_NTPCR_gRNA2	Giulio Superti-Furga
pLENTICRISPR_v2_NTPCR_gRNA3	Giulio Superti-Furga
pLENTICRISPR_v2_NUDT16_gRNA1	Giulio Superti-Furga
pLENTICRISPR_v2_NUDT16_gRNA2	Giulio Superti-Furga
pLENTICRISPR_v2_NUDT16_gRNA3	Giulio Superti-Furga
pLENTICRISPR_v2_NUMB_gRNA1	Giulio Superti-Furga
pLENTICRISPR_v2_NUMB_gRNA2	Giulio Superti-Furga
pLENTICRISPR_v2_NUMB_gRNA3	Giulio Superti-Furga
pLENTICRISPR_v2_PARP1_gRNA1	Giulio Superti-Furga
pLENTICRISPR_v2_PARP1_gRNA2	Giulio Superti-Furga
pLENTICRISPR_v2_PARP1_gRNA3	Giulio Superti-Furga
pLENTICRISPR_v2_PARP12_gRNA1	Giulio Superti-Furga
pLENTICRISPR_v2_PARP12_gRNA2	Giulio Superti-Furga
pLENTICRISPR_v2_PARP12_gRNA3	Giulio Superti-Furga
pLENTICRISPR_v2_PARP2_gRNA1	Giulio Superti-Furga
pLENTICRISPR_v2_PARP2_gRNA2	Giulio Superti-Furga
pLENTICRISPR_v2_PARP2_gRNA3	Giulio Superti-Furga
pLENTICRISPR_v2_PATL1_gRNA1	Giulio Superti-Furga
pLENTICRISPR_v2_PATL1_gRNA2	Giulio Superti-Furga
pLENTICRISPR_v2_PATL1_gRNA3	Giulio Superti-Furga
pLENTICRISPR_v2_PDAP1_gRNA1	Giulio Superti-Furga
pLENTICRISPR_v2_PDAP1_gRNA2	Giulio Superti-Furga
pLENTICRISPR_v2_PDAP1_gRNA3	Giulio Superti-Furga
pLENTICRISPR_v2_PDIA5_gRNA1	Giulio Superti-Furga
pLENTICRISPR_v2_PDIA5_gRNA2	Giulio Superti-Furga
pLENTICRISPR_v2_PDIA5_gRNA3	Giulio Superti-Furga
pLENTICRISPR_v2_PHF6_gRNA1	Giulio Superti-Furga
pLENTICRISPR_v2_PHF6_gRNA2	Giulio Superti-Furga
pLENTICRISPR_v2_PHF6_gRNA3	Giulio Superti-Furga
pLENTICRISPR_v2_PRMT1_gRNA1	Giulio Superti-Furga
pLENTICRISPR_v2_PRMT1_gRNA2	Giulio Superti-Furga
pLENTICRISPR_v2_PRMT1_gRNA3	Giulio Superti-Furga
pLENTICRISPR_v2_PYHIN1_gRNA1	Giulio Superti-Furga
pLENTICRISPR_v2_PYHIN1_gRNA2	Giulio Superti-Furga
pLENTICRISPR_v2_PYHIN1_gRNA3	Giulio Superti-Furga
pLENTICRISPR_v2_QKI_gRNA1	Giulio Superti-Furga

pLENTICRISPR_v2_QKI_gRNA2	Giulio Superti-Furga
pLENTICRISPR_v2_QKI_gRNA3	Giulio Superti-Furga
pLENTICRISPR_v2_R3HCC1_gRNA1	Giulio Superti-Furga
pLENTICRISPR_v2_R3HCC1_gRNA2	Giulio Superti-Furga
pLENTICRISPR_v2_R3HCC1_gRNA3	Giulio Superti-Furga
pLENTICRISPR_v2_RACK1_gRNA1	Giulio Superti-Furga
pLENTICRISPR_v2_RACK1_gRNA2	Giulio Superti-Furga
pLENTICRISPR_v2_RACK1_gRNA3	Giulio Superti-Furga
pLENTICRISPR_v2_RBM14_gRNA1	Giulio Superti-Furga
pLENTICRISPR_v2_RBM14_gRNA2	Giulio Superti-Furga
pLENTICRISPR_v2_RBM14_gRNA3	Giulio Superti-Furga
pLENTICRISPR_v2_RBMS1_gRNA1	Giulio Superti-Furga
pLENTICRISPR_v2_RBMS1_gRNA2	Giulio Superti-Furga
pLENTICRISPR_v2_RBMS1_gRNA3	Giulio Superti-Furga
pLENTICRISPR_v2_RBMS2_gRNA1	Giulio Superti-Furga
pLENTICRISPR_v2_RBMS2_gRNA2	Giulio Superti-Furga
pLENTICRISPR_v2_RBMS2_gRNA3	Giulio Superti-Furga
pLENTICRISPR_v2_RSL1D1_gRNA1	Giulio Superti-Furga
pLENTICRISPR_v2_RSL1D1_gRNA2	Giulio Superti-Furga
pLENTICRISPR_v2_RSL1D1_gRNA3	Giulio Superti-Furga
pLENTICRISPR_v2_SMARCA5_gRNA1	Giulio Superti-Furga
pLENTICRISPR_v2_SMARCA5_gRNA2	Giulio Superti-Furga
pLENTICRISPR_v2_SMARCA5_gRNA3	Giulio Superti-Furga
pLENTICRISPR_v2_STAT1_gRNA1	Giulio Superti-Furga
pLENTICRISPR_v2_STAT1_gRNA2	Giulio Superti-Furga
pLENTICRISPR_v2_STAT1_gRNA3	Giulio Superti-Furga
pLENTICRISPR_v2_STAU1_gRNA1	Giulio Superti-Furga
pLENTICRISPR_v2_STAU1_gRNA2	Giulio Superti-Furga
pLENTICRISPR_v2_STAU1_gRNA3	Giulio Superti-Furga
pLENTICRISPR_v2_STRBP_gRNA1	Giulio Superti-Furga
pLENTICRISPR_v2_STRBP_gRNA2	Giulio Superti-Furga
pLENTICRISPR_v2_STRBP_gRNA3	Giulio Superti-Furga
pLENTICRISPR_v2_SYNCRIP_gRNA1	Giulio Superti-Furga
pLENTICRISPR_v2_SYNCRIP_gRNA2	Giulio Superti-Furga
pLENTICRISPR_v2_SYNCRIP_gRNA3	Giulio Superti-Furga
pLENTICRISPR_v2_TAOK1_gRNA1	Giulio Superti-Furga
pLENTICRISPR_v2_TAOK1_gRNA2	Giulio Superti-Furga
pLENTICRISPR_v2_TAOK1_gRNA3	Giulio Superti-Furga
pLENTICRISPR_v2_TAOK2_gRNA1	Giulio Superti-Furga
pLENTICRISPR_v2_TAOK2_gRNA2	Giulio Superti-Furga
pLENTICRISPR_v2_TAOK2_gRNA3	Giulio Superti-Furga
pLENTICRISPR_v2_TAOK3_gRNA1	Giulio Superti-Furga
pLENTICRISPR_v2_TAOK3_gRNA2	Giulio Superti-Furga
pLENTICRISPR_v2_TAOK3_gRNA3	Giulio Superti-Furga
pLENTICRISPR_v2_TOE1_gRNA1	Giulio Superti-Furga
pLENTICRISPR_v2_TOE1_gRNA2	Giulio Superti-Furga
pLENTICRISPR_v2_TOE1_gRNA3	Giulio Superti-Furga



pLENTICRISPR_v2_TOP1_gRNA1	Giulio Superti-Furga
pLENTICRISPR_v2_TOP1_gRNA2	Giulio Superti-Furga
pLENTICRISPR_v2_TOP1_gRNA3	Giulio Superti-Furga
pLENTICRISPR_v2_TSEN2_gRNA1	Giulio Superti-Furga
pLENTICRISPR_v2_TSEN2_gRNA2	Giulio Superti-Furga
pLENTICRISPR_v2_TSEN2_gRNA3	Giulio Superti-Furga
pLENTICRISPR_v2_UHRF1_gRNA1	Giulio Superti-Furga
pLENTICRISPR_v2_UHRF1_gRNA2	Giulio Superti-Furga
pLENTICRISPR_v2_UHRF1_gRNA3	Giulio Superti-Furga
pLENTICRISPR_v2_VRK1_gRNA1	Giulio Superti-Furga
pLENTICRISPR_v2_VRK1_gRNA2	Giulio Superti-Furga
pLENTICRISPR_v2_VRK1_gRNA3	Giulio Superti-Furga
pLENTICRISPR_v2_XAB2_gRNA1	Giulio Superti-Furga
pLENTICRISPR_v2_XAB2_gRNA2	Giulio Superti-Furga
pLENTICRISPR_v2_XAB2_gRNA3	Giulio Superti-Furga
pLENTICRISPR_v2_XRN1_gRNA1	Giulio Superti-Furga
pLENTICRISPR_v2_XRN1_gRNA2	Giulio Superti-Furga
pLENTICRISPR_v2_XRN1_gRNA3	Giulio Superti-Furga
pLENTICRISPR_v2_YTHDC2_gRNA1	Giulio Superti-Furga
pLENTICRISPR_v2_YTHDC2_gRNA2	Giulio Superti-Furga
pLENTICRISPR_v2_YTHDC2_gRNA3	Giulio Superti-Furga
pLENTICRISPR_v2_ZC3H11A_gRNA1	Giulio Superti-Furga
pLENTICRISPR_v2_ZC3H11A_gRNA2	Giulio Superti-Furga
pLENTICRISPR_v2_ZC3H11A_gRNA3	Giulio Superti-Furga
pLENTICRISPR_v2_ZC3H15_gRNA1	Giulio Superti-Furga
pLENTICRISPR_v2_ZC3H15_gRNA2	Giulio Superti-Furga
pLENTICRISPR_v2_ZC3H15_gRNA3	Giulio Superti-Furga
pLENTICRISPR_v2_ZC3HAV1_gRNA1	Giulio Superti-Furga
pLENTICRISPR_v2_ZC3HAV1_gRNA2	Giulio Superti-Furga
pLENTICRISPR_v2_ZC3HAV1_gRNA3	Giulio Superti-Furga
pLENTICRISPR_v2_ZFP91_gRNA1	Giulio Superti-Furga
pLENTICRISPR_v2_ZFP91_gRNA2	Giulio Superti-Furga
pLENTICRISPR_v2_ZFP91_gRNA3	Giulio Superti-Furga
pLENTICRISPR_v2_ZNF207_gRNA1	Giulio Superti-Furga
pLENTICRISPR_v2_ZNF207_gRNA2	Giulio Superti-Furga
pLENTICRISPR_v2_ZNF207_gRNA3	Giulio Superti-Furga
pLENTICRISPR_v2_ZNF346_gRNA1	Giulio Superti-Furga
pLENTICRISPR_v2_ZNF346_gRNA2	Giulio Superti-Furga
pLENTICRISPR_v2_ZNF346_gRNA3	Giulio Superti-Furga
pLENTICRISPR_v2_ZNF385A_gRNA1	Giulio Superti-Furga
pLENTICRISPR_v2_ZNF385A_gRNA2	Giulio Superti-Furga
pLENTICRISPR_v2_ZNF385A_gRNA3	Giulio Superti-Furga
pLENTICRISPR_v2_ZNFX1_gRNA1	Giulio Superti-Furga
pLENTICRISPR_v2_ZNFX1_gRNA2	Giulio Superti-Furga
pLENTICRISPR_v2_ZNFX1_gRNA3	Giulio Superti-Furga
pLENTICRISPR_v2_NTC	this study
pLIX403_cV5_GW_ratTAOK2(1-451aa)	this study

pLIX403_cV5_GW_ratTAOK2(1-451aa) D151A	this study
pLIX403_cV5_GW_ratTAOK2(1-993aa)	this study
pLIX403_cV5_GW_ratTAOK2(1-993aa) D151A	this study
pLIX403_cV5_GW_eGFP	this study

Other viruses

Virus

HSV-1-Firefly Luc
 Influenza A SC35M NS1_2A_Gaussia_2A_NEP
 SFV
 SFV6-2SG-Gaussia-Luc
 SFV6-2SG-mCherry
 VSV-Firefly Luc

Origin

Søren Riis Paludan
 Peter Reuther
 Georg Kochs
 Andres Merits
 Andres Merits
 Gert Zimmer

Software and databases

Software or database

Affinity Analysis v2.2.4
 CDD batch search
 Cytoscape
 DIOPT - DRSC Integrative Ortholog
 Prediction Tool
 egglog
 EnrichmentMap
 GPP sgRNA designer
 i-control version 1.11
 Illustrator CS6
 IncuCyte S3 Software version 2019B Rev2
 Interferome
 iRegulon
 MaxQuant (version 1.5.0.0/ 1.6.14.0)
 MetaScape IAV
 OptEnrichedSetCover.jl
 Perseus (version 1.5.2.1/ 1.6.13.0)
 Photoshop CS6
 Prism (v8)
 QuickGo
 R (v3.3/ v3.5)
 Reactome Pathway Database
 rstan R package
 Snappene version 4.3.3

 UniProt

 Vi-CELL XR Software

Manufacturer

NanoTemper Technologies MO
 (Marchler-Bauer et al., 2011)
 (Shannon, 2003)
 (Hu et al., 2011)
 (Huerta-Cepas et al., 2019)
 (Merico et al., 2010)
 (Doench et al., 2016)
 Tecan
 Adobe
 Essen Bioscience
 (Rusinova et al., 2012)
 (Janky et al., 2014)
 (Tyanova et al., 2016a)
 (Tripathi et al., 2015)
 Alexey Stukalov
 (Tyanova et al., 2016b)
 Adobe
 Graphpad Software
 (Binns et al., 2009)
 R Project
 (Jassal et al., 2020)
 (Carpenter et al., 2017)
 Snappene
 European Bioinformatics Institute (EMBL-
 EBI), the SIB Swiss Institute of
 Bioinformatics and the Protein Information
 Resource (PIR)
 Beckman Coulter



Methods

Molecular cloning

Molecular cloning encompasses a set of techniques used to assemble recombinant gene expression vectors. The DNA of interest, coined insert, is amplified by PCR from a template using specific primers. After amplification, the insert is fused with the new plasmid vector. The thus resulting final plasmid can be amplified in bacteria. In addition, DNA sequences can also be modified by mutagenesis PCR.

Polymerase Chain Reaction

Polymerase Chain Reaction (PCR) was performed to amplify a DNA sequence of interest from a template such as another plasmid or cDNA. The following reaction mixture was pipetted to a total volume of 50 μ L: 100 ng template DNA, 10 μ L 5x GC Buffer, 1 μ L 10 mM dNTPS, 2.5 μ L 10 μ M forward primer, 2.5 μ L 10 μ M reverse primer and 0.5 μ L Phusion Hot Start II DNA Polymerase (2 U/ μ L) in UltraPure™ DNase/RNase-Free Distilled Water. The reaction mix was amplified in a T100™ Thermal Cycler to amplify the DNA. After an initial denaturation of 2 min at 95°C, a cycle consisting of (i) denaturation at 95°C for 30 sec, (ii) annealing at 55°C for 30 sec and (iii) extension at 72°C for 90 sec was run 35 times. Following the cycling, a final extension was performed at 72°C for 3 min. The PCR product was either analyzed and purified using agarose gel electrophoresis and gel purification or directly purified using NucleoSpin® Gel and PCR Clean-up (Macherey-Nagel) kit according to the manufacturer's protocol.

For SLIC cloning, where a linearized plasmid is required, the reaction procedure is as follows. The reaction mixture was pipetted to a total volume of 50 μ L: 25 ng template DNA, 10 μ L 5x GC Buffer, 2 μ L 10 mM dNTPS, 0.5 μ L 50 pM forward primer, 0.5 μ L 50 pM reverse primer and 1 μ L Phusion Hot Start II DNA Polymerase (2 U/ μ L) in UltraPure™ DNase/RNase-Free Distilled Water. After an initial denaturation of 30 sec at 98°C, a cycle consisting of (i) denaturation at 98°C for 30 sec and (ii) extension at 72°C for 90 sec was run 30 times. Following the cycling, a final extension was performed at 72°C for 10 min. The linearized plasmid is then purified from an agarose gel.

Agarose gel electrophoresis and gel purification

Following PCR or DNA restriction digest, DNA fragments were separated based on size using gel electrophoresis. An electric field is applied to an agarose gel, into which the DNA has been loaded. As the DNA is negatively charged, it moves towards the positively charge electrode within the applied electric field.

A 1% (w/v) agarose gel was prepared in TAE buffer through boiling, with 0.1% (v/v) GelRed™ Nucleic Acid Stain being added. The DNA of interest, as well as a DNA ladder (GeneRuler 100 bp Plus DNA Ladder or GeneRuler 1 kb DNA Ladder) was mixed with Loading Dye and loaded into the set gel in TAE buffer. An electrical current of 120 V was applied for 1 – 1.5 h. The DNA was visualized under UV light in InGenius3. If the DNA was used for further cloning, the bands of interested were excised using a scalpel and purified using NucleoSpin® Gel and PCR Clean-up (Macherey-Nagel) or QIAEX II Gel Extraction Kit (Qiagen) kit according to the manufacturer's protocol.

Gateway cloning

The Gateway® Technology relies on the lambda recombination system to allow transfer of a gene of interest between vectors. To allow this, primers for the isolation of the gene of interest are designed to include the *attB* forward and reverse sequences. 2 µL of the PCR product are incubated at 25°C for 3 h with 150 ng of the donor vector (e.g. pDONR221), 2 µL Gateway BP clonase® II enzyme and 5 µL TE buffer. This facilitates recombination of the *attB* site with the *attP* site to create an *attL* containing entry plasmid. The plasmid preparation is then treated with Proteinase K at 37°C for 10 min to digest the proteins.

Once purified, 50-150 ng of entry plasmid are mixed with 150 ng of destination vector (e.g. pETG-N-His/Venus-GW or pLIX403_cV5_GW) and 2 µL of Gateway LR clonase® II enzyme in UltraPure™ DNase/RNase-Free Distilled Water to a total volume of 10 µL. The mixture is incubated at 25°C for 2 h, which allows for the recombination of *attL* with *attR* to create an *attB* containing expression vector with the gene of interest. The plasmid preparation is treated with Proteinase K at 37°C for 10 min to digest the proteins.



Sequence and Ligation Independent cloning

Sequence and Ligation Independent Cloning (SLIC) is based on homologous recombination in *E. coli* and does not rely on site-specific recombination. Both the vector and the gene of interest are amplified using PCR as previously described. 80-120ng of the linearized plasmid, 1-2 μL of insert, 2 μL RecA recombinase buffer and 1 μL RecA recombinase are mixed and incubated at 37°C for 30 min, catalyzing RecA-mediated recombination.

Lentiviral CRISPR cloning

In order to generate lentiviral CRISPR/Cas9 KO cells, sgRNA containing CRISPR plasmids were generated. For the primary lentiviral CRISPR/Cas9 library, this work was performed in the laboratory of Giulio Superti-Furga.

The previously noted sgRNA oligonucleotides were annealed as follows. 1 μL of 100 μM forward and 1 μL of 100 μM reverse oligo were mixed with 1 μL 10x T4 Ligation Buffer in 10 μL UltraPure™ DNase/RNase-Free Distilled Water. The reaction mix was incubated at 37°C for 30 min, then 95°C for 5 min after which the temperature was reduced by 5°C/min until 25°C was reached. The annealed oligoes were then diluted in water at 1:100. The pLentiCRISPRv2 plasmid was digested with BsmBI. For this 5 μg of plasmid were mixed with 3 μL BsmBI, 3 μL Digestion Buffer 3.1 (NEB) and filled to 30 μL with water. The mixture was incubated for 30 min at 37°C, followed by gel electrophoresis and gel purification. 50 ng of the digested pLentiCRISPRv2, 1 μL of the diluted annealed oligonucleotides, 2 μL 5x Rapid Ligation Buffer and 1 μL T4 DNA ligase were mixed and incubated at room temperature for 10 min.

Site-directed mutagenesis

Site directed mutagenesis was performed to specifically change a single codon within a plasmid sequence and thereby exchanging the amino acid. To this aim, comparatively long primers centering on the desired codon were designed with the mutated nucleotide sequence. The following reaction mixture was pipetted to a total volume of 50 μL : 100 ng template DNA, 5 μL 10x pfu reaction Buffer, 1 μL 10 mM dNTPS, 2.5 μL 10 μM forward primer, 2.5 μL 10 μM reverse primer and 0.5 μL pfu polymerase in UltraPure™ DNase/RNase-Free Distilled Water. The reaction mix was amplified in a T100™ Thermal Cycler to amplify the DNA. After an initial denaturation of 5 min at 95°C, a cycle consisting of (i) denaturation at 95°C for 1 min, (ii) annealing at 65°C for 1 min and (iii) extension at 72°C for 16 min was run 18 times. Following the

cycling, a final extension was performed at 72°C for 32 min. The PCR product was incubated with DpNI for 2h at 37°C to digest the methylated template plasmid and then purified using NucleoSpin® Gel and PCR Clean-up (Macherey-Nagel) kit according to the manufacturer's protocol.

Bacterial Transformation

In order for bacteria to take up DNA from the environment, they need to be competent. Chemically competent bacteria were produced as follows. Using an overnight culture of the bacteria of interest, 100 mL of LB were inoculated and grown at 37°C to 0.22-0.5 OD₅₅₀. The bacteria were chilled on ice for 10 min, centrifuged at 4500 g for 10 min at 4°C and resuspended in 40 mL ice cold TB1 buffer. Again, the bacteria were chilled on ice for 10 min, centrifuged at 4500 g for 10 min at 4°C and resuspended in 40 mL ice cold TB2 buffer. The bacteria were chilled on ice for 15 min, aliquoted, shock-frozen in liquid nitrogen and stored at -80°C until use.

For the transformation, the bacteria were mixed with around 100 ng of plasmid on chilled on ice for 30 min. Afterwards, the bacteria were heat shocked at 42°C for 30 sec, 1 mL of pre-warmed LB- medium was added and they were incubated at 37°C for 1-2 hours. Transformed bacteria were then plated onto LB agar plates containing the relevant antibiotics and incubated overnight at 37°C. Single colonies were then picked and in LB at 37°C with 250 rpm overnight for extraction and analysis of the plasmid.

DNA extraction

Bacterial amplified plasmid DNA was isolated using commercially available plasmid purification kits. For small scale extractions NucleoSpin® Plasmid (Macherey-Nagel) was used, for medium scale extractions NucleoBond™ AX (Macherey-Nagel) and for large scale extractions Nucleobond™ PC 500 (Macherey-Nagel), all according to manufacturer's protocol.

Extracted plasmids were verified through sequencing at Eurofins Genomics, Ebersberg, Germany using promoter or gene specific primers or via test digest. For the test digest 1-2 µg of the plasmid were incubated with 1 µL restriction enzyme in the respective buffer for 30-60 min at the recommended temperature.



Cell culture and handling

Cell culture

All mammalian cells were cultured in a humidified incubator at 37°C with 5% CO₂. HEK293T, HEK293R1, Vero, HeLa and A549 based cell lines were cultured in Duplecco's modified Eagle's medium (DMEM) supplemented with 1% penicillin-streptomycin (P/S) and 10% fetal bovine serum (FBS). THP-1 based cell lines were cultured in RPMI 1640 supplement with 1% P/S and 10% FCS.

Adherent cells were split at a confluency of 80-100% every 2-3 days. The cells were washed once with PBS and then incubated in 0.25% trypsin until they had detached from the plate. Trypsin digest was then inhibited by the addition of medium, the cells were diluted at 1:10 in fresh medium and plated on a cell culture dish. Suspension cells were split every 2-3 days and seeded at a density of approximately 2.5E5 cells / mL.

Where necessary cells were counted either on a Countess or on a Vi-CELL XR Cell Viability Analyzer System. If desired, THP-1 cells were differentiated with 150 nM PMA upon seeding overnight before stimulation.

Freezing and thawing of cells

For long-term storage, cells were frozen with FBS and dimethylsulfoxid. Cells were grown until 60-80% confluency, if necessary trypsinated, and centrifuged. The cell culture medium was removed and the cells were resuspended in cell culture medium with 10% FBS, followed by the slow addition of an equal volume of FBS with 20% dimethylsulfoxid. The cell suspension was aliquoted in cryotubes and frozen at -80°C in an isopropanol-based freezing container. After freezing, the cells were transferred into a liquid nitrogen tank for long-term storage.

As the dimethylsulfoxid can damage the cells, during thawing it is important to quickly remove it. Therefore the cells were quickly thawed in a 37°C waterbath, transferred to a Falcon with prewarmed medium and centrifuged at 800rpm for 5 min. The medium was replaced and the cells were plated.

Creation of stable KO or overexpression cells

THP-1 cells were seeded in at 2E5 cells / well in a 24 well plate in 400 µL of medium. 600 µL of lentivirus stock was added per well, for KO cells 200µL of the three different lentiviral gRNAs targeting a single gene were mixed. After overnight incubation at

37°C, 1 µg/mL of selection antibiotic (puromycin or blasticidin) was added and the cells were incubated for a further 2 days at 37°C. On day 4 after infection, cells were transferred to a 1.5 mL Eppendorf and centrifuged at 2000 g for 10 min. The puromycin containing cell culture medium was refreshed and the cells were transferred to a 12 well plate with a final volume of 2 mL. On day 7 post infection, cells were transferred to a 2 mL Eppendorf and centrifuged at 2000 g for 10 min. The puromycin containing cell culture medium was refreshed and the cells were transferred to a 6 well plate with a final volume of 4 mL. On approx. day 10 post infection if the cells appeared confluent, the cells were transferred to a 10 cm dish in 10 mL of puromycin containing cell culture medium. On approx. day 13 post infection if the cells appeared confluent, the cells were transferred to a 15 cm dish in 20 mL of puromycin containing cell culture medium. Cells were prepared for long-term storage and taken off puromycin selection media at approx. day 16 post infection.

Transient overexpression

HEK293R1 cells were seeded at 2.5E5 cells / well in a 6 well dish. Plasmids were diluted in 50 µL of PBS in the noted concentration and added onto 1 µL Metafectene Pro in 50 µL PBS. The mixture was incubated for 15-20 minutes at room temperature, after which it was added dropwise to the cells. The cells were then incubated at 37°C for 30 min, followed by the addition of 1 µg / mL doxycycline. The cells were then incubated overnight before additional assays were performed.

Cell viability

To determine cell viability, 50 µg/mL of resazurin were added to each well and incubated at 37°C for 30 min, after which the fluorescence (535/590 nm) was measured using an Infinite 200 PRO series micro plate reader.

Live cell imaging

Replication of fluorescently tagged cell lines was measured using the Incucyte S3 light microscopy screening platform. Images were taken every 2-4 hours and subsequently analyzed using the IncuCyte 2019B Rev2 software. Transfection of poly(I:C) was performed using Metafectene Pro (1µL per µg poly(I:C)).



Virus culture, titration and related experiments

Virus stock production

In order to have sufficient viral stocks, the four key viruses used in the human KO screening needed to be cultivated. To do so, Vero E6 cells were seeded and grown to confluency at 37°C. The medium was removed and the cells were infected for 1 h in 5 mL of OptiMEM, after which the inoculum was removed and cell culture medium was added. The virus was harvested between 24 h to -4 days, depending on when cytopathic effects were observable. The supernatant was centrifuged at 3000 rpm, 4°C, for 15 min to remove cell debris. It was then aliquoted, flash frozen in liquid nitrogen and stored at -80°C.

Plaque assays

Plaque assays were used to measure the viral concentration, determined as plaque forming units (pfu) / mL. A 24 well plate was seeded with 2E5 Vero E6 cells / well and incubated overnight at 37°C. A serial 10 fold dilution was prepared from the virus stock in cell culture medium. The medium was then removed from the 24 well plate and replaced with 300 µL of virus dilution. The plate was incubated at 37°C for 1 h and shaken every 15 min. 1.5% (w/v) CMC in cell culture medium was added on top of the viral dilution (1 mL per well) and the plate was then incubated for 2-4 days at 37°C. Afterwards the medium was removed and replaced with 4% formaldehyde. After at least 30 min incubation at room temperature the formaldehyde was removed. To visualize the plaques 1% crystal violet in 10% ethanol staining was added for at least 30 min at room temperature, after which the plate was washed in water and dried. The plaques were then counted and the titer calculated: $titer =$

$$\frac{\text{number of plaques}}{\text{volume of viruses added (mL)} \cdot \text{dilution counted}}$$

Lentivirus production

HEK293T cells were seeded at 5E5 cells / well in a 6 well dish and incubated at 37°C overnight. The following day, the lentiviral plasmid of interest, viral packaging plasmid (psPAX2) and viral envelope plasmid (pMD2G) were mixed at 4:2:1 ratio in PBS. PEI was added at a ratio of 4 µg PEI per µg plasmid. The PEI-plasmid mixture was incubated 15 min at room temperature before being added to the cells and incubated at 37°C overnight. The next morning the cell culture media was refreshed. The

following day, the virus containing supernatant was harvested, centrifuged for 10 min at 2500 rpm to remove cell debris, and stored at -80°C.

Virus replication of luciferase tagged viruses

Gaussia luciferase levels were determined; 20 µL of cell supernatant was mixed with 20 µL of Gaussia Luciferase buffer with 300:1 of a coelenterazine solution (3 mM in acidified methanol) and incubated at RT in the dark for 5 min, after which the luminescence was measured using an Infinite 200 PRO series micro plate reader. The levels of firefly luciferase were measured by first pelleting the non-PMA cells (800g for 5 min) and removing the medium for the pelleted non-PMA and PMA treated cells. The cells were resuspended in 50µL 1x Passive lysis buffer and subjected to a freeze-thaw cycle to break the cell membrane. 20 µL of cell lysate were mixed with 20 µL of firefly substrate and incubated at RT in the dark for 5 min, after which the luminescence was measured using an Infinite 200 PRO series micro plate reader.

Virus replication of fluorescently tagged viruses

Replication of fluorescent viruses was measured using the Incucyte S3 light microscopy screening platform. Images were taken every 2-4 hours and subsequently analyzed using the InCuCyte 2019B Rev2 software.

Protein biochemistry

SDS-PAGE

SDS polyacrylamide gel electrophoresis (SDS-PAGE) allows for the separation of proteins according to their molecular weight. The cells are harvested either in TAP lysis buffer and diluted in 5x Lämmli buffer or harvested directly in 1x SDS buffer, and boiled at 95°C for 5 min. Gels were cast with 2.08 mL water, 1.67 mL acrylamide 1.25 mL 1x Resolving/separating Gel Buffer, 5 µL TEMED and 50 µL APS per gel in a Multi-casting chamber. The gels were covered with isopropanol and allowed to set for 30 min. The isopropanol was removed and the stacking gel with 2.23 mL water, 0.4 mL acrylamide, 0.375 mL 1x Stacking Gel Buffer, 3µL TEMED and 30 µL APS was added. The comb was inserted and the gel was allowed to set for an additional 30 min. The samples were loaded onto the gel, along with PageRuler™ Prestained Protein Ladder, 10 to 180 kDa in a Protein electrophoresis chamber filled with 1x Electrophoresis Running Buffer. An electrical current was applied at 100 V for 60-90 minutes.



In order to visualize proteins on the SDS-PAGE, the gel was stained with Coomassie staining solution for 1 h. After being completely stained the gel was treated with Destaining solution over the course of several hours, with the Destaining solution being replaced when needed.

Western Blot

In a western blot, the proteins separated by SDS-PAGE are transferred to a membrane so that they can be detected by antibodies. To achieve this, the SDS-PAGE gel and the 0.45 or 0.22 Nitrocellulose Membrane were sandwiched between Whatman paper and assembled in a Mini Trans-Blot® Cell in 1x Transfer Buffer. An electrical current was applied limited with 350 mA and set to 100 V for 60 minutes. Afterwards the membrane was blocked in 5% milk powder in PBS for 2h at room temperature or overnight at 4°C. The membrane was then washed three times in PBST, before the primary antibody was added in either 5% BSA or 5% milk powder in PBS. The blot was incubated with primary antibody for 1 h at room temperature or overnight at 4°C. The blot was once more washed three times in PBST, after which the secondary antibody was added in 5% milk powder in PBS. The blot was incubated with secondary antibody for 1 h at room temperature, after which it was washed three times with PBST. Chemiluminescence was measured using SuperSignal™ West Femto or Western Lightning Plus-ECL, Enhanced Chemiluminescence Substrate in a ChemiDoc™ XRS+. If probing with an additional antibody was desired, the horseradish peroxidase (HRP) coupled secondary antibody was deactivated by treating the membrane with 30% H₂O₂ for 15 minutes.

Affinity purification and LC-MS/MS analysis

The AP-MS screening, which was further analyzed in this thesis, was performed by M.H. For better comprehension of the dataset the methodology will be described here.

Triphosphorylated antisense 7SK (7SKas) RNA was synthesized by in vitro transcription with SP6 polymerase (RiboMAX Large Scale RNA Production Systems), in the presence or absence of biotin-16-UTP from linearized plasmid and purified by ammonium-acetate isopropanol precipitation. Aliquots of PPP-RNA were then mock-treated or dephosphorylated with alkaline phosphatase (FastAP). Synthetic oligoribonucleotides with a 3'-terminal C6 amino linker matching the first 22 nucleotides of the 5' untranslated region of Severe Acute Respiratory Syndrome Coronavirus HKU-39849 [PPP-r(AUAUUAGGUUUUUUACCUACCC)-NH₂] and a corresponding 2'-O-

ribose methylated RNA oligomer [PPP-r(AmUAUUAGGUUUUUUACCUACCC)-NH₂] were ordered from ChemGenes Corporation (Wilmington, MA, USA) and capped as described previously using the m7G Capping System. Capped RNA oligomers were then HPLC-purified, biotinylated with biotin-N-hydroxysuccinimide ester according to the manufacturer's instructions and again HPLC-purified. As control we used a corresponding 3'-terminal biotinylated and HPLC-purified oligoribonucleotide harboring a 5' hydroxyl group [OH-r(AUAUUAGGUUUUUUACCUACCCU)-biotin].

For quantitative purification of proteins binding to biotinylated synthetic or in-vitro transcribed nucleic acids, streptavidin affinity resin was first incubated either with 100 pmol aliquots of biotin-labelled 7SKas RNA, 5 nmol of RNA oligomers, 100 pmol 2'5'OAs, 100 pmol ATP or 100 pmol ISD in TAP buffer in the presence of 40 U RNase inhibitor for 60 min at 4°C on a rotary wheel. Poly(C) or Poly(U) agarose beads (20 µl bed volume) were either incubated with excess poly(I) or poly(A) or left untreated in TAP buffer. Beads were washed three times with TAP buffer to remove excess nucleic acids. Cell lysates from murine RAW macrophages, human THP-1 macrophages and drosophila S2 cells were prepared by flash-freezing cells in liquid nitrogen, followed by lysis in TAP buffer for 30 min on ice. Whole flies were mixed with TAP buffer and lysed by bead milling using the FastPrep-24 with Lysing Matrix D at 5500 rpm for 2 times 25 sec. Lysates were clarified by centrifugation at 16,000 × g for 10 min. Nucleic acid coated beads were incubated with 2-mg samples of cell lysates for 60 min, washed three times with TAP buffer, and twice with TAP buffer lacking Nonidet-P40 to remove residual detergent. Four independent affinity purifications were performed for each bait. Bound proteins were denatured by incubation in 6 M urea-2 M thiourea with 1 mM DTT for 30 min and alkylated with 5.5 mM iodoacetamide for 20 min. After digestion with 1 µg LysC at room temperature for 3 h, the suspension was diluted in 50 mM ammonium bicarbonate buffer (pH 8). The beads were removed by filtration through 96-well multiscreen filter plates, and the protein solution was digested with trypsin (Promega) overnight at room temperature. Peptides were purified on stage tips with three C18 Empore filter discs (3M) and analyzed by mass spectrometry as described previously (Rappsilber et al., 2007). Briefly, peptides were eluted from stage tips and separated on either 15cm or 20cm long C18 reversed-phase column by applying a 5% to 30% acetonitrile gradient in 0.5% acetic acid at a flow rate of 250 nl/min over a period of 95 min, using an EASY-nanoLC system. The nanoLC system was directly coupled to the electrospray ion source of an LTQ-Orbitrap XL mass spectrometer operated in



a data dependent mode with a full scan in the Orbitrap cell at a resolution of 60,000 with concomitant isolation and fragmentation of the ten most abundant ions in the linear ion trap.

Mass spectrometry RAW data were processed individually for each species (mouse, human, drosophila) using MaxQuant using the standard settings, label free quantitation and match between runs (match time window 2 min, alignment time window 30 min). The MaxQuant output was further analyzed using Perseus version 1.5.2.1. First, contaminants were removed, as well as the proteins identified by the single peptide. For statistical analysis, the LFQ values were log₂-transformed, missing values were replaced by sampling from the normal distribution (Replace Missing Values from Normal Distribution; settings: width: 0.3, downshift: 1.8, separately for each MS run). To identify enriched proteins, the intensity values in MS runs of NA bait were compared against the controls using two-sided Welch's t-test (S0 1; min. 2 valid values in at least one group) with a permutation-based FDR of 0.05 (for the poly(I:C) enrichment in fly a FDR of 0.001 was used instead). Imputed values were replaced by NaN. Candidate clustering is based on Euclidian distance and ward as agglomeration method.

Protein production in insect cells

The recombinant full length dTao (CG14217) was produced by the Core Facility of the Max Planck Institute of Biochemistry.

pCoofy27_dTao was used for baculovirus based expression in High Five cells (Scholz and Suppmann, 2017). Cells were lysed via douncing (1 mM AEBSF-HCl, 2 µg/mL Aprotinin, 1 µg/mL Leupeptin, 1 µg/mL Pepstatin, 2,4 U/mL Benzonase, 2mM MgCl₂). Protein purification was performed using the coupled N-His6 tag via affinity purification (Ni Sepharose High Performance GE) in His Binding Buffer (50 mM Na-P, 500 mM NaCl, 10 mM Imidazole, 10% Glycerin and 1 mM TCEP, pH 8) at 4°C for 2.5 h and washed with His Wash Buffer (50 mM Na-P, 500 mM NaCl, 20 mM Imidazole, 10 % Glycerin and 1 mM TCEP, pH 8). Purified protein was eluted from the beads using His Elution Buffer (50 mM Na-P, 500 mM NaCl, 250 mM Imidazole, 10 % Glycerin and 1 mM TCEP, pH 8). The protein was further purified by gel filtration (HiLoad 26/60 Superdex 200 GE) and eluted in Storage Buffer (20 mM Tris, 200 mM NaCl, 10 % Glycerin, 0.2 mM EGTA and 1 mM TCEP, pH 8) and concentrated (Amicon Ultra 15) at 3700 rpm, 4°C in 5 min steps. The production was verified using LC-MS.

Fluorescence quenching

Using the recombinant drosophila Tao kinase (dTao) we were then able to perform a fluorescence quenching assay with fluorescently labelled poly(I:C) to determine whether there is a direct interaction between poly(I:C) and dTao kinase. Using a fluorometer (Monolith NT.115), the fluorescence of the FITC-tagged poly(I:C) was measured with an increasing concentration of dTao kinase in Storage Buffer. As a control that the decrease of the fluorescence was not solely due to the increase of protein within the sample, an SD-test was performed. During the SD-test, the remaining sample used during the quenching assay was diluted 1:1 in a 4% SDS solution and boiled at 95°C for 5 minutes, thus denaturing the protein and removing any activation function. The fluorescence intensity of the thus treated samples was then measured. The analysis was performed using NanoTemper Technologies MO. Affinity Analysis v2.2.4 with Initial fluorescence settings.

Kinase assay

The ADP-Glo™ Kinase Assay kit was performed according to the manufacturer's instructions, with the addition of 0.3 mg/mL poly(I:C).

Full proteomic MS analysis

THP-1 cells with KO of TAOK1, -2, -3, STAT1 or NEG4 (control) were pIC- or mock-treated, or infected with SFV or IAV. Cell pellets of quadruplicates were lysed in FP lysis buffer, boiled at 99°C for 10 min and sonicated (15 min, 4°C, 30 sec on, 30 sec off, high setting; Bioruptor Plus). Protein concentrations of cleared lysates were normalized to 50 µg and proteins were pre-digested with 1 µg LysC (37°C, 3 h) followed by a 1:10 dilution (100 mM Tris-HCl pH 8) and overnight digestion with 1 µg trypsin at 30°C. Peptide purification on StageTips with three layers of C18 Empore filter discs (3M) and subsequent mass spectrometry analysis was performed as described previously (Hubel et al., 2019; Scaturro et al., 2018). Briefly, 1.5 µg purified peptides were loaded on a 50 cm HPLC column (60°C; 75 µm inner diameter; packed in-house with ReproSil-Pur C18-AQ 1.9 µm silica beads) and separated using an EASY-nLC system with a 120 min gradient and a binary buffer system, consisting of buffer A and buffer B at a flow rate of 300 nl/min (5-30% buffer B (95 min), 30-95% buffer B (10 min), wash-out at 95% buffer B for 5 min, decreased to 5% buffer B in 5 min, and kept at 5% buffer B for 5 min for re-equilibration). Eluting peptides were directly analyzed on a Q-Exactive HF mass spectrometer via a nano-electrospray source. Data-



dependent acquisition included repeating cycles of one MS1 full scan (300–1650 m/z, resolution of 60,000 at m/z 200) at an automatic gain control (AGC) target of 3×10^6 , followed by 15 MS2 scans of the highest abundant isolated and higher-energy collisional dissociation (HCD) fragmented peptide precursors (resolution of 15,000 at m/z 200). For MS2 scans, collection of isolated peptide precursors was limited by an AGC target of 1×10^5 and a maximum injection time of 25 ms. Isolation and fragmentation of the same peptide precursor was eliminated by dynamic exclusion for 20 s. The isolation window of the quadrupole was set to 1.4 m/z and HCD was set to a normalized collision energy (NCE) of 27%. All data was acquired in profile mode using positive polarity. Raw files were processed with MaxQuant (version 1.6.14.0) using standard settings, label-free quantification (LFQ) and match between run options enabled. Spectra were searched against forward and reverse sequences of the reviewed human proteome including isoforms (UniprotKB, release 10.2019) as well as SFV and IAV protein sequences by the built-in Andromeda search engine.

The output of MaxQuant was analyzed with Perseus (version 1.6.13.0) and visualized with R Studio (version 3.6.0). Detected protein groups within the proteinGroups.txt output table identified as known contaminants, reverse sequence matches, only identified by site or quantified in less than 3 out of 4 replicates in at least one condition were excluded. Following log₂-transformation, missing values of each replicate were imputed by sampling values from a normal distribution, calculated based on the original data distribution (width=0.3 s.d., downshift=-1.8×s.d.). Differentially expressed protein groups between control (NEG4) and TAOK1, -2, -3 or STAT1 KO THP-1 cells for each treatment were identified via two-sided Student's t-test ($S_0 = 0.1$, permutation-based FDR < 0.05, 250 randomizations). Protein groups with less than 3 measured intensities in at least one tested condition were excluded from statistical testing. Annotation with Gene Ontology terms corresponding to biological processes (GOBP), molecular functions (GOMF) and cellular compartments (GOCC) or Kyoto Encyclopedia of Genes and Genomes (KEGG) terms was performed within Perseus (downloaded from <http://annotations.perseus-framework.org>, 06.2019). Testing for the enrichment of annotations within significantly changing protein groups was done using Fisher exact test with the Benjamini-Hochberg-adjusted P-value cutoff set to 0.05.

Cytokine measurements

The cytometric bead array was measured by Silke Hegenbarth (AG Percy Knolle). The IFN- β ELISA, IP-10 ELISA and Bio-Plex sets were used according to the manufacturer's protocol. The ELISA and cytometric bead array were measured using an Infinite 200 PRO series micro plate reader and Bio-Plex 200 Luminex Technology, respectively.

Bioinformatic analysis

Analysis overlap Castello / Metascape IAV and domain enrichment

Protein superfamily domain annotations were identified using the CDD batch search. Metascape IAV hits were taken from (Tripathi et al., 2015) for at least 1 screening and Garcia-Moreno hits were taken from (Garcia-Moreno et al., 2019) Table S1, 18hpi quantitative. Significant enrichment of protein superfamily domains, Metascape IAV annotations and Garcia-Moreno hits within affinity purified protein groups across NA baits was calculated via Fisher exact test (Benjamini-Hochberg adjusted FDR > 0.05).

GO-Term enrichment of AP-MS data

The GO-Term enrichment, was performed by Alexey Stukalov. For better comprehension of the dataset the methodology will be described here.

EnrichmentMap (version 2018.12) was used to annotate the human proteins with Gene Ontology terms. To identify the terms that are specifically enriched among the protein binders of specific NA bait or shared by multiple NA baits, the OptEnrichedSetCover.jl Julia package was used (<https://github.com/alyst/OptEnrichedSetCover.jl>).

Orthologue analysis

For orthologues mapping, the DRSC Integrative Ortholog Prediction Tool was used excluding the orthologous with a DIOPT score less than 2 (low score). Identified human orthologues were filtered against an experimentally determined THP-1 proteome, so as to not include orthologues of proteins that could not be experimentally identified in THP-1 cells in the interspecies comparison.

Selection of Candidate Lists

The candidate list, which was used as the basis for the human KO screening, was selection by M.H. For better comprehension, the methodology will be described here.



After the statistical analysis of the data, a score was calculated for each bait-control comparison; $(foldchange \cdot -\log(p - value))^5 \cdot (proteome\ abundance)^{0.05} \cdot (number\ of\ affinity\ purifications\ with\ valid\ values)^{0.01}$. For each bait, the top 200 protein candidates of human were compared to the 200 best mouse ones. Then, factoring in regulation of potential candidates by type I or Type II interferon (fc >2) (interferome.org) and excluding known nucleic acid sensors and proteins involved in transcription, the final candidate list was manually selected.

Statistical analysis of the KO screening

The statistical analysis of the luminescence and resazurin data was performed in R (v3.3) by Alexey Stukalov.

Both resazurin and luciferase data were fit using the random effects generalized linear Bayesian model, which, in R glm notation, could be expressed as $\log_2(intensity) \sim 1 + batch + virus * gene$. The effects corresponding to the screen batch, the virus infection (*virus*), gene KO (*gene*) and the effect of interaction between the last two model factors were set to have horseshoe prior distribution (Carvalho et al., 2010). The distribution of $\log_2(intensity)$ was set to be Laplacian for robust handling of outliers. The model was fit with No-U-Turn Markov Chain Monte Carlo sampler implemented in rstan R package (ver. 2.15). 2000 iterations of the sampling method (1000 warmup + 1000 sampling) in 8 independent MCMC chains was done. The model parameters samples were collected at each 2nd iteration of MCMC run. To estimate the significance of the viral replication change, the reconstructed batch effect-free posterior distribution of luciferase intensity upon virus infection and gene KO (Luc_{KO}) was compared with the posterior distribution of NT control (Luc_{NT}). The significance was defined as the probability that the \log_2 fold-change of luciferase intensity is different from zero: $P_{value} = 2 \cdot \min(P(\log_2(Luc_{KO}/Luc_{NT}) < 0), P(\log_2(Luc_{KO}/Luc_{NT}) > 0))$. No P-value correction for multiple hypothesis testing was done, since it's handled by the choice of model parameters prior distribution.

Upstream promoter analysis

Upstream promoter analysis was performed using iRegulon in Cytoscape v.3.7.2.

Results

This study was conducted in the research group of Prof. Dr. Andreas Pichlmair at the Technical University of Munich Institute of Virology / Max-Planck Institute of Biochemistry with the help of collaborators from other research groups and institutes. Results from collaborators are indicated as such. This thesis also includes experiments conducted by three students, Simon Giosele, Swayanka Biswas and Teresa-Maria Lavacca, under my supervision.

NA interactor identification using proteomic quantification

The affinity purification based LC-MS/MS approach designed to identify novel NA interacting proteins utilized 17 different NAs. The NAs were selected to resemble NAs found during viral infection but with defined chemical or structural modifications: synthetic double-stranded (ds)RNAs (poly(I:C) and poly(A:U), 5' modified *in vitro* transcribed dsRNA (dsRNA-PPP and dsRNA-CAP0) and 5' modified *in vitro* transcribed single-stranded (ss)RNAs (ssRNA-PPP, ssRNA-CAP, ssRNA-CAP0, ssRNA-CAP1). Matched NAs were used as control baits: poly(C), poly(U), dsRNA-OH and ssRNA-OH. These control baits were selected because they have similar features to the bait, but are not generally considered as immune activators (Alexopoulou et al., 2001; Schmidt et al., 2009; Snead et al., 2013; Sugiyama et al., 2008). Additionally to the RNA baits, interferon stimulatory DNA (ISD), a DNA bait (Stetson and Medzhitov, 2006) and RNA:ISD, a RNA:DNA hybrid bait, were included, as well as the second messenger 2'5OAs, with the control ATP (Table 3).

Table 3: Overview of NA baits and controls used

	Bait	Description	Occurrence	Effect	References
synthetic RNA baits	Poly(I:C)	Heterogenous dsRNA polyinosine:polycytidine	Unknown	Activation of MDA5; Induction of cytokines and apoptosis	(Alexopoulou et al., 2001)
	Poly(C)	ssRNA polycytidine	Poly-C stretch in picornaviruses, e.g. FMDV and Cardiovirus	Unknown	(Alexopoulou et al., 2001; Sangar, 1979)
	Poly(A:U)	Heterogenous dsRNA polyadenylic:polyuridylic	Unknown	Activation of TLR3 and TLR7; Induction of cytokines	(Sugiyama et al., 2008)
	Poly(U)	ssRNA polyuridylic	Poly-U tail of bacterial small RNAs	No known effect	(Ishikawa et al., 2012; Sugiyama et al., 2008)
DNA baits	dsISD	Interferon stimulatory dsDNA	Genomes of most species and many DNA viruses, e.g. herpes-, baculo- and poxviridae	Activation of cGAS; Induction of interferon	(Kranzusch et al., 2013; Stetson and Medzhitov, 2006; Weitzman and Fradet-Turcotte, 2018)



	RNA:ISD	Interferon stimulatory ssISD annealed to antisense ssRNA	Formed during cellular transcription, as well as transcription of DNA viruses and reverse transcription of retroviruses	Activation of cGAS	(Mankan et al., 2014; Nadel et al., 2015)
	ssISD	Interferon stimulatory ssDNA	Parvo and circoviruses	Activation of DNA damage response	(Shulman and Davidson, 2017; Weitzman and Fradet-Turcotte, 2018)
ssRNA baits	ssPPP	ssRNA bearing triphosphate 5' end	Viral RNAs and genomes e.g. rhabd and paramyxoviruses; Inhibitory RNAs expressed by DNA and RNA viruses; RNAi based antiviral defense in fly	Induction of cytokines and apoptosis	(Hornung et al., 2006; Tassetto et al., 2017)
	ssCAP	5' Unmethylated capped ssRNA	Viruses infecting lower eukaryotes and vesicular stomatitis virus mutants	Impaired virus growth	(Decroly et al., 2011; Wang et al., 2007)
	ssCAP0	5' N7 methylated capped ssRNA	Viruses infecting lower eukaryotes, e.g. tobacco mosaic virus mRNA	Impaired virus growth; Induction of cytokines	(Decroly et al., 2011; Furuichi and Shatkin, 2000)
	ssCAP1	5' N7 2'O methylated CAP-ssRNA	mRNA of higher eukaryotes and mRNA of most viruses	Strong binder of translation factors	(Decroly et al., 2011)
	ssOH	5'OH-ssRNA	Unknown	Unknown	(Snead et al., 2013)
dsRNA baits	dsPPP	dsRNA bearing triphosphate end, annealed to antisense 5'OH-RNA	End structures of negative strand-RNA viruses, e.g. influenza virus panhandle structure	Activation of RIG-I; Induction of cytokines and apoptosis	(Schmidt et al., 2009; Weber et al., 2006)
	dsCAP0	5' N7 2'O methylated CAP-dsRNA, annealed to antisense 5'OH-RNA	Unknown	Activation of RIG-I	(Devarkar et al., 2016)
	dsOH	5'OH-dsRNA	Unknown	Unknown	(Schmidt et al., 2009)
other	2'5'OA	2'5' Oligoadenylate	Second messenger, induced by OAS during viral infection	Induction of interferons	(Silverman, 2007)
	ATP	Adenosine Triphosphate	Found in all life forms, required for intracellular energy transfer	Activation of P2 receptors; Induction of cytokines	(Cekic and Linden, 2016)

Using the above noted 11 baits and 6 controls M.H. performed 246 individual affinity enrichments with cell lysates of human (THP-1), mouse (RAW 264.3) and fly (Schneider 2) origin, as well as total fly lysate. In order to differentiate between NA interactors and background we performed a two-sided Welch's t-test comparing the bait to its respective control. Proteins were considered NA interactors only if there was a significantly more protein identified in the bait than in the control. In total, the AP-MS experiment identified 904, 1214 and 1479 NA interactors in human, mouse and fly, respectively.

As an initial verification of the AP-MS data, we surveyed known NA binding proteins for their binding patterns (Fig. 9A). Three prime repair exonuclease 1 (TREX1), which is known for degrading ISD (Schlee and Hartmann, 2016), was identified interacting

with all three ISD containing NAs. Furthermore, known RNA:DNA hybrid nuclease Ribonuclease H1 (RNASEH1) was identified during the RNA:ISD affinity purification, alongside three members of the ribonuclease H2 heterotrimeric complex (RNASEH2A, RNASEH2B and RNASEH2C) (Schlee and Hartmann, 2016). dsRNA activated PRR OAS3 was identified as interacting with poly(I:C) and not with DNA or chemically modified RNA baits (Hornung et al., 2014). Known triple-phosphorylated RNA binding PRR RIG-I was observed binding to PPP-RNA baits, and as anticipated proteins of the IFIT complex associated with chemically triple-phosphorylated and capped RNA baits (Schlee and Hartmann, 2016). Additionally, RNASEL was precipitated with its only known ligand 2'5'OAs (Hornung et al., 2014).

For additional validation, we verified the NA interacting capabilities of selected proteins through western blotting (Fig. 9B). Both in the AP-MS and in the western blot, SMARCA5 interacted with poly(I:C) and PARP12 with poly(A:U). ABCF1 and ABCF3, both members of the ATP-binding cassette (ABC) transporter superfamily, were identified as 2'5'OAs interactors in the AP-MS. Intriguingly, in the western blot we observed interaction with 2'5'OAs but not ATP or dephosphorylated 2'5'OAs, which is indicative of a phosphate dependent interact similar to RNASEL. The high degree of

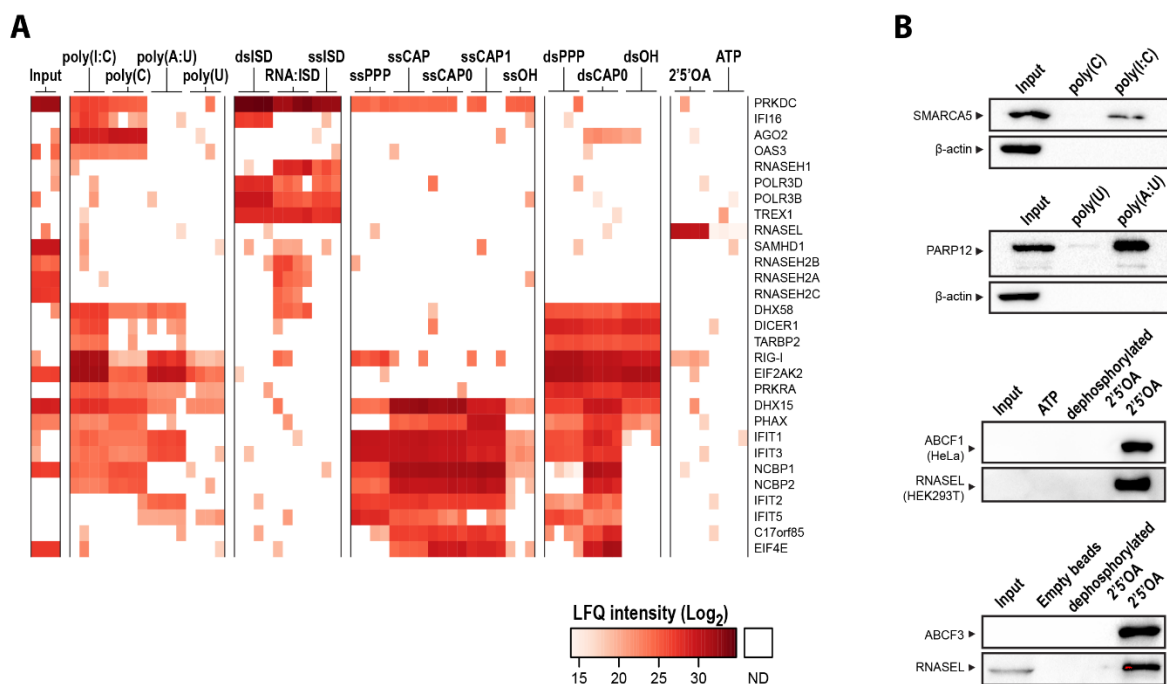


Figure 9: Validation of AP-MS interactors from the THP-1 screen. (A) Log₂ LFQ intensities for a selected set of known nucleic acid binders identified during the AP-MS screen. **(B)** Western Blots of selected candidates confirming NA interactions observed in the AP-MS screen.



similarity between the observed NA binding in the AP-MS and NA binding phenotypes described in literature speaks to the validity of the dataset.

Analysis of NA interactome

To gain an overview of the interactor distribution across the different NA baits, we generated an interaction network of the 904 human identified proteins (Fig. 10). We see a clear distinction between proteins interacting with RNA and with DNA, with 74 proteins interacting with both. Among the DNA and RNA interactors is DNA-PKcs (also known as PRKDC), a DNA-dependent protein kinase which is involved in DNA double strand break repair and was recently shown to also have an RNA-dependent function during ribosome biogenesis (Shao et al., 2020). Another interesting example is CDKN2AIP, a DNA damage regulator, which has also been shown to modulate growth of the PPP-RNA producing IAV (Cheung et al., 2014; Tripathi et al., 2015).

We also observe a clear distinction between the *in vitro* transcribed chemically modified baits, and the unmodified synthetic poly(I:C) and poly(A:U). In line with this, we see large overlaps between structurally similar baits. This is particularly visible when it comes to the CAP structure, with ssCAP1 and ssCAP0 (n=43, with n being the overlapping binding partners), ssCAP1 and ssCAP (n=30), ssCAP0 and ssCAP1 (n=30), as well as ssCAP0 and dsCAP0 (n=44). Among them are the three IFIT proteins, IFIT1, IFIT2 and IFIT3, which were enriched in all capped RNAs. While only IFIT1 has been described as a CAP binder (Habjan et al., 2013), IFIT2 and IFIT3 enhance IFIT1 binding to non-self NAs (Fleith et al., 2018).

Enrichment analysis of the identified NA interacting proteins reveals that 60% are annotated as RNA or DNA binding (478 RNA binding, 147 DNA binding and 69 both) (Binns et al., 2009). Furthermore, Reactome pathway analysis (Jassal et al., 2020) of all enriched proteins, independent of bait, produces 34 overrepresented pathways (FDR < 5.5E-15). Sorting based on the ratio of proteins identified per known proteins of that pathway, termed Reactome entities ratio, reveals that the top four related pathways are metabolism of RNA, cellular response to external stimuli, cellular response to stress and translation (Fig. 11 A). In addition, the remaining highly significant pathways include viral mRNA translation, influenza infection and influenza viral RNA transcription and replication.

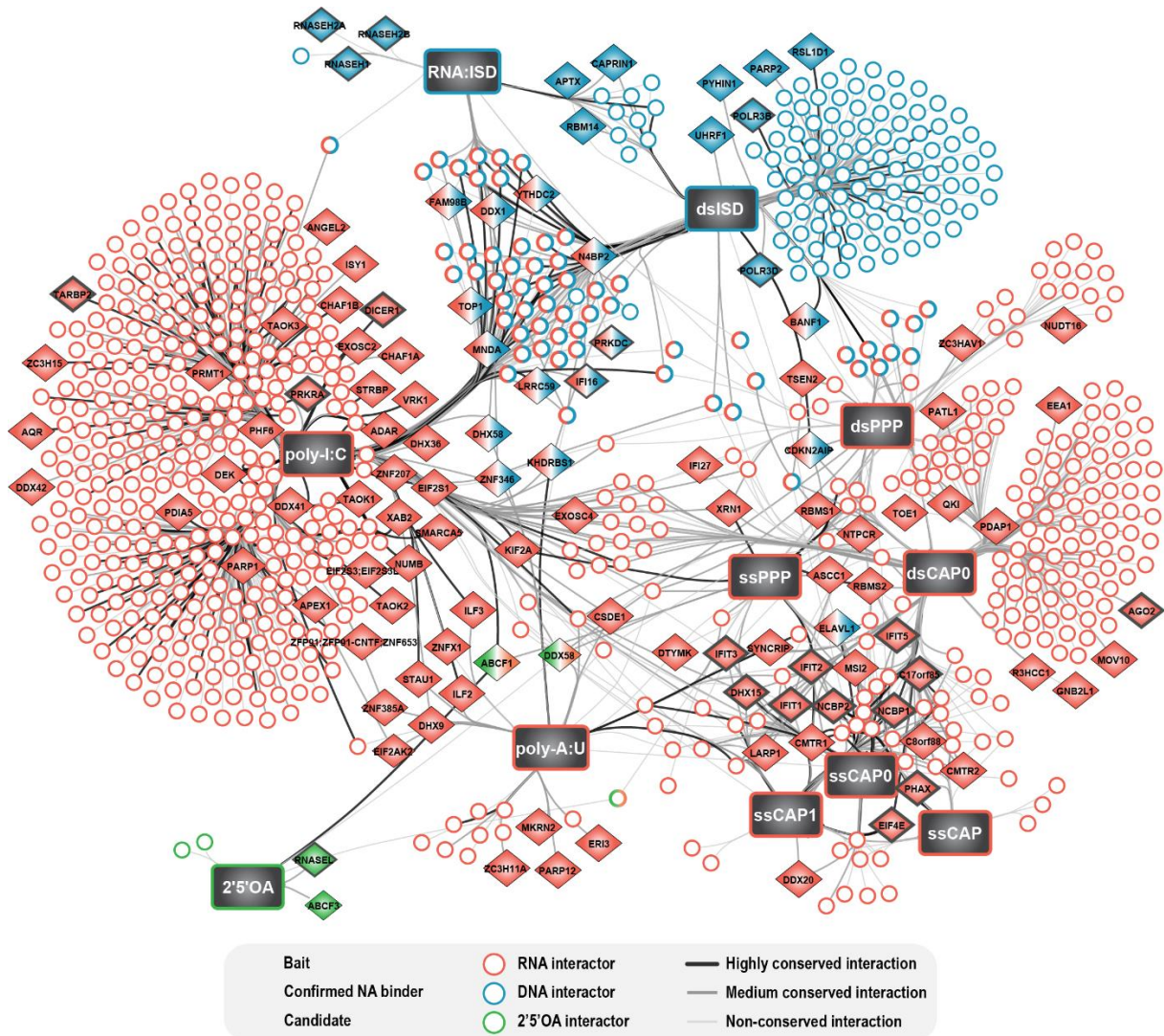


Figure 10: Network analysis of the significantly enriched proteins in the human AP-MS screening. Significance was calculated using the Welch's *t*-test with an FDR of 0.05. Known NA interactors and candidates for the KO screening, as well as conservation of individual interactions across species, are indicated.

As Gene Ontology (GO) term enrichment analysis of the individual affinity purifications reveals highly redundant GO terms, leading us to implement a functional enrichment analysis, performed by Alexey Stukalov. This analysis revealed 27 enriched GO terms across the individual bait control comparisons, 18 of which were GO terms related to NA biology (Fig. 11B). For example, we identified 'cellular response to exogenous dsRNA' for all RNA baits, which is linked to the identified proteins IFIT1, RIG-I and DHX9. DNA related GO terms, such as 'regulation of DNA-directed DNA polymerase activity' and 'nucleotide-excision repair, DNA incision, 5'-lesion' are both primarily linked to DNA baits (RNA:ISD and dsISD). Furthermore, the enrichment features GO terms related to NA degradation, e.g. 'nuclear-transcribed mRNA catabolic processes, nonsense-mediated decay', 'mRNA destabilization' and 'mRNA stabilization'. These

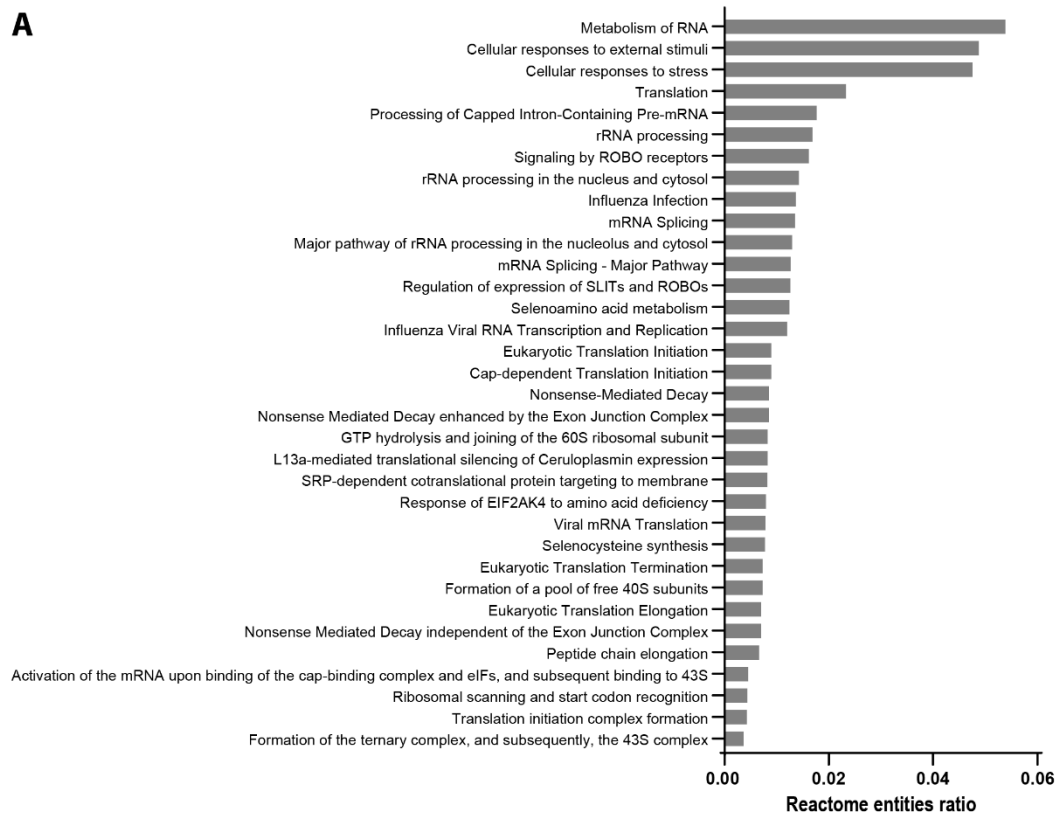


GO terms were identified in all of the RNA baits, and are primarily linked to proteins such as pre-mRNA processor HNRNPR and the RNA helicases MOV10 and DHX36.

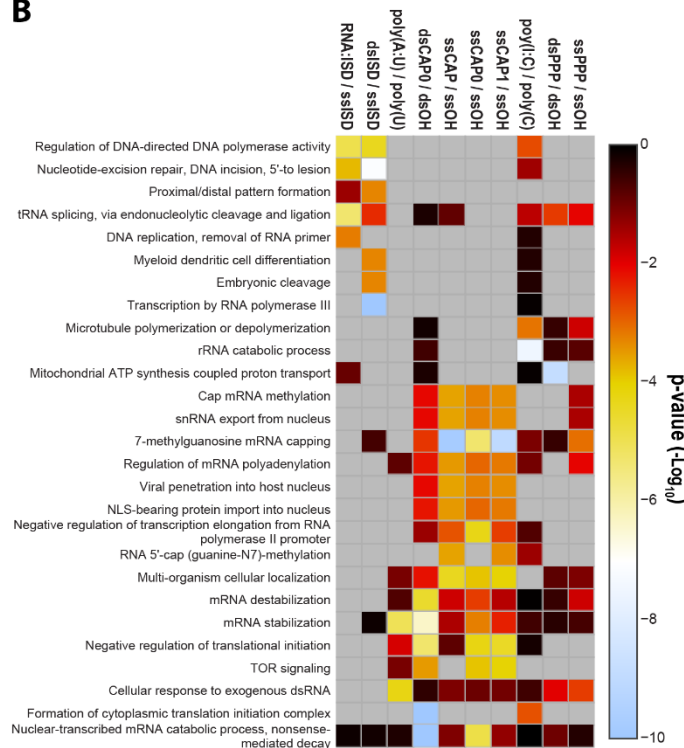
The final enrichment analysis performed on the NA interactome is a protein domain enrichment. As expected, we identify a large number of domains with annotated NA binding capability (Fig. 11C). For instance, the RNA recognition motif (RRM), a putative eukaryotic RNA-binding domain, was enriched among the interactors of poly(I:C), ssPPP, ssCAP0 and dsCAP0. We also observed enrichment of annotated DNA binding domains, bZIP and H1H superfamily domains, among DNA baits. However, this analysis led to some unexpected enrichments such as enrichment of the specific ssRNA/DNA binding R3H domains in dsRNA containing baits (e.g. dsCAP0 RNAs), and HEAT-EZ in ssCAP interacting proteins.

Within our AP-MS screening, the ATPases associated with a variety of cellular activities (AAA) domain superfamily, was enriched for 2'5'OAs, primarily due to the association of ABCF1 and ABCF3. The AAA superfamily members have been identified as key players in a number of cellular processes including protein quality control, cytoskeleton remodeling and membrane dynamics (Puchades et al., 2019). For example, AAA superfamily member VPS4 disassembles the endosomal sorting complex required for transport III (ESCRT-III) polymers (Puchades et al., 2019). ESCRT-III controls membrane fission reactions, and is coopted by many enveloped viruses, including HIV-1 and Herpes simplex virus 1 (HSV-1), to allow for the nuclear export of the virions (Arii et al., 2018; Morita et al., 2011; Votteler and Sundquist, 2013).

A



B



C

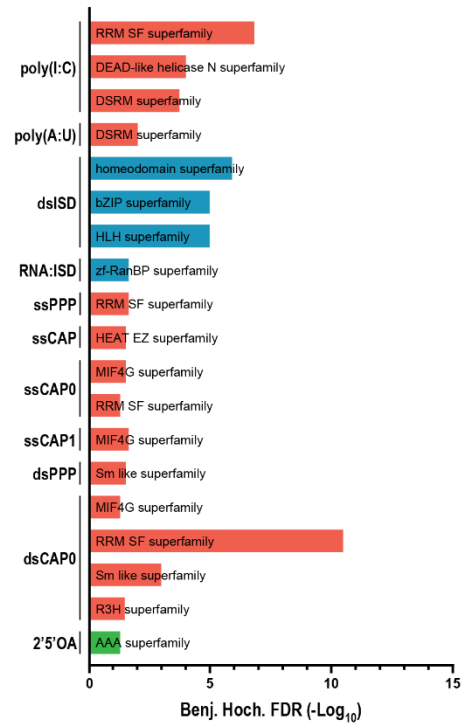


Figure 11: Analysis of AP-MS dataset. (A) Results of the Reactome pathway enrichment analysis across all significantly enriched proteins independent of bait. All pathways with an FDR lower than $5.22E-15$ are shown. The Reactome entities ratio indicates the highest number of identified proteins per pathway compared to the number of known proteins in this pathway. **(B)** Gene Ontology Biological Processes terms enriched in the identified NA interacting proteins. The color indicates the $-\log_{10}(p\text{-value})$ of the Fisher Exact Test (one-sided, unadjusted) for the enrichment of a given Gene Ontology Biological process term. Gene Ontology Biological Processes terms enrichment was performed by



Alexey Stukalov. (C) Enrichment of known NA binding domains per bait. Significance was calculated via Fisher exact test (Benjamini-Hochberg adjusted FDR < 0.05).

Comparative analysis of NA interactome with viral datasets

In order to gain an initial approximation of whether the proteins identified in the AP-MS are linked to the antiviral immune response, we intersected our dataset with published screenings studying the impact of protein depletion on viral replication or protein levels during viral infection. Intersection of the AP-MS data with an RNA binding interactome in cells infected with the ssRNA virus SINV (Garcia-Moreno et al., 2019) reveals an overlap of 96 different proteins, most of which interacted with an RNA bait (n=81). Included in the overlapping proteins is a cluster of proteins belonging to the HEXIM1-DNA-PK-paraspeckle components-ribonucleoprotein complex (HDP-RNP): MATR3 SFPQ, PSPC1, NONO and RBM14. Functions of the HDP-RNP include controlling gene expression through nuclear retention of A->I hyperedited RNA and mediating cGAS-STING activation (Bond and Fox, 2009; Morchikh et al., 2017). Furthermore, SFPQ and NONO have also been shown to regulate HIV-1 replication by binding to *cis*-acting regulatory elements found on HIV-1 mRNA, causing mRNA downregulation (Zolotukhin et al., 2003), with NONO also directly interacting with both the HIV-1 capsid and cGAS (Lahaye et al., 2018). Another HDP-RNP complex member, MATR3 also post-transcriptionally regulates HIV-1 replication, though it appears to act as a cofactor to the viral Rev protein (Sarracino et al., 2018).

Intersection of the AP-MS data with a meta-analysis of genome-wide RNAi depletion datasets followed by the assessment of ssRNA virus IAV replication (Tripathi et al., 2015), identified 150 overlapping proteins. Of these 134 are IAV host factors and 12 are IAV antiviral restriction factors and four are noted as both (KHSRP, CIRBP, RRP1B and PPAN) (Tripathi et al., 2015). As with the SINV interactome, a large portion of the overlapping proteins interacted with RNA baits (n=127). In addition, over half of the proteins identified in the overlap had previously been annotated as RNA binders (n=97) (Binns et al., 2009), six of which have well established antiviral activity (DHX15, PRKRA, EIF2AK2, IFIT2, POLR3B and IFIT5). PRKRA, which was enriched with poly(I:C) in our AP-MS screen, is a noted restriction factor for IAV (Tripathi et al., 2015). A previous study shows that EIF2AK2A binds to foreign dsRNA, upon which it activates a viral restriction factor EIF2AK2 (also known as PKR) (Samuel, 2001). EIF2AK2, which was also identified both in our AP-MS data set and the IAV replication meta-

analysis database, is an IFN-inducible, dsRNA-dependent protein kinase (Samuel, 2001) that as previously noted phosphorylates EIF2 α , thereby inducing a global stop of protein synthesis (Hur, 2019). Taken together, this shows that not only do the identified proteins directly interact with viral RNA, but that some of the identified proteins are capable of participating in and modulating the immune response.

Intersection of AP-MS from human, mouse and fly

In addition to the AP-MS in human cell lysates, M.H. performed the AP-MS analysis in mouse (RAW 264.3) and *D. melanogaster* (total flies and Schneider S2 cells). We detected 1214 significantly enriched proteins in mouse and 1480 in fly (1230 in whole fly lysate, 144 in S2 cells and 106 in both), with a similar distribution for the individual baits as in humans (Fig. 12A, B).

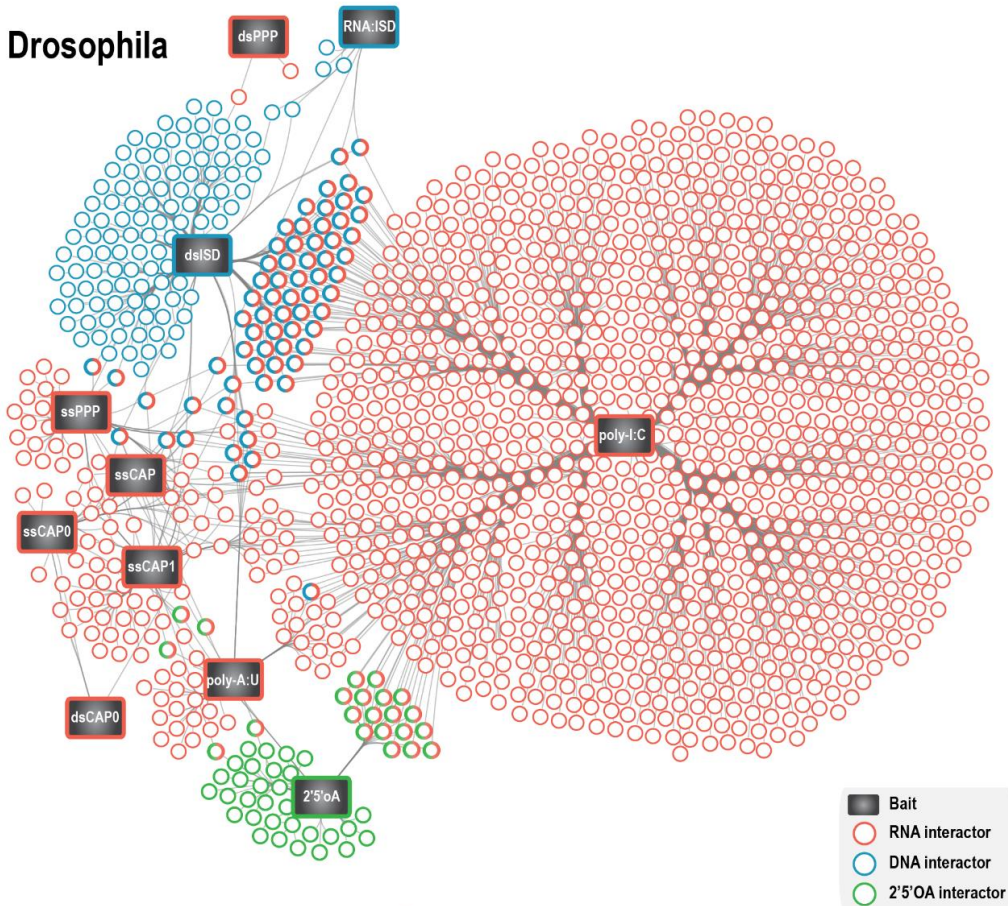
As the aim of the project is to use evolution to identify conserved, and therefore hopefully relevant, NA interactors, we next identified the human orthologues of the significantly enriched proteins in mouse and fly using the DRSC Integrative Ortholog Prediction Tool (DIOPT) (Hu et al., 2011). Of the identified human proteins, 63% were also found in mouse and 44% in flies. Comparison of the AP-MS data per bait across the different species allowed for the identification of conserved NA interactors. For example 127 proteins were conserved across all three species in the poly(I:C) AP-MS, among them the previously noted nucleic acid interactor Adar. Six proteins were conserved across all three species in the ssPPP affinity purification (Fig. 13A). In the 2'5'OA precipitate, only ABCF1 was conserved across all three species.

In order to prioritize the 904 identified human candidates M.H. calculated a strength score for each protein. The strength score is based on the interaction strength between the NA bait and interactor, specifically favoring generally less abundant proteins. The score was calculated for human and mouse NA interactors in parallel. The 200 proteins with the highest strength score of human and mouse were intersected. Factoring in IFN regulation and GO terms related to NA interaction of these proteins led to a selection of 90 candidates (Fig. 13B).



A

Drosophila



B

Mouse

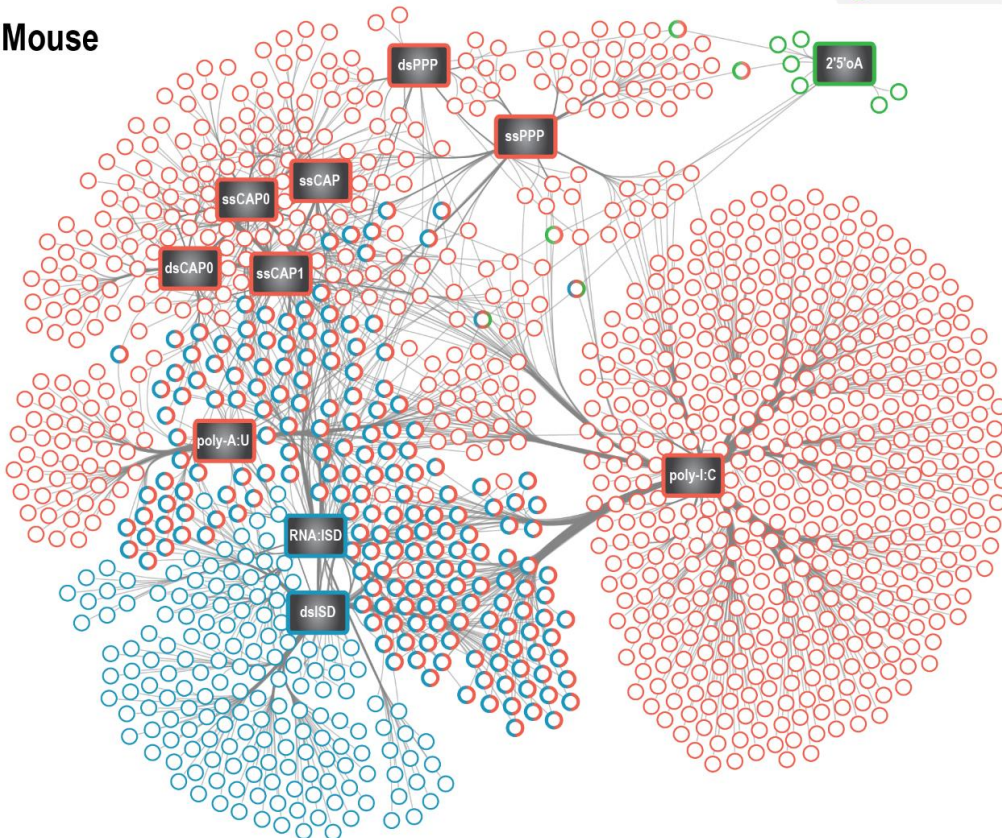


Figure 12: Network analysis of the significantly enriched proteins in the fly (A) and mouse (B) AP-MS screening. Significance was calculated using the Welch's *t*-test with an FDR of 0.05. For the whole fly poly(I:C) samples the FDR was reduced to 0.001.

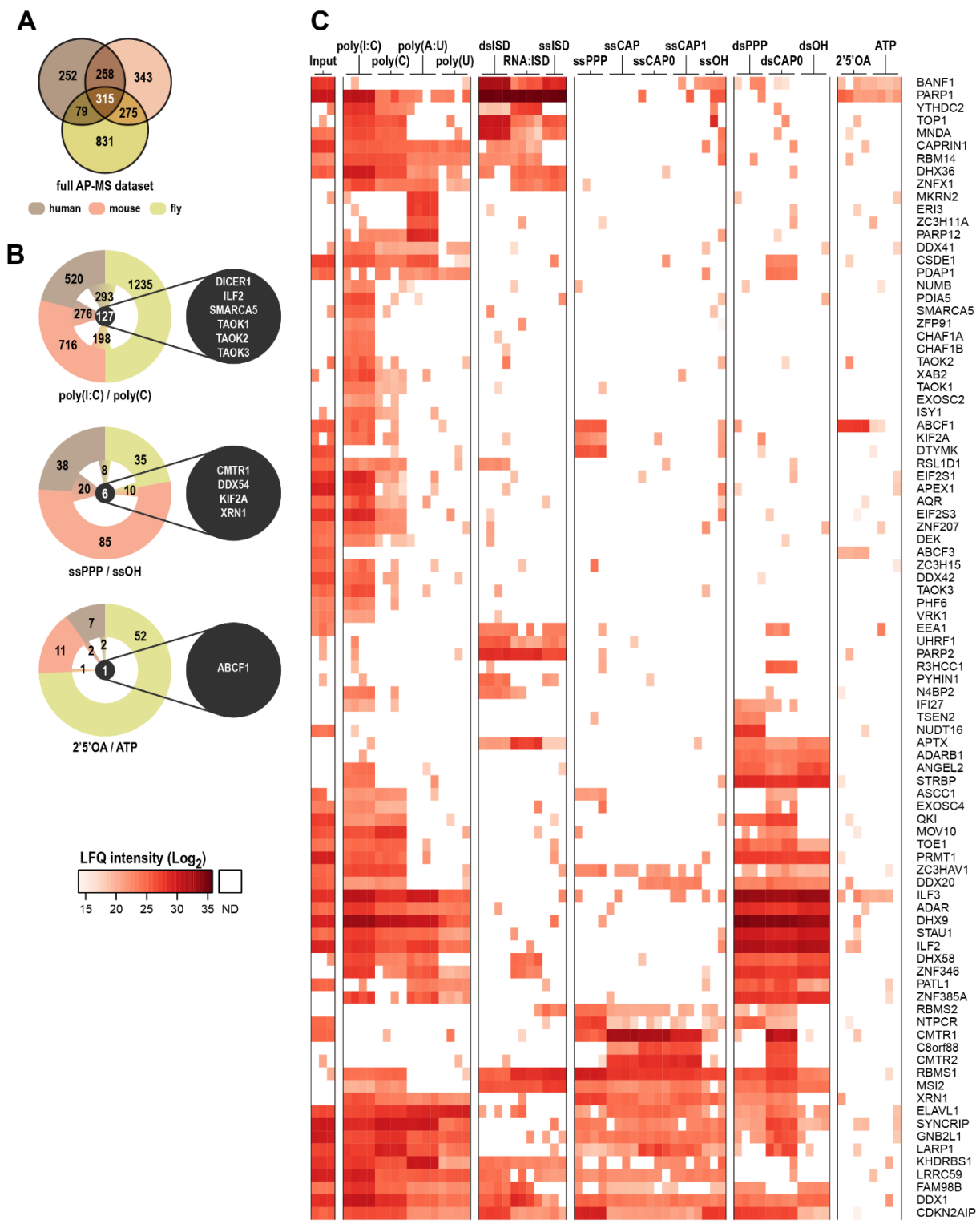


Figure 13: Orthologue analysis and selection of candidates. (A) Venn diagram of all enriched proteins identified in the AP-MS screen, independent of bait. (B) Significantly enriched proteins identified for poly(I:C) (top), ssPPP (middle) and 2'5'OAs (bottom) considering overlap of orthologues. Selected proteins enriched in all three species are listed in the callout circle. (C) Heatmap displaying log₂ LFQ intensities of the 90 candidates selected by M.H.. ND: not detected.



Lentivirus based arrayed CRISPR Cas9 screening of the candidate list

In order to identify which of the proteins selected from the NA AP-MS are functionally relevant, we conducted a lentivirus based arrayed CRISPR Cas9 knockout (KO) screening in human monocytes (THP-1) with four different viruses. To this end, KO cells for each of the 90 proteins of interest were generated and either left undifferentiated or differentiated with PMA into macrophages (Fig. 14A). The KO cells were then infected with a panel of luciferase tagged viruses: vesicular stomatitis virus (VSV, non-segmented neg. strand ssRNA), IAV (segmented neg. strand ssRNA), semliki forest virus (SFV, pos. strand ssRNA) and HSV-1 (dsDNA). The level of viral replication and gene expression was measured by luciferase activity. In order to exclude toxicity effects caused by deletion of the protein of interest, a cell viability assay was performed in addition to the evaluation of the viral luciferase levels (Fig. 14B). Furthermore, in order to assure the functionality of the screen, depletion of STAT1, a well-known ISG transcriptional activator, was included as a positive control as well as the addition of four non-targeting negative controls. As anticipated, comparison of the non-targeting controls and the STAT1 KO showed an increase in luciferase signals for all of the tested viruses (Fig. 14C).

Of the 89 candidates tested (one candidate had to be excluded due to technical reasons), KO of 64 candidates led to a significant change in luciferase activity for at least one virus in non-differentiated or differentiated cells (Fig. 14C). For 43 of the proteins, we noted an increase in luciferase activity, indicating that these proteins are viral restriction factors, whereas 13 appear to be host factors, leading to a decrease in luciferase activity (Table 4).

Table 4: Number of potential anti- and pro-viral factors, sorted both by virus and by THP-1 treatment.

	IAV		HSV		SFV		VSV		Summary	
	-	+	-	+	-	+	-	+	-	+
PMA										
Antiviral	27	23	4	18	9	5	1	8	32	42
Pro-viral	1	0	3	1	14	3	3	2	19	6



using resazurin. The color indicates the mean relative cell viability of three repeats compared to the control. The two-sided P -value is defined as probability that $\log_2(\text{LucKO}/\text{LucC})$ is different from 0; significant changes ($P\text{-value} \leq 0.05$; $\text{LucKO}/\text{LucC} \geq \log_2(1.5)$) are highlighted with dots. Data represents the median of biological triplicates. **(C)** \log_2 Fold change of the luciferase signal during the depletion screening compared to the control. The two-sided P -value is defined as probability that $\log_2(\text{LucKO}/\text{LucC})$ is different from 0; significant changes ($P\text{-value} \leq 0.05$; unadjusted) are highlighted with dots. Data represents the median of biological triplicates.

We were also able to identify functional connections between the NA affinity and the antiviral activity observed for individual candidates. In general we observe that proteins interacting with RNA baits in the AP-MS screening display overall more pronounced effects during infection with RNA viruses ($n=53$), but also more specific traits of the individual viruses can be found reflected in the NA affinity. Notable examples of this include the PPP-RNA interactors NTPCR, TSEN2 and RBMS2, which when depleted led to an increase in viral growth for the PPP-RNA generating IAV, while not affecting viral replication of the other tested viruses. We also observed that depletion of the DNA interactor UHRF1 led to an increase of replication in the dsDNA virus HSV-1.

Similarly, depletion of dsRNA interactors KHDRBS1, APEX1 and MKRN2 led to a decrease in SFV growth. The effect of the dsRNA interactors on the ssRNA virus SFV is noteworthy, as SFV replication causes the accumulation of dsRNA in the cytosol (Bauernfried et al., 2020). Strikingly MKRN2 was previously shown to negatively regulate the NF- κ B subunit p65 after stimulation with LPS, with depletion of MKRN2 causing an increase of the pro-inflammatory cytokines IL-6 and TNF- α (Shin et al., 2017). If MKRN2 also acts as a negative regulator of the NF- κ B induced immune response during viral infection, this may explain why depletion of MKRN2 leads to a decrease in viral replication.

Two other interesting examples of virus specific effects are KIF2A and XRN1, both of which were identified as interacting with PPP-RNA and poly(I:C). The depletion indicated that both were proviral for SFV, which produces large amounts of dsRNA, and antiviral for IAV, which generates PPP-RNA. Furthermore, the proviral effect of XRN1 in SFV is in line with an upregulation of XRN1 during infection with SINV (Garcia-Moreno et al., 2019), which belongs to the same family as SFV, the *Togaviridae*.

We also identified a number of proteins that appear to have a broad antiviral phenotype, as indicated by the increase in luciferase activity for multiple viruses. Particularly striking are TAOK2 (HSV-1, SFV and IAV), RSL1D1 (HSV-1, IAV and VSV) and ZFP91 (HSV-1, IAV and VSV).

TAO kinases as antiviral proteins

The three human TAO kinases, their respective mouse orthologues, and the single fly Tao kinase were all identified as synthetic dsRNA interactors in the AP-MS screening. Furthermore, in the KO screening TAOK1 and TAOK3 were antiviral during IAV infection, while TAOK2 was antiviral during HSV-1, SFV and IAV infection. Similarly, in a parallel shRNA knockdown screen in *D. melanogaster*, *D. melanogaster* Tao (dTao) displayed an antiviral phenotype for Drosophila C Virus (DCV) and VSV. These results indicate that both the NA interaction and the antiviral activity of TAO kinases are conserved across species and warranting further investigation.

Validation of TAOK2 screening phenotypes

To validate the AP-MS results, we first repeated the affinity purification of THP-1 lysates with poly(I:C) as bait. The affinity purification was evaluated by western blot (Fig. 16A) and this verified the association of human TAO kinases with poly(I:C), but not the poly(C) negative control.

We wanted to confirm the observed antiviral phenotype. To do so, we infected TAOK2 and control KO THP-1 cells with SFV expressing mCherry (SFV-mCherry) (Fig. 16B) and using fluorescence time-lapse microscopy we were able to quantify the fluorescence signal of SFV-mCherry over time. We observed that loss of TAOK2 ($p < 0.05$ at 15 hpi) and STAT1 ($p < 0.05$ at 21 hpi) led to an increase in SFV-mCherry

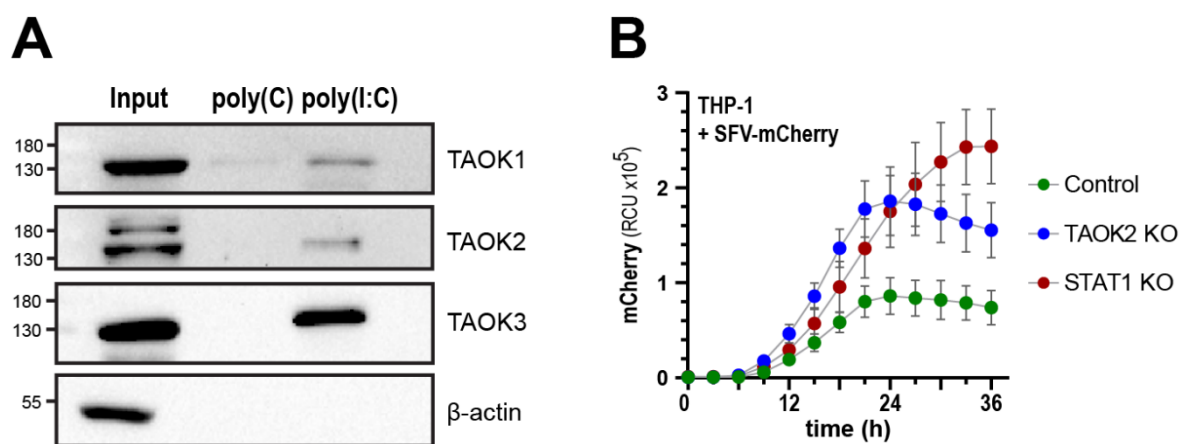


Figure 15: Validation of TAOK2 phenotypes observed in AP-MS and KO screening. (A) THP-1 cell lysate was incubated with poly(I:C) and poly(C) coupled agarose beads. The co-precipitating proteins were then analyzed via Western Blotting. (B) THP-1 TAOK2 KO, STAT1 KO and scrambled control cells were infected with SFV-mCherry (MOI 5). Red fluorescence intensity was measured every 3 hours using an Incucyte S3 live cell imaging system. The graph shows mean integrated red intensity / cell confluence per image (RCU) (y -axis) \pm SD over time (x -axis). Two-way ANOVA with Geissser-Greenhouse correction and Sidak's multiple comparisons test was performed to evaluate the significance.



fluorescence when compared to the scrambled control, thereby confirming the phenotype observed in the screening.

TAOK2 can be transiently, but not stably overexpressed

As we were unable to clone full-length human TAOK2, we acquired plasmids with two truncated versions of rat (*rattus norvegicus*) TAOK2 from M. Cobb (Chen et al., 1999). The two truncated versions of TAOK2 encompass amino acids (i) 1-451 and (ii) 1-993 of the total 1235 aa (Fig. 17A). The protein sequence of rat TAOK2 and human TAOK2 are highly similar, with 93% amino acid sequence overlap. Both versions include the protein kinase domain, while 1-993 aa also includes the first section of the transmembrane domains. Both truncated versions of TAOK2 were cloned into a doxycycline inducible plasmid and transiently transfected into HEK293R1 cells. One hour after transfection the expression of TAOK2 was induced using doxycycline and cell viability was measured following overnight incubation. We observed that induction with doxycycline leads to a decrease in cell viability (Fig. 17B). Despite the decrease in cell viability, we were still able to detect the overexpression of both truncated versions by western blot against the included V5-tag (Fig. 17C).

We next attempted to create stable, inducible, TAOK2 overexpression cell lines using lentiviral transduction of THP-1 followed by selection with puromycin for two weeks. In doing so, we also created a kinase dead version by mutating aspartic acid 151 within the active site of the kinase into an alanine (D151A). When the TAOK2 expression were induced with doxycycline, we observe overexpression of both WT and D151A 1-451 aa truncated TAOK2 based on the detection of the V5-tag, but we do not observe any expression of 1-993 aa truncated TAOK2 (Fig. 17D). Similarly, staining the membrane with a direct TAOK2 antibody did not indicate overexpression of 1-993 aa truncated TAOK2. While the transient overexpression of 1-993aa is possible, the creation of a stable 1-993aa expressing cell line is not.

In order to differentiate between TAO kinases interacting with poly(I:C) directly or as part of a complex, recombinant TAO kinase was required. Due to post-translational modifications, expression of mammalian kinases in bacteria is difficult. We therefore opted to collaborate with the Core Facility at the Max-Planck Institute of Biochemistry to overexpress and isolate both truncated versions of TAOK2 as well as dTao using the baculovirus insect cell expression system. Again, while 1-451 aa truncated TAOK2

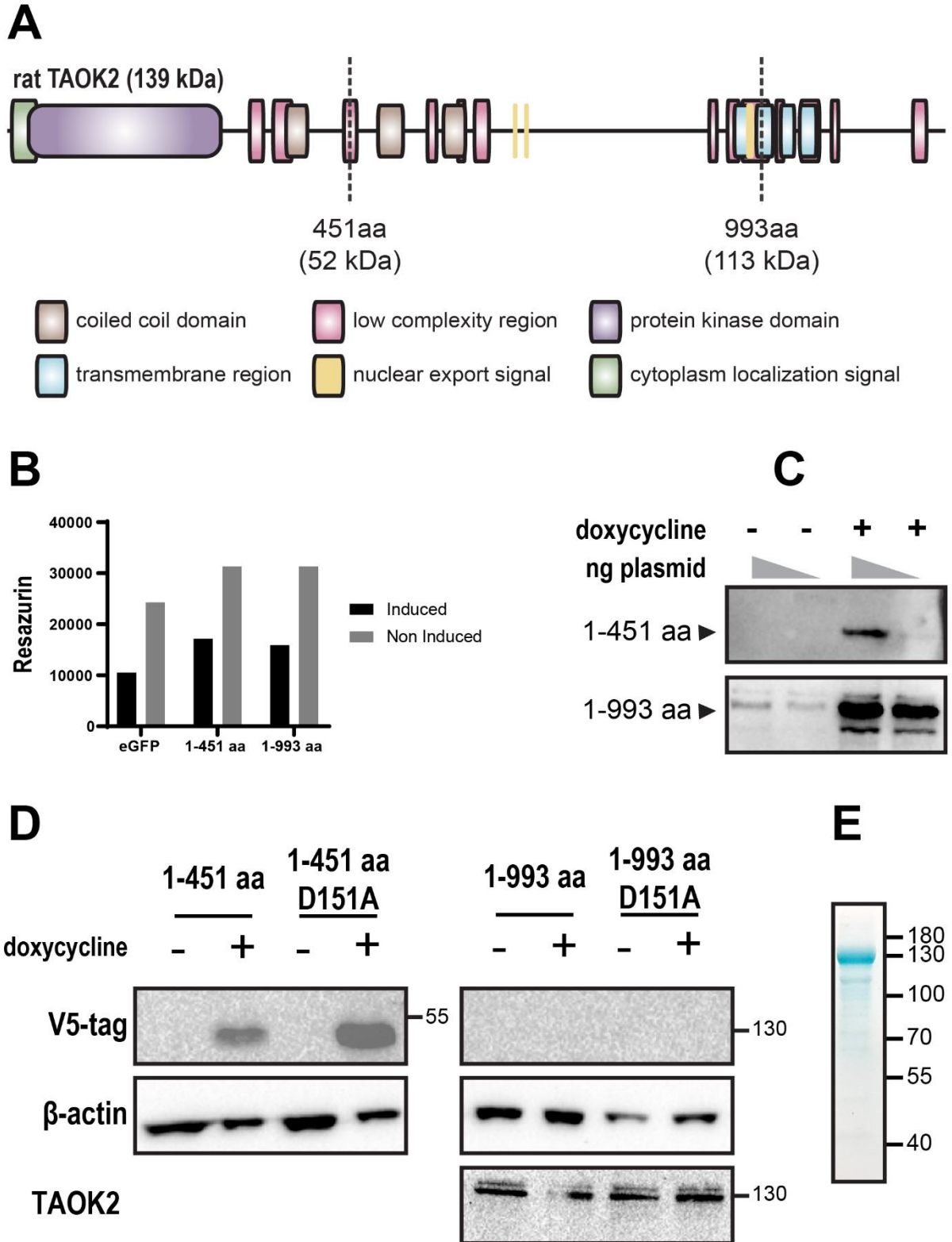


Figure 17: Transient and stable TAOK2 overexpression. (A) Schematic of rat TAOK2 depicting fragment sizes. (B) Results of cell viability assay on TAOK2 overexpressing cells. HEK293R1 cells were transfected with 200 ng of 1-451 aa and 500 ng of 1-993 aa. (C) Western Blot for the C-terminally fused V5 tag on both truncated TAOK2 plasmids. Both plasmids were tested at 100 and 200ng /500 μ L in HEK293R1 cells. (D) Stable TAOK2 overexpressing cell lines. TAOK2 overexpression lentivirus was generated and used to infect THP-1 cells. Cells were maintained on selection media for 16 days before TAOK2 expression was induced with doxycyclin. (E) Coomassie stain of recombinant dTAO produced by the Max-Planck Institute for Biochemistry CoreFacility.

was able to be expressed and isolated, 1-993 aa truncated TAOK2 did not express. We were also able to express and isolate full-length dTao (Fig. 17E).

dTao directly interacts with poly(I:C) and the interaction affects kinase activity

Having expressed and isolated recombinant dTao, we were able to test if the observed interaction between TAO kinases and poly(I:C) is due to a direct interaction or not. In order to so, we performed a fluorescence quenching assay. Increasing concentrations of dTao were incubated with FITC tagged poly(I:C), after which the fluorescent signal was measured. We observed a direct interaction between dTao and poly(I:C) with a K_d of 42 ± 15.66 nM (Fig. 18A) and denaturing of dTao with SDS terminated the interaction (Fig. 18B).

Our next question was whether the interaction between dTao and poly(I:C) impacts kinase activity. To this end, we performed a kinase assay, measuring the ATP consumption of dTao with and without poly(I:C). We noted a distinct increase in kinase activity upon the addition of poly(I:C), while poly(I:C) itself did not modulate the assay (Fig. 18C). This indicates that dTao interacts directly with poly(I:C) and that the kinase activity is impacted by the interaction with poly(I:C).

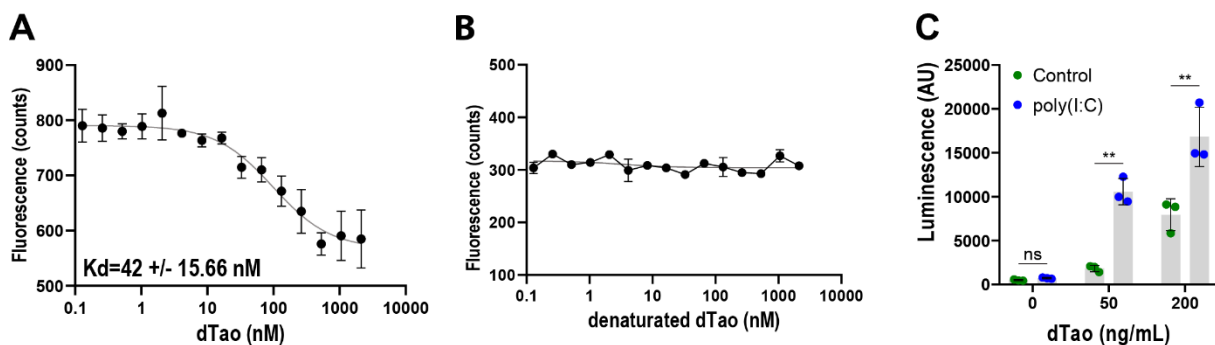


Figure 18: dTao directly binds poly(I:C) and this interaction affects kinase activity. (A) Fluorescence quenching assay showing fluorescence of FITC-tagged poly(I:C) incubated with increase concentration of dTao kinase. Shown is the mean fluorescence intensity (\pm SD) of three measurements. The indicated K_d was calculated using Affinity Analysis v2.2.4 (NanoTemper Technologies). **(B)** Fluorescence quenching assay showing fluorescence of FITC-tagged poly(I:C) incubated with increase concentration of denatured dTao kinase. dTao was denatured by 1:1 dilution in 4% SDS and boiling at 95°C for 5 minutes. Shown is the mean fluorescence intensity (\pm SD) of two measurements. **(C)** dTao was incubated with and without 0.3 mg/mL poly(I:C) and kinase activity was measured using a luminescence based ATP consumption assay. The histogram shows the mean of three parallel measurements \pm SD and is representative of three independent repeats. ** $p < 0.01$ (unpaired Welch's t -test), AU: arbitrary units.

Loss of TAOK2 leads to a decrease in ISG expression

Our next aim was to gain a deeper understanding of TAO kinase function in context of viral infection. Consequently, we generated lentivirus based CRISPR Cas9 KO cells of the three TAOKs as well as scrambled controls, using the same gRNA as in the KO screening and the loss of TAOK expression was successfully validated via western blot (Fig. 19A). We then performed a full proteomic analysis of the KO cells in SFV infected and uninfected conditions, which allowed us to evaluate the expression patterns of 5272 proteins in parallel. Overall, we noted that depletion of TAOKs lead to a significant expression difference in numerous proteins compared to the scrambled control in the SFV infected samples. Especially in TAOK2 KO cells, we observed negative

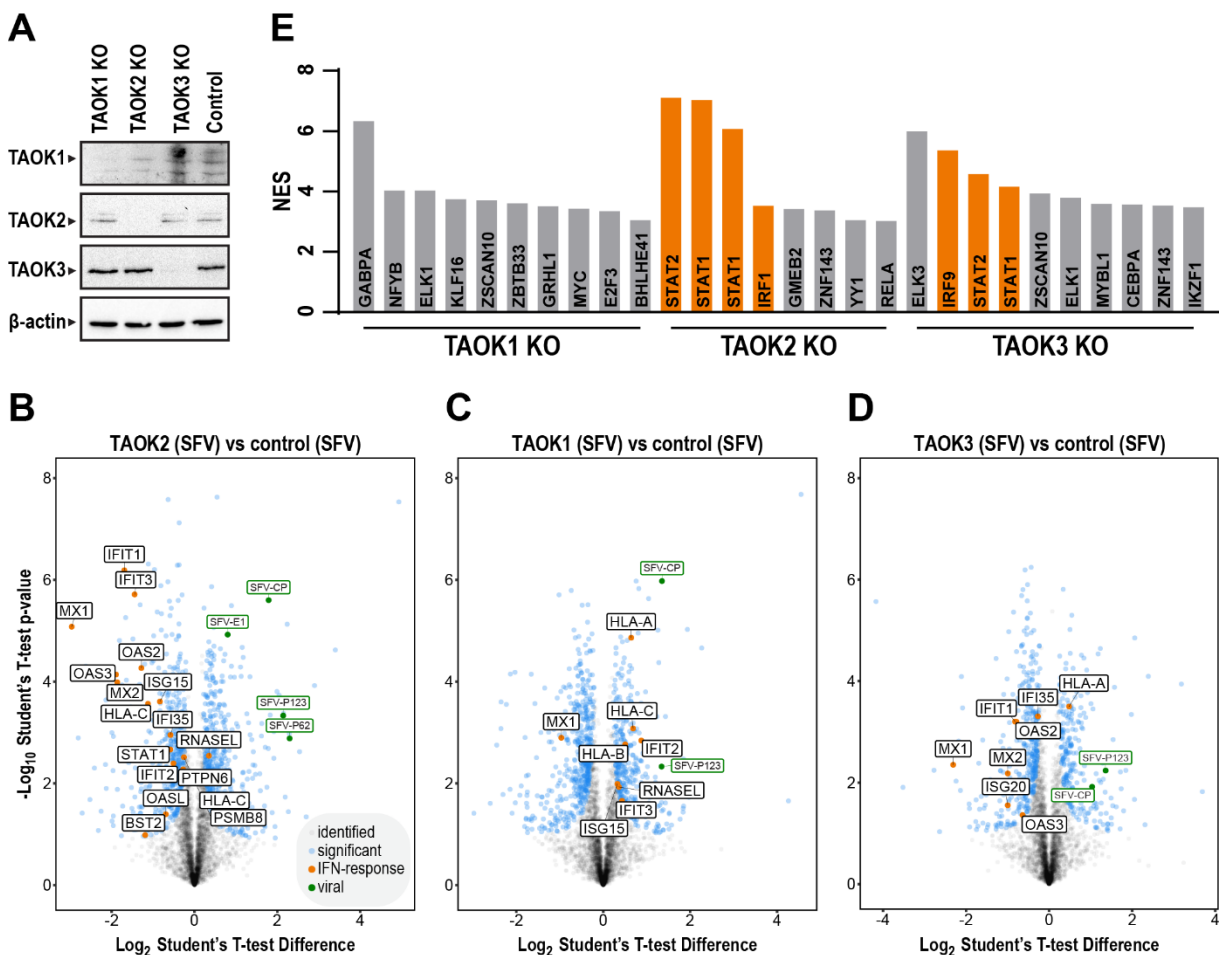


Figure 19: TAOK2 affects ISG expression. (A) Western Blot confirming depletion of TAO kinases in THP-1 cells. (B-D) THP-1 KO and scrambled control cells were infected with SFV (MOI 10) for 24 h and the proteome expression was analyzed using MS. Volcano blots depict protein expression patterns during infection for TAOK1 (C), TAOK2 (B) and TAOK3 (D) compared to the scrambled control. Proteins with significantly different expression are highlighted in blue, proteins belonging to the GO-Term 'cellular response to type I interferon' are marked in orange and viral proteins in green. The data shown is averaged across four biological repeats and significance was determined using two-sided Student's t-test (permutation-based FDR <0.05). (E) Upstream promoter analysis of proteins with a significant lack of upregulation during SFV infection in TAOK2 KO cells compared to scrambled control. Transcription factors linked to interferon-regulated innate immunity, based on Reactome pathway enrichment analysis, are marked in orange. Normalized Enrichment Score (NES) indicates the enrichment score of the given transcription factor.

differential expression of proteins belonging to the innate antiviral immune response, including MX1, MX2, OAS3 and IFIT1 (Fig. 19B). Interestingly, MX1 expression in particular was also reduced in infected TAOK1 and TAOK3 KO cells (Fig. 19C, D). Unbiased GO-term analysis of differentially expressed proteins in control VS TAOK2 KO cells highlighted the enrichment for proteins involved in ‘cellular response to type I interferon’ and ‘type I interferon-mediated signaling’, fitting with the predominant differential regulation of ISGs. An unbiased promoter analysis (Janky et al., 2014) performed on all proteins that failed to be upregulated in SFV infected TAOK2 KO cells compared to the scrambled control cells indicated the involvement of eight transcription factors, including STAT1, IRF1 and STAT2 (Fig. 19E), further supporting the link between IFN based immunity and TAOK2.

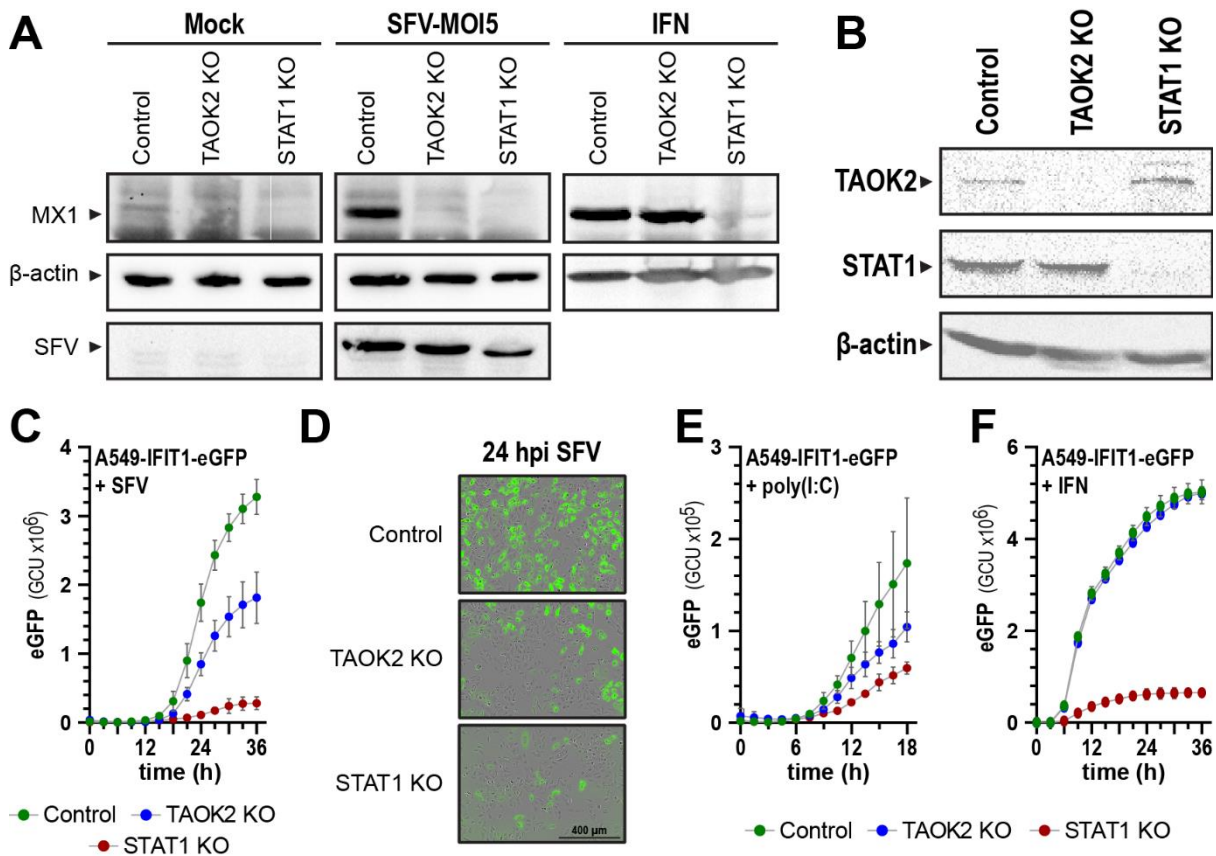


Figure 20: TAOK2 is required for ISG expression in infected, but not in IFN treated cells. (A) Scrambled control, TAOK2 KO and STAT1 KO were left unstimulated (mock), infected with SFV (MOI 5) or treated with IFN- α B/D (1000 units/mL) for 24 h. Obtained cell lysates were used for western blotting against MX1, β -actin and SFV. **(B)** Western Blot confirming depletion of TAO kinases in A549-IFIT1-eGFP cells. **(C)** A549-IFIT1-eGFP control, TAOK2 KO and STAT1 KO cells were infected with SFV (MOI5). Green fluorescence intensity was measured every 3 h using an Incucyte S3 live cell imaging system. Mean green intensity/cell confluence per image (GCU) \pm SD (y-axis) is shown over time (x-axis). **(D)** Representative fluorescence microscopy images of (C) 24 hours after SFV infection. **(E-F)** As (C), but transfected with poly(I:C) (2 μ g/mL) (E) or stimulated with IFN- α B/D (1000 units/mL) (F). Two-way ANOVA with Geissser-Greenhouse correction and Sidak's multiple comparisons test was performed to evaluate the significance of (C), (E) and (F).

Western blotting of SFV infected TAOK2 and STAT1 KO THP-1 cells confirmed the decrease of MX1 expression compared to the control (Fig. 20A). In order to further validate the ISG dependent antiviral phenotype of TAOK2 and gain quantitative kinetic data, we generated TAOK2 and STAT1 KOs in an A54-IFIT1-eGFP reporter cell line (Fig. 20B). This cell line expresses GFP under the control of the IFIT1 promoter, so that GFP levels can be used as a proxy for IFIT1 expression. As previously observed in the full proteomic MS, infection of the TAOK2 KO cells with SFV, led to a significant reduction in GFP and thus IFIT1 ($p < 0.005$ 15 hpi, $p < 0.0005$ 18 hpi) (Fig. 20C). Similarly, poly(I:C) transfection also led to a reduction in GFP signaling in the TAOK2 KO cells compared to the scrambled control ($p < 0.005$ 15 hpi, $p < 0.0005$ 18 hpi) (Fig. 20E).

In order to determine whether the effect of TAOK2 was on IFN induction or signaling, we treated the KO cells with recombinant IFN- α B/D and looked for induction of MX1 expression by western blotting. As anticipated, no MX1 induction was observed in the STAT1 KO cells. However, the expression level of MX1 in the TAOK2 KO cells was comparable to the scrambled control (Fig. 20A). To confirm this phenotype, the A549-IFIT1-GFP reporter cells were similarly treated with recombinant IFN- α B/D. In line with the unaffected MX1 levels in the western blot experiment, TAOK2 KO and control cells showed similar induction of IFIT1-GFP (Fig. 20F). This indicates that the signaling downstream of IFN is unaffected by the loss of TAOK2 and speaks to TAOK2 affecting ISG expression by playing a role in IFN induction.

TAOK2 impacts expression of IFN genes/proteins, but not of TNF- α or ILs

Having noted the lack of upregulation of ISGs in SFV infected but not in IFN treated TAOK2 cells, our hypothesis is that TAOK2 is active in the PRR signaling upstream of IFN. Therefore, we next assessed the cytokine levels in the supernatants of SFV infected THP-1 TAOK2 KO and control cells using cytometric bead array (performed by Silke Hegenbarth, Institute of Molecular Immunology and Experimental Oncology, TUM) and ELISA.

We observed a significant decrease of IFN- β ($p < 0.005$) (Fig. 21A) and IP-10 ($p < 0.05$) (Fig. 21B) induction in TAOK2 KO cells compared to the scrambled control. A similar decrease of induction was observed for the chemokines MCP-1 (Fig. 21C) and MIP-1b (Fig. 21D). Expression MCP-1 is induced via NF- κ B and IFN expression, while MIP1-1b is induced via NF- κ B and IRF3 (Andersen et al., 2008; Lehmann et al., 2016).

Surprisingly, loss of TAOK2 did not appear to affect IL-6 (Fig. 21F), IL-8 (Fig. 21G) and TNF- α (Fig. 21E) expression. Granulocyte colony-stimulating factor (G-CSF) was similarly unaffected by viral infection (Fig. 21H). Taken together, we observe a clear impact of TAOK2 depletion in SFV infected cells on IFN and IFN-related cytokines, but not on cytokines induced via NF- κ B.

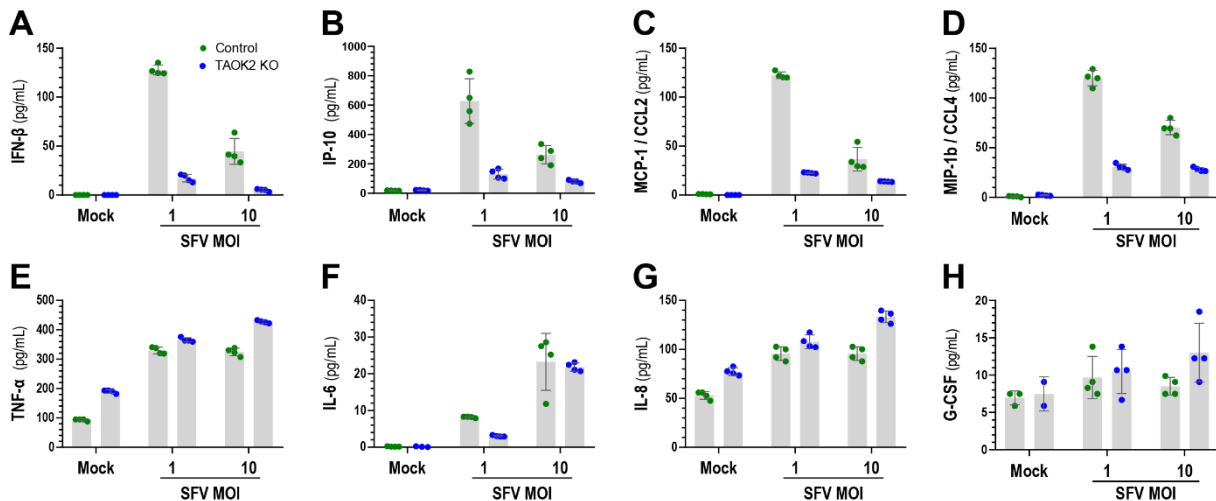


Figure 21: Loss of TAOK2 directly impacts IFN but not TNF- α secretion. (A-H) THP-1 cells were infected with SFV at the indicated MOI and 24h later the accumulation of cytokines in the supernatant was measured by ELISA (IFN- β (A) and IP-10 (B)) and cytometric bead array (MCP-1/CCL2 (C), MIP-1b/CCL4 (D), TNF- α (E), IL-6 (F), IL-8 (G) and G-CSF (H)). Data presented is averaged across four biological repeats \pm SD. Unpaired Welch's *t*-test was performed to evaluate the significance.

Targeting of TAOK2 using kinase inhibitors

Kinases are a frequent target for pharmacological intervention in many different diseases, predominantly in cancer and autoimmune disorders such as rheumatoid arthritis. To identify a TAOK2 inhibitor, we mined a kinase inhibitor database. Of particular interest was a MS-based screening approach, which had identified RAF265 as a TAOK2 inhibitor (Klaeger et al., 2017). RAF265 was initially identified as a BRAF inhibitor, and mouse experiments indicated a potential use in cancer treatment (Williams et al., 2015). However, in phase I clinical RAF265 treatment trials in patients with advanced or metastatic melanoma, a response to treatment was observed in only 12% of the patients and this response was independent of the BRAF status of the patients (Izar et al., 2017). This indicates that RAF265 may have additional targets besides BRAF.

An initial trial was conducted with RAF265 in poly(I:C) pre-stimulated IFIT1-GLuc tagged THP-1 cells. IFIT1-GLuc tagged THP-1 cells express Gaussia luciferase in control of the IFIT1 promoter. The levels of luciferase can be measured and used as

a proxy for IFIT1. Following RAF265 treatment we observed a decrease of luciferase, indicating that RAF265 impacts IFIT1 expression (Fig. 22A). We therefore proceeded to monitor the RAF265 impact over time in the A549-IFIT1-eGFP cells infected with mCherry-tagged SFV. To exclude that the observed phenotype was due to inhibition of BRAF, we included the known BRAF inhibitor, Dabrafenib as a control. RAF265 treatment in SFV infected A549-IFIT1-eGFP cells led to a significant increase in SFV-mCherry growth ($p < 0.05$ 45 hpi) (Fig. 22B) and a significant decrease in IFIT1-eGFP expression ($p < 0.0005$ 24 hpi) (Fig. 22C). We did not observe any distinct changes in the SFV-mCherry or IFIT1-eGFP expression in the Dabrafenib treated cells, indicating that the RAF265 phenotype is not due to targeting of BRAF. The phenotype observed upon RAF265 treatment is in line with the previously observed TAOK2 KO phenotype.

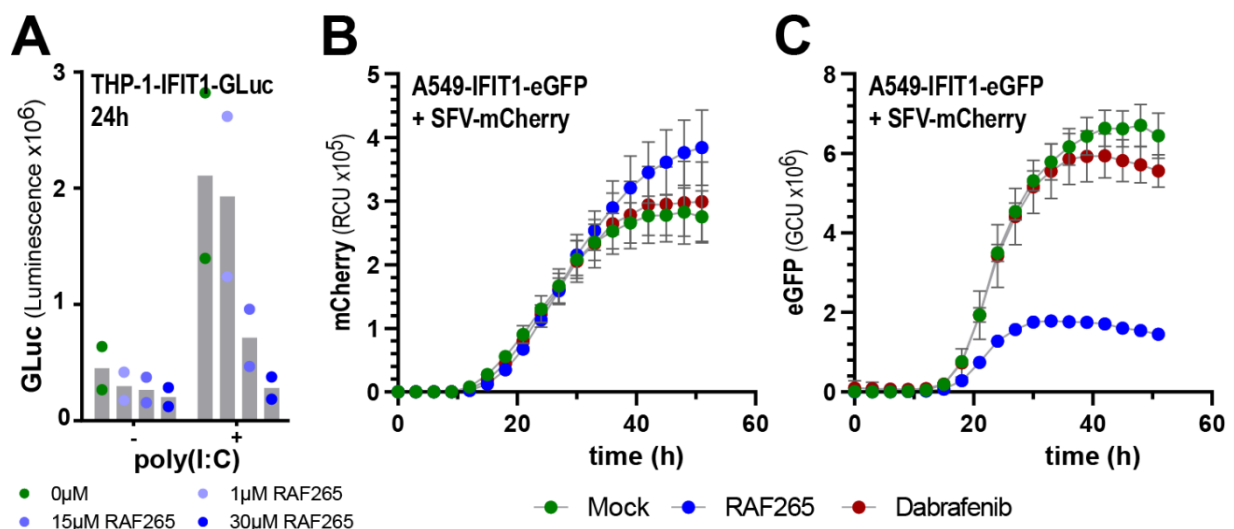
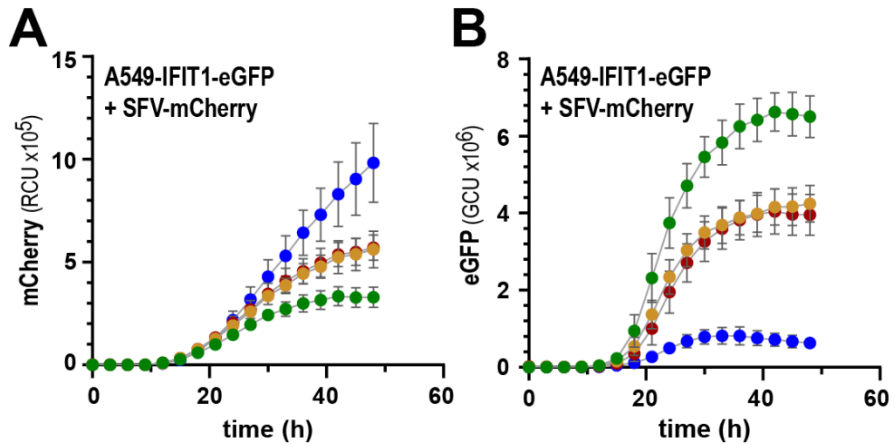


Figure 22: Effect of TAOK2 inhibitors on viral replication. (A) TAOK2 inhibitor RAF265 was titrated in THP-1-IFIT1-GLuc cells. The cells were prestimulated with poly(I:C) (0.5 μ g/mL) for 3 h before addition of the inhibitor. Gaussia levels were measured 24 hours after inhibitor addition. The histogram shows two technical repeats of a single trial experiment. (B-C) SFV replication (B) and IFIT1 expression (C) was monitored in A549 IFIT1-eGFP cells with and without RAF265 / Dabrafenib treatment. A549 IFIT1-eGFP cells were seeded at 5E3 cells/ well. After overnight incubation the cells were infected with SFV-mCherry (MOI 5) and simultaneously treated with RAF265 (500nM) / Dabrafenib (500nM). Fluorescence intensity was measured every 3 hours for 48 hours. The Y-axis is displayed as Integrated Intensity (RCU/Image)/ Confluence (%) $\times 10^5$ and Integrated Intensity (GCU/Image)/ Confluence (%) $\times 10^6$. Data presented is representative of three biological repeats. Two-way ANOVA with Geisser-Greenhouse correction and Sidak's multiple comparisons test was performed to evaluate the significance of (B) and (C)..

Next, we treated the A549-IFIT1-eGFP TAOK2 KO cells with both of the inhibitors to determine if RAF265 is TAOK2 specific. Notably, Dabrafenib showed no additive effect on the expression of SFV-mCherry and IFIT1-eGFP in TAOK2 KO cells, whereas RAF265 led to an increase in virus replication and reduction of IFIT1 expression (Fig. 23A, B). The additional decrease of IFIT1 expression and increase of virus replication

could be due to additional inhibitor targets, which were not identified in the MS-based screening approach (Klaeger et al., 2017).



● Mock ● TAOK2KO ● TAOK2KO + RAF265 ● TAOK2KO + Dabrafenib

Figure 23: Effect of TAOK2 inhibitors in TAOK2 KO cells. (A-B) SFV replication (B) and IFIT1 expression (C) monitored in A549 IFIT1-eGFP cells control and TAOK2 KO with RAF265 / Dabrafenib treatment. A549 IFIT1-eGFP cells were seeded at 5E3 cells/ well. After overnight incubation the cells were infected with SFV-mCherry (MOI 5) and simultaneously treated with RAF265 (500nM) / Dabrafenib (500nM). Fluorescence intensity was measured every 3 hours. Mean green or red intensity/cell confluence per image (GCU / RCU) \pm SD (y-axis) is shown over time (x-axis). Representative of three biological repeats. Two-way ANOVA with Geissser-Greenhouse correction and Sidak's multiple comparisons test was performed to evaluate the significance.

Discussion

The eukaryotic innate immune system evolved over millions of years under constant selective pressure from pathogens such as viruses (Fumagalli et al., 2011; Theze et al., 2011). This co-evolution resulted in the conserved antiviral NA interactors, such as RIG-I and cGAS (Kranzusch et al., 2015; Paro et al., 2015). My predecessor M.H. used affinity enrichment with viral NAs in three species to identify conserved NA interactors, with the hypothesis that these proteins may have conserved antiviral functions related to their NA interacting capability. Overall, we identified a set of conserved NA interactors, which highlights the ancient origin of antiviral innate immunity (Martins, 2020) and a number of species-specific candidates, which indicates differences in the evolutionary paths of the antiviral immune system when confronted with species-specific viruses (Duggal and Emerman, 2012).

Candidates from the CRISPR Cas9 KO screening

Lentivirus based CRISPR/Cas9 mediated depletion of selected NA interactors revealed the anti- /pro-viral activity of the 90 candidates against an array of viruses. As previously noted, 64 of the 89 tested candidates affected luciferase activity for at least one of the tested viruses. In the following, I will discuss the observed phenotypes of individual candidates in the context of previously published studies.

The dsRNA interactor PARP12 has pan-antiviral activity

Here we identified PARP12, a member of the Poly-ADP-Ribose Polymerases, as a poly(A:U) interactor in human and mouse. Poly-ADP-Ribose Polymerases are capable of catalyzing the transfer of ADP-ribose to other proteins (Morales et al., 2014). During the KO screening, depletion of PARP12 led to increased replication of IAV. Previous studies have also shown PARP12 to be active against VSV, Murine gammaherpesvirus 68, Venezuelan equine encephalitis virus and Zika virus, though for most viruses the molecular function of PARP12 has not been fully elucidated (Atasheva et al., 2014; Li et al., 2018a; Liu et al., 2012). This indicates that although we only observed a PARP12 phenotype for one virus tested in this project, PARP12 seems to have a broad antiviral phenotype. While PARP12 antiviral activity against Zika virus has been linked to its ability to target and induce degradation of viral proteins NS1 and NS3 (Li et al., 2018a), the broad antiviral activity may be explained with its affinity for NAs.



The RNA binding capability of PARP12 is most likely due to four CCCH type zinc finger motifs, which is a known NA binding motif (Guo et al., 2004). The presence of the four CCCH type zinc finger motifs of PARP12 are particularly noteworthy as only two other members of the PARP family, PARP7 and PARP13, contain them (Vyas et al., 2013).

Even more so, while other PARP family members have been identified as being involved in DNA damage repair and chromatin dynamics (Morales et al., 2014), the only PARP member linked to antiviral immunity is PARP13. PARP13 has been shown to bind viral RNA and recruits the RNA processing exosome to degrade it (Guo et al., 2004; Guo et al., 2007). PARP13 inhibits viral replication by preventing viral RNA accumulation in the cytoplasm, a phenotype that has been confirmed in SINV infection as well as for retroviral Moloney murine leukemia virus (Bick et al., 2003; Gao et al., 2002). It is quite possible that PARP12 antiviral function has a similar mechanism as PARP13.

The dsDNA interactor RSL1D1 is involved in the DNA damage response

Not all candidates identified during the screening are necessarily directly linked to viral NA based antiviral response. They may also be NA interactors that are peripherally activated during the antiviral response. For instance, RSL1D1 is known to be involved in the DNA damage response (DDR) after UV irradiation (Li et al., 2012). In line with this, RSL1D1 its mouse orthologue Rsl1d1 and its fly orthologue CG13096 were all identified as DNA binders in our NA affinity studies, but during the KO screen, we also observed a broad antiviral phenotype, with activity against HSV-1, IAV and VSV. The involvement in the DNA damage response could serve as a potential explanation for the broad antiviral phenotype since IAV and VSV are both known to induce DNA damage (Hajime Koyama, 1995; Li et al., 2015). As opposed to IAV and VSV, HSV-1 has a more complex relationship with the DDR pathway. Upon HSV-1 infection, the DDR kinase ATM is upregulated in order to aid HSV-1 viral replication (Lilley et al., 2005), but simultaneously, HSV-1 protein ICP0 prevents the full activation of the DDR-ATM pathway (Lilley et al., 2010). Similarly, ATR kinase, from a parallel DDR response pathway, is also recruited to the HSV-1 viral replication site without activation of the full ATR mediated DDR response pathway (Mohani et al., 2010). The direct inhibition of DDR activation in HSV-1 infected cells makes it unlikely that the broad antiviral phenotype observed is solely due to the involvement of RSL1D1 in the DDR pathway during viral infection.

Another potential explanation could be that RSL1D1 has also been shown to negatively regulate phosphatase and tensin homolog (PTEN) (Ma et al., 2008). PTEN in turn negatively regulates phosphatidylinositol-3-kinase (PI3K) signaling (Engelman et al., 2006), which in turn can impact the antiviral response (Hrincius et al., 2011; Sarkar et al., 2004). In line with the broad antiviral activity observed for RSL1D1, the PI3K pathway has been shown to be activated by a wide array of viruses, including IAV, WNV, Hepatitis B virus and Dengue virus (Hrincius et al., 2011; Lee et al., 2005; Shih et al., 2000; Wang et al., 2017). Loss of RSL1D1 releases the inhibition on PTEN, thereby indirectly inhibiting PI3K (Engelman et al., 2006). As PI3K interfaces with the innate immune system, inhibition of PI3K leads to an increase of virus growth (Wang et al., 2017).

The dsRNA interactor SMARCA5 belongs to a family of known antiviral proteins

SMARCA5 and its respective orthologues in mouse and fly were identified in the poly(I:C) APs, and we observed an antiviral effect against VSV, IAV and HSV-1. SMARCA5 is a member of the SWI/SNF family, a family best known for its involvement in the chromatin remodeling process. While human SMARCA5 has been studied as a factor in cell invasion and migration in cancer (Chetty and Serra, 2020), it has not previously been studied in the context of viral infection. However, mouse SMARCA5 was identified as a retroviral element silencer (Golding et al., 2010). Furthermore, fly SMARCA5 orthologue ISWI is a RNA interactor and is upregulated during SINV infection (Mudiganti et al., 2010; Onorati et al., 2011).

Additionally, two other SWI/SNF family members, SMARCA2 and SMARCA4, have been linked to viral phenotypes (Dornfeld et al., 2018; Dudek et al., 2018). Both are differentially expressed during viral infection and regulate the response to poly(I:C) (Dudek et al., 2018), while SMARCA2 also impairs IAV growth (Dornfeld et al., 2018). Overall, this highlights a more prominent role of the SWI/SNF family in antiviral immunity, and indicates that follow-up experiments on these proteins could be most interesting.

Overlap between human and fly depletion screening

In parallel to our lentivirus based CRISPR Cas9 KO screening, collaborators were performing a siRNA based knockdown screening in flies with 92 different candidates identified in the fly and S2 AP-MS (Assel Mussabekova, Carine Meignin and Jean-Luc 90

Imler, Université de Strasbourg, CNRS). They used transgenic flies containing shRNA or inverted repeat transgenes under the control of a temperature sensitive promoter, allowing temperature-inducible depletion of candidate genes. After activation of RNAi by temperature, the flies were infected with the Drosophila C virus (DCV, pos. strand ssRNA), Cricket paralysis Virus (CrPV, pos. strand ssRNA), Flock house virus (FHV, pos. strand ssRNA), SINV and VSV for 2 or 3 days and virus growth was monitored by

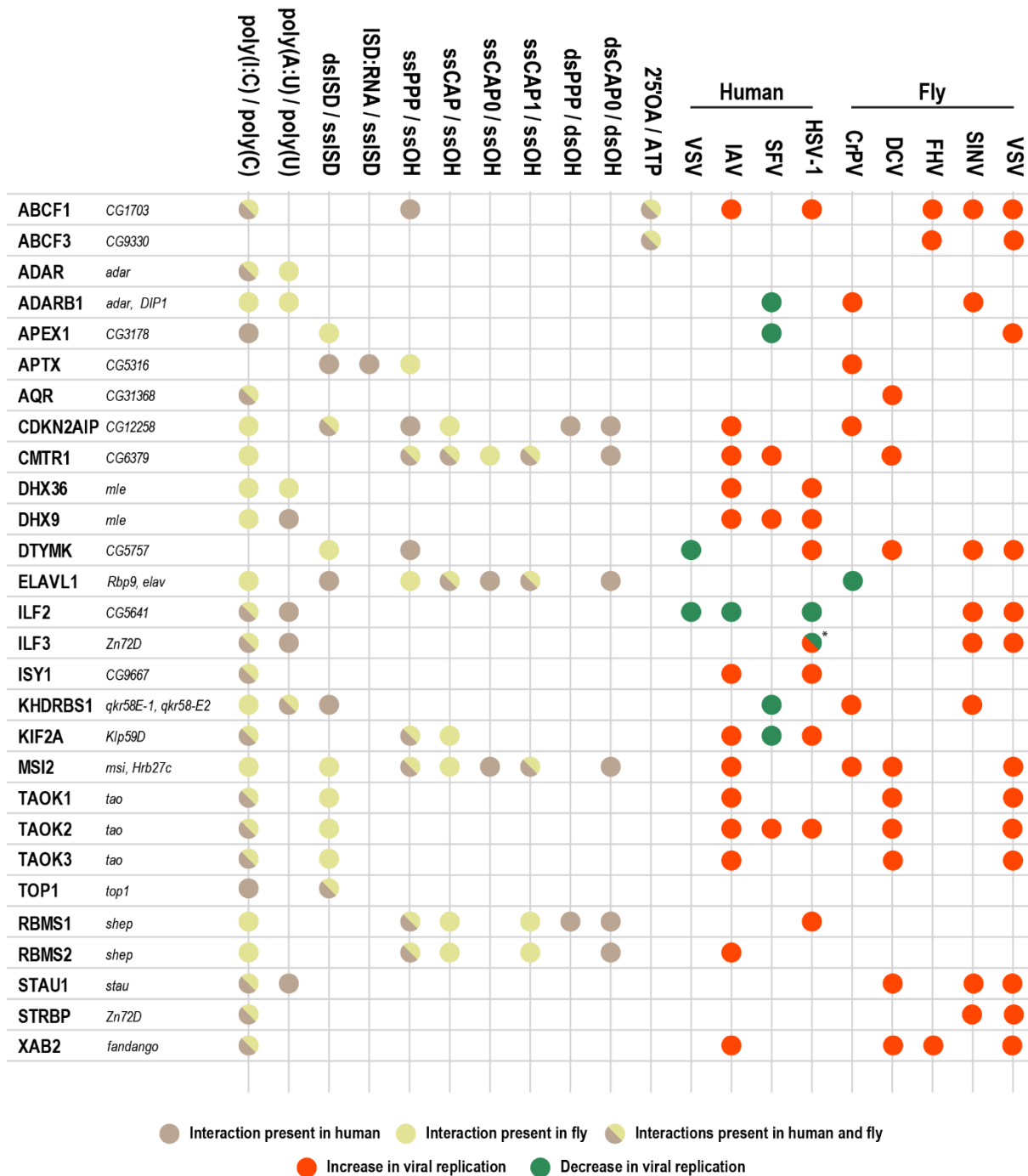


Figure 24: Overview of the results gathered in the three separate screenings (AP-MS, human KO and fly KD) for the 28 overlapping proteins from the human KO and fly KD screening. For some proteins, e.g. TAO kinases, there is only one fly orthologue for multiple human proteins, each was treated as a separate orthologue pair in this figure. *for ILF3 we observed an increase of viral replication in PMA treated THP-1 cells, but a decrease of viral replication in the untreated THP-1 cells.

RT-qPCR. Of the 92 candidates selected for the fly screening, 55 had human orthologues and of these 55, 28 were included in our lentiviral screening. Given that the premise of this project was the identification of evolutionary conserved NA interactors, comparison of the viral phenotypes of the 28 candidates and their fly orthologues is particularly interesting. Of the 28 candidates, 14 had a phenotype in both species (Fig. 24).

ABCF1 and ABCF3 are novel 2'5'OA interactors with antiviral effects

As previously noted, ABCF1 is a member of the ABC transporter family, carries the AAA domain, which was enriched in the 2'5'OA AP-MS, and is the sole protein conserved across all three species for 2'5'OA in the AP-MS. We also observed an increase of viral replication for both HSV-1 and IAV replication in PMA treated THP-1 ABCF1 KO cells. Taken together, this indicates that not only is the ABCF1 – 2'5'OA interaction highly conserved, it could also be immunologically relevant. ABCF1 has been identified as an immune regulator in various cancers (Fung et al., 2019; Seborova et al., 2019) and is thought to act as an E2 ligase mediating MyD88 and TRIF-dependent signaling (Arora et al., 2019). Infection of ABCF1 siRNA knockdown mouse embryonic fibroblasts leads to a significant decrease in IFN- β expression, further indicating the relevance of ABCF1 for PRR signaling (Lee et al., 2013). The conserved interaction between 2'5'OA and ABCF1 suggests that 2'5'OA might have additional intracellular targets, besides RNASEL, through which it mediates inflammatory conditions.

ABCF3, another ABC transporter family member, was also identified as a 2'5'OA interactor during the AP-MS. While we did not observe a virus-related phenotype for ABCF3 in the CRISPR Cas9 KO screening, another KO screening using SARS-CoV-2 identified ABCF3 as a strong antiviral candidate (Valter Bergant, internal communication). In addition, loss of fly orthologue of ABCF3, CG9330, lead to an increase of FHV and VSV in the fly shRNA screening. ABCF3 has been noted as an interactor of the mouse Oas1b (Courtney et al., 2012). Oas1b is considered an orthologue of human OAS1 (Hu et al., 2011), although Oas1b does not have 2'5'OAs activity, similar to OASL (Ibsen et al., 2015; Kakuta et al., 2002). Given the 2'5'OAs binding capability of ABCF3 in humans and in flies and the observed antiviral phenotype in human and fly, ABCF3 may also act as an immune modulator downstream of 2'5'OAs production.



NA interactors MSI2 and CDK2AIP have conserved antiviral phenotypes in human and flies

Another interesting set of proteins is MSI2 and CDKN2AIP, for which similar NA binding patterns and viral phenotypes are observable in humans and flies. Both MSI2 and CDKN2AIP were identified as ssRNA and dsDNA interactors in humans and flies, and both proteins displayed antiviral phenotypes for IAV (human lentiviral screening) and CrPV (fly shRNA screening), with MSI2 also appearing antiviral against DCV and VSV (fly shRNA screening).

This is particularly noteworthy as neither protein has previously been directly linked to a viral phenotype, though MSI2 has been linked to an increased recurrence and mortality rate in Hepatitis B virus related hepatocellular carcinoma (Wang et al., 2015). They are, however, known to be involved in the human WNT- β -catenin signaling pathway (Kalra et al., 2018; Wang et al., 2015) that has been linked to the regulation of the IFN- β response in humans and to the Toll-regulated NF- κ B response in flies (Baril et al., 2013; Gordon et al., 2005). It is therefore plausible that MSI2 and CDKN2AIP detect foreign NA and then induce immune signaling, though follow-up experiments would be required to determine if this is indeed the case.

Human proviral factor KHDRBS1 is antiviral in flies

Intriguingly, for four of the 14 proteins displaying viral phenotypes in both humans and flies (ADARB1, APEX1, ILF2 and KHDRBS1), the human protein is proviral while the drosophila orthologue is antiviral.

KHDRBS1, also known as Sam68, is a noted NA-binding proviral host factor for HIV-1, Foot-and-mouth-disease virus (FMDV), Enterovirus 71 (EV71) and Hepatitis C virus (Liu et al., 2011; Qin et al., 2019; Rai et al., 2015; Zhang et al., 2015). This is in line with the reduced viral replication we observed during SFV infection in the KHDRBS1 KO cells. KHDRBS1 appears to have two different modes of action. First, KHDRBS1 interacts with the viral polymerase in poliovirus and Hepatitis C virus infections (McBride et al., 1996; Qin et al., 2019) and thereby most likely affects viral replication. Second, KHDRBS1 directly interacts with the viral RNA, via the internal ribosome entry site (IRES) as seen in FMDV and Hepatitis C virus infections, likely affecting viral translation (Qin et al., 2019; Rai et al., 2015).

Little is known about KHDRBS1 fly orthologues, though two potential orthologues appear to be involved in alternative splicing (Brooks et al., 2015). Our data also indicates that the RNA binding affinity is conserved, though the effects on viral replication show a contrasting result. While the phenotype of the human KO cells showed a decrease of viral replication, we observe an increase in viral replication for both CrPV and SINV in the fly shRNA screening. The contrasting phenotypes in the two species are particularly surprising, as SINV and SFV are closely related viruses, both belonging to the Togaviridae family and CrPV, FMDV, EV71, poliovirus and rhinovirus all belonging to the order Picornavirales. It remains uncertain how and why these contradicting viral phenotypes occur in humans and flies, though it may reflect the differential adaptation of the different viruses to their respective hosts (Woolhouse et al., 2001).

TAO kinases as antiviral proteins

One of the candidate clusters where we observed a high degree of conservation in both NA interaction and antiviral function was the group of three human TAO kinases, TAOK1, TAOK2 and TAOK3 as well as the single fly orthologue Tao kinase (noted as dTao). All four kinases interact with poly(I:C), and dTao furthermore interacts with dsISD. We confirmed that the interaction between dTao and poly(I:C) was a direct affinity interaction, with affinity for dsRNA in the nanomolar range and intriguingly, poly(I:C) appears to be able to directly impact kinase activity *in vitro*. In the lentiviral KO screen, all three human TAO kinases displayed antiviral activity against IAV and in addition, TAOK2 also showed antiviral activity against SFV and HSV-1. In the fly KD screening, dTao was antiviral against DCV and VSV. Proteomic analysis of TAOK2 depleted cells revealed a surprising involvement of TAOK2 in the induction of innate immune proteins, specifically induction of ISGs. Similarly, cytokine profiling suggests that loss of TAOK2 selectively impairs IRF3 dependent cytokines like IFN- β and IL-10, without affecting NF- κ B dependent cytokines like TNF- α and IL-6. Intriguingly, a recent single-cell genomics study in SARS-CoV-2 infected patients noted a decrease of TAOK1 expression (Bost et al., 2020), further indicating that TAOKs are in fact relevant in antiviral immunity.

It is particularly noteworthy, that a TAOK2 mutation has been identified in two patients with treatment-resistant generalized verrucosis lesions caused by unimpaired growth of human papillomavirus (Molho-Pessach et al., 2017). The identified TAOK2 mutation



(C2908T) causes an amino acid change from arginine to cysteine at amino acid 700 (Molho-Pessach et al., 2017), located between the kinase (28-281aa) and the transmembrane domain (955-1063aa). Sanger sequencing confirmed that both patients, who are siblings, have the homozygous C2908T mutation, whereas the third sibling and the parents are heterozygous carriers and do not show clinical symptoms (Molho-Pessach et al., 2017). Notably, arginine mutations account for almost 15% of known disease mutations, with over half of the observed mutations being to a cysteine (Vitkup et al., 2003). An arginine to cysteine mutation can affect various interactions, such as hydrogen-bonds and the new free thiol of the cysteine could form unexpected disulfide bridges (Gallego-Villar et al., 2017). In consequence, approximately 8% of genetic diseases caused by missense mutations are impacted by arginine to cysteine mutations (Gallego-Villar et al., 2017; Vitkup et al., 2003).

Human papillomaviruses contain circular dsDNA genomes, and like many DNA viruses most likely generates dsRNA through convergent transcription (Weber et al., 2006). Production of dsRNA during HPV replication is further supported by an ADAR1 KD leading to enhanced human papillomavirus replication (Pujantell et al., 2019), as well as modulation of EIF2AK2 activity by human papillomavirus (Hebner et al., 2006). Our data suggests that perhaps the inability to control human papilloma virus replication and the TAOK2 mutation observed in the patients are both linked to the innate immune regulating and dsRNA binding properties of TAOK2.

The exact function of TAOK2 in the induction of the immune system remains uncertain, though it may be via the previously published TAOK2 regulation of JNK (Chen and Cobb, 2001), as there is some evidence that MEK4/7-JNK signaling directly and specifically regulates IFN production. For example in MEK4/7 depleted cells, poly(I:C) stimulation led to a decrease of IP-10 and IFN- β , while the phosphorylation levels of NF- κ B regulator I κ B were unaffected (Yoshizawa et al., 2008). Additionally, chemical JNK inhibition of poly(I:C) stimulated cells inhibited IRF3 phosphorylation and dimerization (Zhang et al., 2009). A potential hypothesis would thus be that TAOK2 interacts with viral dsRNA, which increases TAOK2 activity, leading to the phosphorylation and activation of MEK4/7. This in turn could cause a specific activation of JNK and a cytokine response.

Concluding Remarks

Using an AP-MS approach across three different species and 17 different NAs we identified 904, 1214 and 1479 NA interactors in human, mouse and fly, respectively. Through orthologue analysis between the different species we were able to identify highly conserved NA interactors, such as the dsRNA binding TAOK family and the 2'5'OAs binding ABCF1 protein. Factoring in the interaction strength and data available from literature, 90 candidates were selected. A CRISPR CAS9 lentiviral knockout screening of the selected candidates revealed 43 viral restriction factors and 13 host factors. Furthermore, cross-referencing with a siRNA based fly depletion screening showed that 14 of the candidates, including TAO kinases, displaying phenotypes in the human KO screening also had a viral phenotype in the fly screening. Follow-up experiments with TAOK2 revealed that TAOK2 directly influences IFN expression and thereby the expression of ISGs.

The here described AP-MS dataset is novel in its aim to use evolutionary conservation as an asset to identify NA interactors. We show how considering evolution in the identification of NA interactors is beneficial to the identification of immunologically relevant PRRs. It would therefore be interesting to intersect the AP-MS data from human, mouse and fly with other species. For example, as many PRRs first appear in members of the Cnidaria phylum, e.g. cGAS and TLRs (Gilmore and Wolenski, 2012; Kranzusch et al., 2015) or in Nematodes, e.g. RLRs (Paro et al., 2015), intersecting with AP-MS data from species belonging to these families could be particularly revealing.

However, even taken the human dataset by itself is a valuable resource for other scientists studying anti- / pro-viral proteins. Other scientists could intersection our dataset with their own, similar to the comparative analysis we performed for the genome-wide RNAi depletion study measuring IAV replication (Tripathi et al., 2015), to highlight interesting candidates for follow-up experiments. Factoring in the mouse and the fly dataset provides further value to the dataset, as for example, the evolutionary progression of protein family specific NA affinities can be tracked across species.

References

Ablasser, A., and Chen, Z.J. (2019). cGAS in action: Expanding roles in immunity and inflammation. *Science* 363.

Ablasser, A., and Hur, S. (2020). Regulation of cGAS- and RLR-mediated immunity to nucleic acids. *Nat Immunol* 21, 17-29.

Akdis, M., Burgler, S., Cramer, R., Eiwegger, T., Fujita, H., Gomez, E., Klunker, S., Meyer, N., O'Mahony, L., Palomares, O., et al. (2011). Interleukins, from 1 to 37, and interferon- γ : Receptors, functions, and roles in diseases. *Journal of Allergy and Clinical Immunology* 127, 701-721.e770.

Akira, S., and Takeda, K. (2004). Toll-like receptor signalling. *Nat Rev Immunol* 4, 499-511.

Alexopoulou, L., Holt, A.C., Medzhitov, R., and Flavell, R.A. (2001). Recognition of double-stranded RNA and activation of NF- κ B by Toll-like receptor 3. *Nature* 413, 732-738.

Andersen, J., VanScoy, S., Cheng, T.F., Gomez, D., and Reich, N.C. (2008). IRF-3-dependent and augmented target genes during viral infection. *Genes Immun* 9, 168-175.

Antonczyk, A., Krist, B., Sajek, M., Michalska, A., Piaszyk-Borychowska, A., Plens-Galaska, M., Wesoly, J., and Bluysen, H.A.R. (2019). Direct Inhibition of IRF-Dependent Transcriptional Regulatory Mechanisms Associated With Disease. *Frontiers in Immunology* 10.

Arii, J., Watanabe, M., Maeda, F., Tokai-Nishizumi, N., Chihara, T., Miura, M., Maruzuru, Y., Koyanagi, N., Kato, A., and Kawaguchi, Y. (2018). ESCRT-III mediates budding across the inner nuclear membrane and regulates its integrity. *Nature Communications* 9.

Arora, H., Wilcox, S.M., Johnson, L.A., Munro, L., Eyford, B.A., Pfeifer, C.G., Welch, I., and Jefferies, W.A. (2019). The ATP-Binding Cassette Gene ABCF1 Functions as an E2 Ubiquitin-Conjugating Enzyme Controlling Macrophage Polarization to Dampen Lethal Septic Shock. *Immunity* 50, 418-431 e416.

Atasheva, S., Frolova, E.I., and Frolov, I. (2014). Interferon-stimulated poly(ADP-Ribose) polymerases are potent inhibitors of cellular translation and virus replication. *J Virol* 88, 2116-2130.

Baril, M., Es-Saad, S., Chatel-Chaix, L., Fink, K., Pham, T., Raymond, V.A., Audette, K., Guenier, A.S., Duchaine, J., Servant, M., et al. (2013). Genome-wide RNAi screen reveals a new role of a WNT/CTNNB1 signaling pathway as negative regulator of virus-induced innate immune responses. *PLoS Pathog* 9, e1003416.

Bauernfried, S., Scherr, M.J., Pichlmair, A., Duderstadt, K.E., and Hornung, V. (2020). Human NLRP1 is a sensor for double-stranded RNA. *Science*, eabd0811.

Belgnaoui, S.M., Paz, S., and Hiscott, J. (2011). Orchestrating the interferon antiviral response through the mitochondrial antiviral signaling (MAVS) adapter. *Curr Opin Immunol* 23, 564-572.

Bermejo-Jambrina, M., Eder, J., Helgers, L.C., Hertoghs, N., Nijmeijer, B.M., Stunnenberg, M., and Geijtenbeek, T.B.H. (2018). C-Type Lectin Receptors in Antiviral Immunity and Viral Escape. *Front Immunol* 9, 590.

Bick, M.J., Carroll, J.-W.N., Gao, G., Goff, S.P., Rice, C.M., and MacDonald, M.R. (2003). Expression of the Zinc-Finger Antiviral Protein Inhibits Alphavirus Replication. *Journal of Virology* 77, 11555-11562.

Binns, D., Dimmer, E., Huntley, R., Barrell, D., O'Donovan, C., and Apweiler, R. (2009). QuickGO: a web-based tool for Gene Ontology searching. *Bioinformatics* 25, 3045-3046.

Blasius, A.L., and Beutler, B. (2010). Intracellular Toll-like Receptors. *Immunity* 32, 305-315.

Bond, C.S., and Fox, A.H. (2009). Paraspeckles: nuclear bodies built on long noncoding RNA. *J Cell Biol* 186, 637-644.

Bost, P., Giladi, A., Liu, Y., Bendjelal, Y., Xu, G., David, E., Blecher-Gonen, R., Cohen, M., Medaglia, C., Li, H., et al. (2020). Host-Viral Infection Maps Reveal Signatures of Severe COVID-19 Patients. *Cell* 181, 1475-1488 e1412.

Brennan, J.J., Gilmore, T.D., and Newfeld, S. (2018). Evolutionary Origins of Toll-like Receptor Signaling. *Molecular Biology and Evolution* 35, 1576-1587.



- Brocker, C., Thompson, D., Matsumoto, A., Nebert, D.W., and Vasiliou, V. (2010). Evolutionary divergence and functions of the human interleukin (IL) gene family. *Hum Genomics* 5, 30-55.
- Brooks, A.N., Duff, M.O., May, G., Yang, L., Bolisetty, M., Landolin, J., Wan, K., Sandler, J., Booth, B.W., Celniker, S.E., et al. (2015). Regulation of alternative splicing in *Drosophila* by 56 RNA binding proteins. *Genome Res* 25, 1771-1780.
- Brown, G.D., Willment, J.A., and Whitehead, L. (2018). C-type lectins in immunity and homeostasis. *Nat Rev Immunol* 18, 374-389.
- Brubaker, S.W., Bonham, K.S., Zanoni, I., and Kagan, J.C. (2015). Innate immune pattern recognition: a cell biological perspective. *Annu Rev Immunol* 33, 257-290.
- Carpenter, B., Gelman, A., Hoffman, M.D., Lee, D., Goodrich, B., Betancourt, M., Brubaker, M., Guo, J., Li, P., and Riddell, A. (2017). Stan: A Probabilistic Programming Language. *Journal of Statistical Software* 76.
- Carvalho, C.M., Polson, N.G., and Scott, J.G. (2010). The horseshoe estimator for sparse signals. *Biometrika* 97, 465-480.
- Cekic, C., and Linden, J. (2016). Purinergic regulation of the immune system. *Nat Rev Immunol* 16, 177-192.
- Cervantes, J.L., Weinerman, B., Basole, C., and Salazar, J.C. (2012). TLR8: the forgotten relative revindicated. *Cell Mol Immunol* 9, 434-438.
- Chen, Z., and Cobb, M.H. (2001). Regulation of stress-responsive mitogen-activated protein (MAP) kinase pathways by TAO2. *J Biol Chem* 276, 16070-16075.
- Chen, Z., Hutchison, M., and Cobb, M.H. (1999). Isolation of the Protein Kinase TAO2 and Identification of Its Mitogen-activated Protein Kinase/Extracellular Signal-regulated Kinase Kinase Binding Domain. *The Journal of Biological Chemistry* 274, 28803-28807.
- Chen, Z., Raman, M., Chen, L., Lee, S.F., Gilman, A.G., and Cobb, M.H. (2003). TAO (thousand-and-one amino acid) protein kinases mediate signaling from carbachol to p38 mitogen-activated protein kinase and ternary complex factors. *J Biol Chem* 278, 22278-22283.

Cheng, Z., Dai, T., He, X., Zhang, Z., Xie, F., Wang, S., Zhang, L., and Zhou, F. (2020). The interactions between cGAS-STING pathway and pathogens. *Signal Transduction and Targeted Therapy* 5.

Chetty, R., and Serra, S. (2020). SMARCA family of genes. *J Clin Pathol* 73, 257-260.

Cheung, C.T., Singh, R., Kalra, R.S., Kaul, S.C., and Wadhwa, R. (2014). Collaborator of ARF (CARF) regulates proliferative fate of human cells by dose-dependent regulation of DNA damage signaling. *J Biol Chem* 289, 18258-18269.

Courtney, S.C., Di, H., Stockman, B.M., Liu, H., Scherbik, S.V., and Brinton, M.A. (2012). Identification of Novel Host Cell Binding Partners of Oas1b, the Protein Conferring Resistance to Flavivirus-Induced Disease in Mice. *Journal of Virology* 86, 7953-7963.

Cyster, J.G., and Allen, C.D.C. (2019). B Cell Responses: Cell Interaction Dynamics and Decisions. *Cell* 177, 524-540.

Daugherty, M.D., and Malik, H.S. (2012). Rules of engagement: molecular insights from host-virus arms races. *Annu Rev Genet* 46, 677-700.

de Oliveira Mann, C.C., Orzalli, M.H., King, D.S., Kagan, J.C., Lee, A.S.Y., and Kranzusch, P.J. (2019). Modular Architecture of the STING C-Terminal Tail Allows Interferon and NF- κ B Signaling Adaptation. *Cell Reports* 27, 1165-1175.e1165.

Decker, T., Kovarik, P., and Meinke, A. (1997). GAS Elements: A Few Nucleotides with a Major Impact on Cytokine-Induced Gene Expression. *Journal of Interferon & Cytokine Research* 17, 121-134.

Decroly, E., Ferron, F., Lescar, J., and Canard, B. (2011). Conventional and unconventional mechanisms for capping viral mRNA. *Nat Rev Microbiol* 10, 51-65.

Deddouche, S., Matt, N., Budd, A., Mueller, S., Kemp, C., Galiana-Arnoux, D., Dostert, C., Antoniewski, C., Hoffmann, J.A., and Imler, J.L. (2008). The DExD/H-box helicase Dicer-2 mediates the induction of antiviral activity in drosophila. *Nat Immunol* 9, 1425-1432.

Deng, P., Khan, A., Jacobson, D., Sambrani, N., McGurk, L., Li, X., Jayasree, A., Hejatko, J., Shohat-Ophir, G., O'Connell, M.A., et al. (2020). Adar RNA editing-



dependent and -independent effects are required for brain and innate immune functions in *Drosophila*. *Nat Commun* 11, 1580.

Devarkar, S.C., Wang, C., Miller, M.T., Ramanathan, A., Jiang, F., Khan, A.G., Patel, S.S., and Marcotrigiano, J. (2016). Structural basis for m7G recognition and 2'-O-methyl discrimination in capped RNAs by the innate immune receptor RIG-I. *Proc Natl Acad Sci U S A* 113, 596-601.

Dinarello, C.A. (2011). Interleukin-1 in the pathogenesis and treatment of inflammatory diseases. *Blood* 117, 3720-3732.

Doench, J.G., Fusi, N., Sullender, M., Hegde, M., Vaimberg, E.W., Donovan, K.F., Smith, I., Tothova, Z., Wilen, C., Orchard, R., et al. (2016). Optimized sgRNA design to maximize activity and minimize off-target effects of CRISPR-Cas9. *Nat Biotechnol* 34, 184-191.

Dolasia, K., Bisht, M.K., Pradhan, G., Udgata, A., and Mukhopadhyay, S. (2018). TLRs/NLRs: Shaping the landscape of host immunity. *Int Rev Immunol* 37, 3-19.

Dornfeld, D., Dudek, A.H., Vausselin, T., Gunther, S.C., Hultquist, J.F., Giese, S., Khokhlova-Cubberley, D., Chew, Y.C., Pache, L., Krogan, N.J., et al. (2018). SMARCA2-regulated host cell factors are required for MxA restriction of influenza A viruses. *Sci Rep* 8, 2092.

Dudek, A.H., Pfaff, F., Bolte, H., Waguia Kontchou, C., and Schwemmle, M. (2018). Partial Inactivation of the Chromatin Remodelers SMARCA2 and SMARCA4 in Virus-Infected Cells by Caspase-Mediated Cleavage. *J Virol* 92.

Engelman, J.A., Luo, J., and Cantley, L.C. (2006). The evolution of phosphatidylinositol 3-kinases as regulators of growth and metabolism. *Nature Reviews Genetics* 7, 606-619.

Fernandes-Alnemri, T., Yu, J.W., Datta, P., Wu, J., and Alnemri, E.S. (2009). AIM2 activates the inflammasome and cell death in response to cytoplasmic DNA. *Nature* 458, 509-513.

Fleith, R.C., Mears, H.V., Leong, X.Y., Sanford, T.J., Emmott, E., Graham, S.C., Mansur, D.S., and Sweeney, T.R. (2018). IFIT3 and IFIT2/3 promote IFIT1-mediated translation inhibition by enhancing binding to non-self RNA. *Nucleic Acids Research* 46, 5269-5285.

Fumagalli, M., Sironi, M., Pozzoli, U., Ferrer-Admetlla, A., Pattini, L., and Nielsen, R. (2011). Signatures of environmental genetic adaptation pinpoint pathogens as the main selective pressure through human evolution. *PLoS Genet* 7, e1002355.

Fung, S.W., Cheung, P.F., Yip, C.W., Ng, L.W., Cheung, T.T., Chong, C.C., Lee, C., Lai, P.B., Chan, A.W., Tsao, G.S., et al. (2019). The ATP-binding cassette transporter ABCF1 is a hepatic oncofetal protein that promotes chemoresistance, EMT and cancer stemness in hepatocellular carcinoma. *Cancer Lett* 457, 98-109.

Furuichi, Y., and Shatkin, A.J. (2000). Viral and cellular mRNA capping: past and prospects. *Adv Virus Res* 55, 135-184.

Gallego-Villar, L., Hannibal, L., Häberle, J., Thöny, B., Ben-Omran, T., Nasrallah, G.K., Dewik, A.-N., Kruger, W.D., and Blom, H.J. (2017). Cysteamine revisited: repair of arginine to cysteine mutations. *Journal of Inherited Metabolic Disease* 40, 555-567.

Gao, G., Guo, X., and Goff, S.P. (2002). Inhibition of Retroviral RNA Production by ZAP, a CCCH-Type Zinc Finger Protein. *Science* 297, 1703.

Garcia-Moreno, M., Noerenberg, M., Ni, S., Jarvelin, A.I., Gonzalez-Almela, E., Lenz, C.E., Bach-Pages, M., Cox, V., Avolio, R., Davis, T., et al. (2019). System-wide Profiling of RNA-Binding Proteins Uncovers Key Regulators of Virus Infection. *Mol Cell* 74, 196-211 e111.

Gee, K., Guzzo, C., Che Mat, N.F., Ma, W., and Kumar, A. (2009). The IL-12 family of cytokines in infection, inflammation and autoimmune disorders. *Inflamm Allergy Drug Targets* 8, 40-52.

Gilmore, T.D., and Wolenski, F.S. (2012). NF- κ B: where did it come from and why? *Immunological Reviews* 246, 14-35.

Golding, M.C., Zhang, L., and Mann, M.R. (2010). Multiple epigenetic modifiers induce aggressive viral extinction in extraembryonic endoderm stem cells. *Cell Stem Cell* 6, 457-467.

Gordon, M.D., Dionne, M.S., Schneider, D.S., and Nusse, R. (2005). WntD is a feedback inhibitor of Dorsal/NF-kappaB in *Drosophila* development and immunity. *Nature* 437, 746-749.



Guo, X., Carroll, J.W., Macdonald, M.R., Goff, S.P., and Gao, G. (2004). The zinc finger antiviral protein directly binds to specific viral mRNAs through the CCCH zinc finger motifs. *J Virol* 78, 12781-12787.

Guo, X., Ma, J., Sun, J., and Gao, G. (2007). The zinc-finger antiviral protein recruits the RNA processing exosome to degrade the target mRNA. *Proceedings of the National Academy of Sciences* 104, 151.

Guo, X., Zhang, R., Wang, J., Ding, S.W., and Lu, R. (2013). Homologous RIG-I-like helicase proteins direct RNAi-mediated antiviral immunity in *C. elegans* by distinct mechanisms. *Proc Natl Acad Sci U S A* 110, 16085-16090.

Habjan, M., Hubel, P., Lacerda, L., Benda, C., Holze, C., Eberl, C.H., Mann, A., Kindler, E., Gil-Cruz, C., Ziebuhr, J., et al. (2013). Sequestration by IFIT1 impairs translation of 2'O-unmethylated capped RNA. *PLoS Pathog* 9, e1003663.

Habjan, M., and Pichlmair, A. (2015). Cytoplasmic sensing of viral nucleic acids. *Curr Opin Virol* 11, 31-37.

Hajime Koyama, A. (1995). Induction of apoptotic DNA fragmentation by the infection of vesicular stomatitis virus. *Virus Research* 37, 285-290.

Hartmann, R., Justesen, J., Sarkar, S.N., Sen, G.C., and Yee, V.C. (2003). Crystal Structure of the 2'-Specific and Double-Stranded RNA-Activated Interferon-Induced Antiviral Protein 2'-5'-Oligoadenylate Synthetase. *Molecular Cell* 12, 1173-1185.

Hebner, C.M., Wilson, R., Rader, J., Bidder, M., and Laimins, L.A. (2006). Human papillomaviruses target the double-stranded RNA protein kinase pathway. *Journal of General Virology* 87, 3183-3193.

Hille, F., Richter, H., Wong, S.P., Bratovic, M., Ressel, S., and Charpentier, E. (2018). The Biology of CRISPR-Cas: Backward and Forward. *Cell* 172, 1239-1259.

Honda, K., Takaoka, A., and Taniguchi, T. (2006). Type I Interferon Gene Induction by the Interferon Regulatory Factor Family of Transcription Factors. *Immunity* 25, 349-360.

Hornung, V., Ellegast, J., Kim, S., Brzozka, K., Jung, A., Kato, H., Poeck, H., Akira, S., Conzelmann, K.K., Schlee, M., et al. (2006). 5'-Triphosphate RNA is the ligand for RIG-I. *Science* 314, 994-997.

Hornung, V., Hartmann, R., Ablasser, A., and Hopfner, K.P. (2014). OAS proteins and cGAS: unifying concepts in sensing and responding to cytosolic nucleic acids. *Nat Rev Immunol* 14, 521-528.

Hrincius, E.R., Dierkes, R., Anhlan, D., Wixler, V., Ludwig, S., and Ehrhardt, C. (2011). Phosphatidylinositol-3-kinase (PI3K) is activated by influenza virus vRNA via the pathogen pattern receptor Rig-I to promote efficient type I interferon production. *Cell Microbiol* 13, 1907-1919.

Hu, Y., Flockhart, I., Vinayagam, A., Bergwitz, C., Berger, B., Perrimon, N., and Mohr, S.E. (2011). An integrative approach to ortholog prediction for disease-focused and other functional studies. *BMC Bioinformatics* 12.

Hubel, P., Urban, C., Bergant, V., Schneider, W.M., Knauer, B., Stukalov, A., Scaturro, P., Mann, A., Brunotte, L., Hoffmann, H.H., et al. (2019). A protein-interaction network of interferon-stimulated genes extends the innate immune system landscape. *Nat Immunol* 20, 493-502.

Huerta-Cepas, J., Szklarczyk, D., Heller, D., Hernández-Plaza, A., Forslund, S.K., Cook, H., Mende, D.R., Letunic, I., Rattei, T., Jensen, Lars J., et al. (2019). eggNOG 5.0: a hierarchical, functionally and phylogenetically annotated orthology resource based on 5090 organisms and 2502 viruses. *Nucleic Acids Research* 47, D309-D314.

Hur, S. (2019). Double-Stranded RNA Sensors and Modulators in Innate Immunity. *Annu Rev Immunol* 37, 349-375.

Hurst, L.D., and Smith, N.G.C. (1999). Do essential genes evolve slowly? *Current Biology* 9, 747-750.

Hutchison, M., Berman, K.S., and Cobb, M.H. (1998). Isolation of TAO1, a Protein Kinase That Activates MEKs in Stress-activated Protein Kinase Cascades. *The Journal of Biological Chemistry* 273, 28625-28632.

Ibsen, M.S., Gad, H.H., Andersen, L.L., Hornung, V., Julkunen, I., Sarkar, S.N., and Hartmann, R. (2015). Structural and functional analysis reveals that human OASL binds dsRNA to enhance RIG-I signaling. *Nucleic Acids Research* 43, 5236-5248.

Ishikawa, H., Otaka, H., Maki, K., Morita, T., and Aiba, H. (2012). The functional Hfq-binding module of bacterial sRNAs consists of a double or single hairpin preceded by a U-rich sequence and followed by a 3' poly(U) tail. *RNA* 18, 1062-1074.



Iurescia, S., Fioretti, D., and Rinaldi, M. (2018). Targeting Cytosolic Nucleic Acid-Sensing Pathways for Cancer Immunotherapies. *Frontiers in Immunology* 9.

Izar, B., Sharfman, W., Hodi, F.S., Lawrence, D., Flaherty, K.T., Amaravadi, R., Kim, K.B., Puzanov, I., Sosman, J., Dummer, R., et al. (2017). A first-in-human phase I, multicenter, open-label, dose-escalation study of the oral RAF/VEGFR-2 inhibitor (RAF265) in locally advanced or metastatic melanoma independent from BRAF mutation status. *Cancer Med* 6, 1904-1914.

Janky, R., Verfaillie, A., Imrichova, H., Van de Sande, B., Standaert, L., Christiaens, V., Hulselmans, G., Hertzen, K., Naval Sanchez, M., Potier, D., et al. (2014). iRegulon: from a gene list to a gene regulatory network using large motif and track collections. *PLoS Comput Biol* 10, e1003731.

Jassal, B., Matthews, L., Viteri, G., Gong, C., Lorente, P., Fabregat, A., Sidiropoulos, K., Cook, J., Gillespie, M., Haw, R., et al. (2020). The reactome pathway knowledgebase. *Nucleic Acids Res* 48, D498-D503.

Jefferies, C.A. (2019). Regulating IRFs in IFN Driven Disease. *Front Immunol* 10, 325.

Jonsson, K.L., Laustsen, A., Krapp, C., Skipper, K.A., Thavachelvam, K., Hotter, D., Egedal, J.H., Kjolby, M., Mohammadi, P., Prabakaran, T., et al. (2017). IFI16 is required for DNA sensing in human macrophages by promoting production and function of cGAMP. *Nat Commun* 8, 14391.

Kaech, S.M., and Cui, W. (2012). Transcriptional control of effector and memory CD8+ T cell differentiation. *Nature Reviews Immunology* 12, 749-761.

Kakuta, S., Shibata, S., and Iwakura, Y. (2002). Genomic Structure of the Mouse 2',5'-Oligoadenylate Synthetase Gene Family. *Journal of Interferon & Cytokine Research* 22, 981-993.

Kalra, R.S., Chaudhary, A., Yoon, A.R., Bhargava, P., Omar, A., Garg, S., Yun, C.O., Kaul, S.C., and Wadhwa, R. (2018). CARF enrichment promotes epithelial-mesenchymal transition via Wnt/beta-catenin signaling: its clinical relevance and potential as a therapeutic target. *Oncogenesis* 7, 39.

Kim, B., Arcos, S., Rothamel, K., Jian, J., Rose, K.L., McDonald, W.H., Bian, Y., Reasoner, S., Barrows, N.J., Bradrick, S., et al. (2020). Discovery of Widespread Host

Protein Interactions with the Pre-replicated Genome of CHIKV Using VIR-CLASP. *Mol Cell* 78, 624-640 e627.

Klaeger, S., Heinzlmeir, S., Wilhelm, M., Polzer, H., Vick, B., Koenig, P.A., Reinecke, M., Ruprecht, B., Petzoldt, S., Meng, C., et al. (2017). The target landscape of clinical kinase drugs. *Science* 358.

Kosugia, S., Hasebea, M., Tomitaa, M., and Yanagawa, H. (2009). Systematic identification of cell cycle-dependent yeast nucleocytoplasmic shuttling proteins by prediction of composite motifs. *PNAS* 106, 10171-10176.

Kranzusch, P.J., Lee, A.S., Berger, J.M., and Doudna, J.A. (2013). Structure of human cGAS reveals a conserved family of second-messenger enzymes in innate immunity. *Cell Rep* 3, 1362-1368.

Kranzusch, P.J., Wilson, S.C., Lee, A.S., Berger, J.M., Doudna, J.A., and Vance, R.E. (2015). Ancient Origin of cGAS-STING Reveals Mechanism of Universal 2',3' cGAMP Signaling. *Mol Cell* 59, 891-903.

la Cour, T., Kiemer, L., Molgaard, A., Gupta, R., Skriver, K., and Brunak, S. (2004). Analysis and prediction of leucine-rich nuclear export signals. *Protein Eng Des Sel* 17, 527-536.

Lahaye, X., Gentili, M., Silvin, A., Conrad, C., Picard, L., Jouve, M., Zueva, E., Maurin, M., Nadalin, F., Knott, G.J., et al. (2018). NONO Detects the Nuclear HIV Capsid to Promote cGAS-Mediated Innate Immune Activation. *Cell* 175, 488-501 e422.

Langevin, C., Aleksejeva, E., Passoni, G., Palha, N., Levraud, J.-P., and Boudinot, P. (2013). The Antiviral Innate Immune Response in Fish: Evolution and Conservation of the IFN System. *Journal of Molecular Biology* 425, 4904-4920.

Lee, C.J., Liao, C.L., and Lin, Y.L. (2005). Flavivirus activates phosphatidylinositol 3-kinase signaling to block caspase-dependent apoptotic cell death at the early stage of virus infection. *J Virol* 79, 8388-8399.

Lee, M.N., Roy, M., Ong, S.E., Mertins, P., Villani, A.C., Li, W., Dotiwala, F., Sen, J., Doench, J.G., Orzalli, M.H., et al. (2013). Identification of regulators of the innate immune response to cytosolic DNA and retroviral infection by an integrative approach. *Nat Immunol* 14, 179-185.



Lehmann, M.H., Torres-Dominguez, L.E., Price, P.J., Brandmuller, C., Kirschning, C.J., and Sutter, G. (2016). CCL2 expression is mediated by type I IFN receptor and recruits NK and T cells to the lung during MVA infection. *J Leukoc Biol* 99, 1057-1064.

Letunic, I., and Bork, P. (2018). 20 years of the SMART protein domain annotation resource. *Nucleic Acids Res* 46, D493-D496.

Li, L., Zhao, H., Liu, P., Li, C., Quanquin, N., Ji, X., Sun, N., Du, P., Qin, C.-F., Lu, N., et al. (2018a). PARP12 suppresses Zika virus infection through PARP-dependent degradation of NS1 and NS3 viral proteins. *Science Signaling* 11, eaas9332.

Li, N., Parrish, M., Chan, T.K., Yin, L., Rai, P., Yoshiyuki, Y., Abolhassani, N., Tan, K.B., Kiraly, O., Chow, V.T., et al. (2015). Influenza infection induces host DNA damage and dynamic DNA damage responses during tissue regeneration. *Cell Mol Life Sci* 72, 2973-2988.

Li, N., Zhao, G., Chen, T., Xue, L., Ma, L., Niu, J., and Tong, T. (2012). Nucleolar protein CSIG is required for p33ING1 function in UV-induced apoptosis. *Cell Death Dis* 3, e283.

Li, S.-f., Gong, M.-j., Zhao, F.-r., Shao, J.-j., Xie, Y.-l., Zhang, Y.-g., and Chang, H.-y. (2018b). Type I Interferons: Distinct Biological Activities and Current Applications for Viral Infection. *Cellular Physiology and Biochemistry* 51, 2377-2396.

Lilley, C.E., Carson, C.T., Muotri, A.R., Gage, F.H., and Weitzman, M.D. (2005). DNA repair proteins affect the lifecycle of herpes simplex virus 1. *Proceedings of the National Academy of Sciences of the United States of America* 102, 5844.

Lilley, C.E., Chaurushiya, M.S., Boutell, C., Landry, S., Suh, J., Panier, S., Everett, R.D., Stewart, G.S., Durocher, D., and Weitzman, M.D. (2010). A viral E3 ligase targets RNF8 and RNF168 to control histone ubiquitination and DNA damage responses. *EMBO J* 29, 943-955.

Littman, D.R., and Rudensky, A.Y. (2010). Th17 and Regulatory T Cells in Mediating and Restraining Inflammation. *Cell* 140, 845-858.

Liu, J., Henao-Mejia, J., Liu, H., Zhao, Y., and He, J.J. (2011). Translational regulation of HIV-1 replication by HIV-1 Rev cellular cofactors Sam68, eIF5A, hRIP, and DDX3. *J Neuroimmune Pharmacol* 6, 308-321.

- Liu, S., Cai, X., Wu, J., Cong, Q., Chen, X., Li, T., Du, F., Ren, J., Wu, Y.T., Grishin, N.V., et al. (2015). Phosphorylation of innate immune adaptor proteins MAVS, STING, and TRIF induces IRF3 activation. *Science* 347, aaa2630.
- Liu, S.Y., Sanchez, D.J., Aliyari, R., Lu, S., and Cheng, G. (2012). Systematic identification of type I and type II interferon-induced antiviral factors. *Proc Natl Acad Sci U S A* 109, 4239-4244.
- Liu, T., Zhang, L., Joo, D., and Sun, S.C. (2017). NF-kappaB signaling in inflammation. *Signal Transduct Target Ther* 2.
- Liu, Y., Shepherd, E.G., and Nelin, L.D. (2007). MAPK phosphatases--regulating the immune response. *Nat Rev Immunol* 7, 202-212.
- Loo, Y.M., and Gale, M., Jr. (2011). Immune signaling by RIG-I-like receptors. *Immunity* 34, 680-692.
- Ma, L., Chang, N., Guo, S., Li, Q., Zhang, Z., Wang, W., and Tong, T. (2008). CSIG inhibits PTEN translation in replicative senescence. *Mol Cell Biol* 28, 6290-6301.
- Mankan, A.K., Schmidt, T., Chauhan, D., Goldeck, M., Honing, K., Gaidt, M., Kubarenko, A.V., Andreeva, L., Hopfner, K.P., and Hornung, V. (2014). Cytosolic RNA:DNA hybrids activate the cGAS-STING axis. *EMBO J* 33, 2937-2946.
- Marchler-Bauer, A., Lu, S., Anderson, J.B., Chitsaz, F., Derbyshire, M.K., DeWeese-Scott, C., Fong, J.H., Geer, L.Y., Geer, R.C., Gonzales, N.R., et al. (2011). CDD: a Conserved Domain Database for the functional annotation of proteins. *Nucleic Acids Res* 39, D225-229.
- Matsumoto, M., Oshiumi, H., and Seya, T. (2011). Antiviral responses induced by the TLR3 pathway. *Rev Med Virol* 21, 67-77.
- McBride, A.E., Schlegel, A., and Kirkegaard, K. (1996). Human protein Sam68 relocalization and interaction with poliovirus RNA polymerase in infected cells. *Proceedings of the National Academy of Sciences of the United States of America* 93, 2296-2301.
- Medzhitov, R. (2007). Recognition of microorganisms and activation of the immune response. *Nature* 449, 819-826.



Merico, D., Isserlin, R., Stueker, O., Emili, A., and Bader, G.D. (2010). Enrichment map: a network-based method for gene-set enrichment visualization and interpretation. *PLoS One* 5, e13984.

Mitchell, S., Vargas, J., and Hoffmann, A. (2016). Signaling via the NFkappaB system. *Wiley Interdiscip Rev Syst Biol Med* 8, 227-241.

Mogensen, T.H. (2019). IRF and STAT Transcription Factors - From Basic Biology to Roles in Infection, Protective Immunity, and Primary Immunodeficiencies. *Frontiers in Immunology* 9.

Mohni, K.N., Livingston, C.M., Cortez, D., and Weller, S.K. (2010). ATR and ATRIP are recruited to herpes simplex virus type 1 replication compartments even though ATR signaling is disabled. *J Virol* 84, 12152-12164.

Molho-Pessach, V., Ramot, Y., Mogilevsky, M., Cohen-Daniel, L., Eisenstein, E.M., Abu-Libdeh, A., Siam, I., Berger, M., Karni, R., and Zlotogorski, A. (2017). Generalized verrucosis and abnormal T cell activation due to homozygous TAOK2 mutation. *J Dermatol Sci* 87, 123-129.

Morales, J., Li, L., Fattah, F.J., Dong, Y., Bey, E.A., Patel, M., Gao, J., and Boothman, D.A. (2014). Review of poly (ADP-ribose) polymerase (PARP) mechanisms of action and rationale for targeting in cancer and other diseases. *Crit Rev Eukaryot Gene Expr* 24, 15-28.

Morchikh, M., Cribier, A., Raffel, R., Amraoui, S., Cau, J., Severac, D., Dubois, E., Schwartz, O., Bennasser, Y., and Benkirane, M. (2017). HEXIM1 and NEAT1 Long Non-coding RNA Form a Multi-subunit Complex that Regulates DNA-Mediated Innate Immune Response. *Mol Cell* 67, 387-399 e385.

Morita, E., Sandrin, V., McCullough, J., Katsuyama, A., Baci Hamilton, I., and Sundquist, W.I. (2011). ESCRT-III Protein Requirements for HIV-1 Budding. *Cell Host & Microbe* 9, 235-242.

Mudiganti, U., Hernandez, R., and Brown, D.T. (2010). Insect response to alphavirus infection--establishment of alphavirus persistence in insect cells involves inhibition of viral polyprotein cleavage. *Virus Res* 150, 73-84.

- Muñoz-Wolf, N., and Lavelle, E.C. (2016). Innate Immune Receptors. In *NLR Proteins: Methods and Protocols*, F. Di Virgilio, and P. Pelegrín, eds. (New York, NY: Springer New York), pp. 1-43.
- Mussabekova, A., Daeffler, L., and Imler, J.L. (2017). Innate and intrinsic antiviral immunity in *Drosophila*. *Cell Mol Life Sci* 74, 2039-2054.
- Nadel, J., Athanasiadou, R., Lemetre, C., Wijetunga, N.A., P, O.B., Sato, H., Zhang, Z., Jeddeloh, J., Montagna, C., Golden, A., et al. (2015). RNA:DNA hybrids in the human genome have distinctive nucleotide characteristics, chromatin composition, and transcriptional relationships. *Epigenetics Chromatin* 8, 46.
- Negishi, H., Taniguchi, T., and Yanai, H. (2018). The Interferon (IFN) Class of Cytokines and the IFN Regulatory Factor (IRF) Transcription Factor Family. *Cold Spring Harbor Perspectives in Biology* 10.
- Nehyba, J., Hrdlickova, R., and Bose, H.R. (2009). Dynamic Evolution of Immune System Regulators: The History of the Interferon Regulatory Factor Family. *Molecular Biology and Evolution* 26, 2539-2550.
- Onorati, M.C., Lazzaro, S., Mallik, M., Ingrassia, A.M., Carreca, A.P., Singh, A.K., Chaturvedi, D.P., Lakhotia, S.C., and Corona, D.F. (2011). The ISWI chromatin remodeler organizes the hsomega ncRNA-containing omega speckle nuclear compartments. *PLoS Genet* 7, e1002096.
- Palmer, D.H., and Kronforst, M.R. (2015). Divergence and gene flow among Darwin's finches: A genome-wide view of adaptive radiation driven by interspecies allele sharing. *Bioessays* 37, 968-974.
- Paro, S., Imler, J.L., and Meignin, C. (2015). Sensing viral RNAs by Dicer/RIG-I like ATPases across species. *Curr Opin Immunol* 32, 106-113.
- Peck, K.M., and Lauring, A.S. (2018). Complexities of Viral Mutation Rates. *Journal of Virology* 92, e01031-01017.
- Plotnikov, A., Zehorai, E., Procaccia, S., and Seger, R. (2011). The MAPK cascades: signaling components, nuclear roles and mechanisms of nuclear translocation. *Biochim Biophys Acta* 1813, 1619-1633.



Puchades, C., Sandate, C.R., and Lander, G.C. (2019). The molecular principles governing the activity and functional diversity of AAA+ proteins. *Nature Reviews Molecular Cell Biology* 21, 43-58.

Pujantell, M., Badia, R., Galván-Femenía, I., Garcia-Vidal, E., de Cid, R., Alcalde, C., Tarrats, A., Piñol, M., Garcia, F., Chamorro, A.M., et al. (2019). ADAR1 function affects HPV replication and is associated to recurrent human papillomavirus-induced dysplasia in HIV coinfecting individuals. *Scientific Reports* 9.

Qi, Z., Nie, P., Secombes, C.J., and Zou, J. (2010). Intron-Containing Type I and Type III IFN Coexist in Amphibians: Refuting the Concept That a Retroposition Event Gave Rise to Type I IFNs. *The Journal of Immunology* 184, 5038-5046.

Qin, Y., Xun, Z., Guo, Y., Chen, S., and Zhu, H. (2019). Sam68 Promotes Hepatitis C Virus Replication by Interaction with Stem-Loop 2 of Viral 5' Untranslated Region. *Journal of virology* 93.

Rai, D.K., Lawrence, P., Kloc, A., Schafer, E., and Rieder, E. (2015). Analysis of the interaction between host factor Sam68 and viral elements during foot-and-mouth disease virus infections. *Virology* 12, 224.

Raman, M., Earnest, S., Zhang, K., Zhao, Y., and Cobb, M.H. (2007). TAO kinases mediate activation of p38 in response to DNA damage. *EMBO J* 26, 2005-2014.

Rappsilber, J., Mann, M., and Ishihama, Y. (2007). Protocol for micro-purification, enrichment, pre-fractionation and storage of peptides for proteomics using StageTips. *Nat Protoc* 2, 1896-1906.

Reich, D.P., Tyc, K.M., and Bass, B.L. (2018). *C. elegans* ADARs antagonize silencing of cellular dsRNAs by the antiviral RNAi pathway. *Genes Dev* 32, 271-282.

Rodero, M.P., and Crow, Y.J. (2016). Type I interferon-mediated monogenic autoinflammation: The type I interferonopathies, a conceptual overview. *Journal of Experimental Medicine* 213, 2527-2538.

Rusinova, I., Forster, S., Yu, S., Kannan, A., Masse, M., Cumming, H., Chapman, R., and Hertzog, P.J. (2012). INTERFEROME v2.0: an updated database of annotated interferon-regulated genes. *Nucleic Acids Research* 41, D1040-D1046.

Samuel, C.E. (2001). Antiviral actions of interferons. *Clin Microbiol Rev* 14, 778-809, table of contents.

Samuel, C.E. (2019). Adenosine deaminase acting on RNA (ADAR1), a suppressor of double-stranded RNA-triggered innate immune responses. *J Biol Chem* 294, 1710-1720.

Sangar, D.V. (1979). The Replication of Picornaviruses. *Journal of General Virology* 45, 1-13.

Sanjuán, R., Nebot, M.R., Chirico, N., Mansky, L.M., and Belshaw, R. (2010). Viral Mutation Rates. *Journal of Virology* 84, 9733.

Sarkar, S.N., Peters, K.L., Elco, C.P., Sakamoto, S., Pal, S., and Sen, G.C. (2004). Novel roles of TLR3 tyrosine phosphorylation and PI3 kinase in double-stranded RNA signaling. *Nat Struct Mol Biol* 11, 1060-1067.

Sarracino, A., Gharu, L., Kula, A., Pasternak, A.O., Avettand-Fenoel, V., Rouzioux, C., Bardina, M., De Wit, S., Benkirane, M., Berkhout, B., et al. (2018). Posttranscriptional Regulation of HIV-1 Gene Expression during Replication and Reactivation from Latency by Nuclear Matrix Protein MATR3. *mBio* 9.

Saxena, M., and Yeretssian, G. (2014). NOD-Like Receptors: Master Regulators of Inflammation and Cancer. *Front Immunol* 5, 327.

Scaturro, P., Stukalov, A., Haas, D.A., Cortese, M., Draganova, K., Plaszczyca, A., Bartenschlager, R., Gotz, M., and Pichlmair, A. (2018). An orthogonal proteomic survey uncovers novel Zika virus host factors. *Nature* 561, 253-257.

Schlee, M., and Hartmann, G. (2016). Discriminating self from non-self in nucleic acid sensing. *Nat Rev Immunol* 16, 566-580.

Schmidt, A., Schwerd, T., Hamm, W., Hellmuth, J.C., Cui, S., Wenzel, M., Hoffmann, F.S., Michallet, M.-C., Besch, R., Hopfner, K.-P., et al. (2009). 5'-triphosphate RNA requires base-paired structures to activate antiviral signaling via RIG-I. *Proceedings of the National Academy of Sciences* 106, 12067.

Scholz, J., and Suppmann, S. (2017). A new single-step protocol for rapid baculovirus-driven protein production in insect cells. *BMC Biotechnol* 17, 83.



Schwartz, S.L., and Conn, G.L. (2019). RNA regulation of the antiviral protein 2'-5'-oligoadenylate synthetase. *Wiley Interdiscip Rev RNA* 10, e1534.

Seborova, K., Vaclavikova, R., Soucek, P., Elsnerova, K., Bartakova, A., Cernaj, P., Bouda, J., Rob, L., Hrudá, M., and Dvorak, P. (2019). Association of ABC gene profiles with time to progression and resistance in ovarian cancer revealed by bioinformatics analyses. *Cancer Med* 8, 606-616.

Secombes, C.J., and Zou, J. (2017). Evolution of Interferons and Interferon Receptors. *Frontiers in Immunology* 8.

Shannon, P. (2003). Cytoscape: A Software Environment for Integrated Models of Biomolecular Interaction Networks. *Genome Research* 13, 2498-2504.

Shao, Z., Flynn, R.A., Crowe, J.L., Zhu, Y., Liang, J., Jiang, W., Aryan, F., Aoude, P., Bertozzi, C.R., Estes, V.M., et al. (2020). DNA-PKcs has KU-dependent function in rRNA processing and haematopoiesis. *Nature* 579, 291-296.

Shih, W.L., Kuo, M.L., Chuang, S.E., Cheng, A.L., and Doong, S.L. (2000). Hepatitis B virus X protein inhibits transforming growth factor-beta -induced apoptosis through the activation of phosphatidylinositol 3-kinase pathway. *J Biol Chem* 275, 25858-25864.

Shin, C., Ito, Y., Ichikawa, S., Tokunaga, M., Sakata-Sogawa, K., and Tanaka, T. (2017). MKRN2 is a novel ubiquitin E3 ligase for the p65 subunit of NF-kappaB and negatively regulates inflammatory responses. *Sci Rep* 7, 46097.

Shulman, L.M., and Davidson, I. (2017). Viruses with Circular Single-Stranded DNA Genomes Are Everywhere! *Annu Rev Virol* 4, 159-180.

Silverman, R.H. (2007). Viral encounters with 2',5'-oligoadenylate synthetase and RNase L during the interferon antiviral response. *J Virol* 81, 12720-12729.

Snead, N.M., Wu, X., Li, A., Cui, Q., Sakurai, K., Burnett, J.C., and Rossi, J.J. (2013). Molecular basis for improved gene silencing by Dicer substrate interfering RNA compared with other siRNA variants. *Nucleic Acids Res* 41, 6209-6221.

Stetson, D.B., and Medzhitov, R. (2006). Recognition of cytosolic DNA activates an IRF3-dependent innate immune response. *Immunity* 24, 93-103.

Sugiyama, T., Hoshino, K., Saito, M., Yano, T., Sasaki, I., Yamazaki, C., Akira, S., and Kaisho, T. (2008). Immunoadjuvant effects of polyadenylic:polyuridylic acids through TLR3 and TLR7. *Int Immunol* 20, 1-9.

Sun, L., Wu, J., Du, F., Chen, X., and Chen, Z.J. (2012). Cyclic GMP-AMP Synthase Is a Cytosolic DNA Sensor That Activates the Type I Interferon Pathway. *Science* 339, 786-791.

Tassetto, M., Kunitomi, M., and Andino, R. (2017). Circulating Immune Cells Mediate a Systemic RNAi-Based Adaptive Antiviral Response in *Drosophila*. *Cell* 169, 314-325 e313.

Theze, J., Bezier, A., Periquet, G., Drezen, J.M., and Herniou, E.A. (2011). Paleozoic origin of insect large dsDNA viruses. *Proc Natl Acad Sci U S A* 108, 15931-15935.

Ting, J.P.Y., Lovering, R.C., Alnemri, E.S., Bertin, J., Boss, J.M., Davis, B.K., Flavell, R.A., Girardin, S.E., Godzik, A., Harton, J.A., et al. (2008). The NLR Gene Family: A Standard Nomenclature. *Immunity* 28, 285-287.

Tripathi, S., Pohl, M.O., Zhou, Y., Rodriguez-Frandsen, A., Wang, G., Stein, D.A., Moulton, H.M., DeJesus, P., Che, J., Mulder, L.C., et al. (2015). Meta- and Orthogonal Integration of Influenza "OMICs" Data Defines a Role for UBR4 in Virus Budding. *Cell Host Microbe* 18, 723-735.

Troegeler, A., Mercier, I., Cougoule, C., Pietretti, D., Colom, A., Duval, C., Vu Manh, T.-P., Capilla, F., Poincloux, R., Pingris, K., et al. (2017). C-type lectin receptor DCIR modulates immunity to tuberculosis by sustaining type I interferon signaling in dendritic cells. *Proceedings of the National Academy of Sciences* 114, E540.

Tyanova, S., Temu, T., and Cox, J. (2016a). The MaxQuant computational platform for mass spectrometry-based shotgun proteomics. *Nat Protoc* 11, 2301-2319.

Tyanova, S., Temu, T., Sinitcyn, P., Carlson, A., Hein, M.Y., Geiger, T., Mann, M., and Cox, J. (2016b). The Perseus computational platform for comprehensive analysis of (prote)omics data. *Nat Methods* 13, 731-740.

Valen, L.V. (1973). A new evolutionary law.

Vitkup, D., Sander, C., and Church, G.M. (2003). The amino-acid mutational spectrum of human genetic disease. *Genome Biol* 4, R72-R72.



Votteler, J., and Sundquist, Wesley I. (2013). Virus Budding and the ESCRT Pathway. *Cell Host & Microbe* 14, 232-241.

Vyas, S., Chesarone-Cataldo, M., Todorova, T., Huang, Y.-H., and Chang, P. (2013). A systematic analysis of the PARP protein family identifies new functions critical for cell physiology. *Nature Communications* 4.

Wang, J.T., McElvain, L.E., and Whelan, S.P. (2007). Vesicular stomatitis virus mRNA capping machinery requires specific cis-acting signals in the RNA. *J Virol* 81, 11499-11506.

Wang, L., Yang, L., Fikrig, E., and Wang, P. (2017). An essential role of PI3K in the control of West Nile virus infection. *Sci Rep* 7, 3724.

Wang, M.-H., Qin, S.-Y., Zhang, S.-G., Li, G.-X., Yu, Z.-H., Wang, K., Wang, B., Teng, M.-J., and Peng, Z.-H. (2015). Musashi-2 promotes hepatitis B virus related hepatocellular carcinoma progression via the Wnt/ β -catenin pathway. In *Am J Cancer Res*, pp. 1089-1100.

Wang, P.-H., and He, J.-G. (2019). Nucleic Acid Sensing in Invertebrate Antiviral Immunity. In *Nucleic Acid Sensing and Immunity - Part B*, pp. 287-360.

Weber, F., Wagner, V., Rasmussen, S.B., Hartmann, R., and Paludan, S.R. (2006). Double-stranded RNA is produced by positive-strand RNA viruses and DNA viruses but not in detectable amounts by negative-strand RNA viruses. *J Virol* 80, 5059-5064.

Weitzman, M.D., and Fradet-Turcotte, A. (2018). Virus DNA Replication and the Host DNA Damage Response. *Annu Rev Virol* 5, 141-164.

Williams, T.E., Subramanian, S., Verhagen, J., McBride, C.M., Costales, A., Sung, L., Antonios-McCrea, W., McKenna, M., Louie, A.K., Ramurthy, S., et al. (2015). Discovery of RAF265: A Potent mut-B-RAF Inhibitor for the Treatment of Metastatic Melanoma. *ACS Med Chem Lett* 6, 961-965.

Wilson, A.M., Hubel, T.Y., Wilshin, S.D., Lowe, J.C., Lorenc, M., Dewhirst, O.P., Bartlam-Brooks, H.L.A., Diack, R., Bennitt, E., Golabek, K.A., et al. (2018). Biomechanics of predator-prey arms race in lion, zebra, cheetah and impala. *Nature* 554, 183-188.

Woolhouse, M.E.J., Taylor, L.H., and Haydon, D.T. (2001). Population Biology of Multihost Pathogens. *Science* 292, 1109.

Yang, S.H., Sharrocks, A.D., and Whitmarsh, A.J. (2013). MAP kinase signalling cascades and transcriptional regulation. *Gene* 513, 1-13.

Yoneyama, M., Onomoto, K., Jogi, M., Akaboshi, T., and Fujita, T. (2015). Viral RNA detection by RIG-I-like receptors. *Curr Opin Immunol* 32, 48-53.

Yong, H.Y., and Luo, D. (2018). RIG-I-Like Receptors as Novel Targets for Pan-Antivirals and Vaccine Adjuvants Against Emerging and Re-Emerging Viral Infections. *Frontiers in Immunology* 9.

Yoshizawa, T., Hammaker, D., Sweeney, S.E., Boyle, D.L., and Firestein, G.S. (2008). Synoviocyte Innate Immune Responses: I. Differential Regulation of Interferon Responses and the JNK Pathway by MAPK Kinases. *The Journal of Immunology* 181, 3252.

Zhang, B., Li, M., Chen, L., Yang, K., Shan, Y., Zhu, L., Sun, S., Li, L., and Wang, C. (2009). The TAK1-JNK cascade is required for IRF3 function in the innate immune response. *Cell Research* 19, 412-428.

Zhang, H., Song, L., Cong, H., and Tien, P. (2015). Nuclear Protein Sam68 Interacts with the Enterovirus 71 Internal Ribosome Entry Site and Positively Regulates Viral Protein Translation. *J Virol* 89, 10031-10043.

Zhou, H., Møhlenberg, M., Terczyńska-Dyla, E., Winther, K.G., Hansen, N.H., Vad-Nielsen, J., Laloli, L., Dijkman, R., Nielsen, A.L., Gad, H.H., et al. (2020). The IFNL4 Gene Is a Noncanonical Interferon Gene with a Unique but Evolutionarily Conserved Regulation. *Journal of Virology* 94, e01535-01519.

Zihni, C., Mitsopoulos, C., Tavares, I.A., Baum, B., Ridley, A.J., and Morris, J.D. (2007). Prostate-derived sterile 20-like kinase 1-alpha induces apoptosis. JNK- and caspase-dependent nuclear localization is a requirement for membrane blebbing. *J Biol Chem* 282, 6484-6493.

Zolotukhin, A.S., Michalowski, D., Bear, J., Smulevitch, S.V., Traish, A.M., Peng, R., Patton, J., Shatsky, I.N., and Felber, B.K. (2003). PSF acts through the human immunodeficiency virus type 1 mRNA instability elements to regulate virus expression. *Mol Cell Biol* 23, 6618-6630.



Zou, J., Chang, M., Nie, P., and Secombes, C.J. (2009). Origin and evolution of the RIG-I like RNA helicase gene family. *BMC Evol Biol* 9, 85.

List of Tables and Figures

List of Figures

Figure 1: Overview of components of the innate and the adaptive immune system....	2
Figure 2: Schematic of NA sensing PRR signaling.	4
Figure 3: Schematic of IFN signaling pathways.	12
Figure 4: Comparative view of the domains identified in human RIG-I and C. elegans orthologue DRH1.	14
Figure 5: Cladogram indicating the evolution of various elements of the innate immune system.....	17
Figure 6: Schematic detailing AP-MS procedure.	18
Figure 7: Schematic representation of experimental design and outline..	20
Figure 8: TAO kinase structures and functions.	21
Figure 9: Validation of AP-MS interactors from the THP-1 screen.	66
Figure 10: Network analysis of the significantly enriched proteins in the human AP-MS screening.	68
Figure 11: Analysis of AP-MS dataset.	70
Figure 12: Network analysis of the significantly enriched proteins in the fly (A) and mouse (B) AP-MS screening.	73
Figure 13: Orthologue analysis and selection of candidates.	74
Figure 14: Antiviral activity of candidates in human depletion screening.	76
Figure 16: Validation of TAOK2 phenotypes observed in AP-MS and KO screening..	78
Figure 17: Transient and stable TAOK2 overexpression.	80
Figure 18: dTao directly binds poly(I:C) and this interaction affects kinase activity. ..	81
Figure 19: TAOK2 affects ISG expression.....	82
Figure 20: TAOK2 is required for ISG expression in infected, but not in IFN treated cells.....	83
Figure 21: Loss of TAOK2 directly impacts IFN but not TNF- α secretion.....	85
Figure 22: Effect of TAOK2 inhibitors on viral replication.....	86



Figure 23: Effect of TAOK2 inhibitors in TAOK2 KO cells.....87

Figure 24: Overview of the results gathered in the three separate screenings (AP-MS, human KO and fly KD) for the 28 overlapping proteins from the human KO and fly KD screening.91

List of Tables

Table 1: Overview of selected NA binding PRRs8

Table 2: Overview of IRFs induced by NA sensing PRRs..... 10

Table 3: Overview of NA baits and controls used64

Table 4: Number of potential anti- and pro-viral factors, sorted both by virus and by THP-1 treatment.....75

Acknowledgements

First and foremost I would like to thank my supervisor Andreas Pichlmair. Your expertise has been invaluable; from developing research questions to devising an experimental approach. You always had an open door and helpful advice. Your support when I was left unable to use my hands was incredibly meaningful and something I will continue to be grateful for.

Many thanks to my TAC members, Dietmar Zehn, Colin Crump and Anne Krug as well as my mentor Timothy Soh. Your scientific input helped me to develop new ideas and strengthen my project.

I would also like to thank our collaborators, Jean-Luc Imler, Carine Meignin, Assel Mussabekova, Enrico Girardi, Giulio Superti-Furga, Rasha Boulos, Rune Hartmann, Stephan Uebel, Leopold Urich, Sabine Suppmann and Silke Hegenbarth for their work and the scientific exchange.

I would sincerely like to thank all the members of the 'Innate Lab', in particular Lila, Chris, Alexey, Vincent, Teresa and Line. The scientific discussions, the collaborations, the tea breaks and the happy hours were always a great time. Line, you have been my friend, my flatmate, my lab buddy, my hands and I don't think my project would have come out as nicely as it did without you!

Finally, I would like to thank my boyfriend Frits. You are my rock through all the storms.